Appendices

A. Calculations & supportive data

B. List of Publications and

Seminars attended

APPENDIX A(I)

Calculations from Chapter 3

Table A1. Peak potential value of peak A (Figure 3.1)

Potential (V)	$\overline{X}$	di	di^2	Σdi^2	S	RSD
0.31	0.30	0.01	0.0001	0.0002	0.01	3.33%
0.31		0.01	0.0001			
0.30		0.0	0.0			

Table A2. Peak current value of peak A (Figure 3.1)

Current, Ax 10^{-6}	$\overline{X}$	di	di^2	Σdi^2	S	RSD
5.37	5.35	0.02	0.0004	0.0005	0.02	0.37%
5.34		-0.01	0.0001			
5.35		0.0	0.0			

Table A3. Peak potential value of peak B (Figure 3.1)

Potential (V)	$\overline{X}$	di	di^2	Σdi^2	S	RSD
0.61	0.60	0.01	0.0001	0.0002	0.01	1.66%
0.59		-0.01	0.0001			
0.60		0.0	0.0			

Appendix A

Table A4. Peak potential value of peak B (Figure 3.1)

Potential (V)	$\bar{X}$	di	di^2	Σdi^2	S	RSD
0.92	0.90	0.02	0.0004	0.0006	0.02	2.22%
0.91		0.01	0.0001			
0.89		-0.01	0.0001			

Table A5. Peak potential value of peak C (Figure 3.1)

Potential (V)	$\bar{X}$	di	di^2	Σdi^2	S	RSD
0.103	0.102	0.001	0.000001	0.000009	0.003	2.94%
0.104		0.002	0.000004			
0.100		-0.002	0.000004			

Table A6. Peak potential value of peak D (Figure 3.1)

Potential (V)	$\bar{X}$	di	di^2	Σdi^2	S	RSD
0.051	0.051	0.0	0.0	0.000002	0.001	1.96%
0.052		0.001	0.000001			
0.050		-0.001	0.000001			

Table A7. Peak current value of peak A (Figure 3.2A)

Current, Ax 10^{-6}	$\bar{X}$	di	di^2	Σdi^2	S	RSD
20.65	20.67	-0.02	0.0004	0.0013	0.03	0.14%
20.67		0.0	0.0			
20.70		0.03	0.0009			

Table A8. Peak current value of peak A (Figure 3.2B)

Current, Ax 10^{-6}	$\bar{X}$	di	di^2	Σdi^2	S	RSD
10.50	10.45	0.05	0.0025	0.0042	0.06	0.57%
10.41		-0.04	0.0016			
10.46		0.01	0.0001			

Table A9. Peak current value of peak A (Figure 3.4A)

Current, Ax 10^{-6}	$\bar{X}$	di	di^2	Σdi^2	S	RSD
13.01	12.98	0.03	0.0009	0.0019	0.04	0.30%
12.95		-0.03	0.0009			
12.99		0.01	0.0001			

Table A10. Peak current value of peak A (Figure 3.4B)

Current, Ax 10^{-6}	$\bar{X}$	di	di^2	Σdi^2	S	RSD
12.98	12.95	0.03	0.0009	0.0013	0.03	0.23%
12.95		0.0	0.0			
12.93		-0.02	0.0004			

Table A11. Peak current value of peak A (Figure 3.5A)

Current, Ax 10^{-6}	$\bar{X}$	di	di^2	Σdi^2	S	RSD
15.22	15.20	0.02	0.0004	0.0009	0.03	0.19%
15.21		0.01	0.0001			
15.18		-0.02	0.0004			

Table A12. Peak current value of peak A (Figure 3.5B)

Current, Ax 10^{-6}	$\bar{X}$	di	di^2	Σdi^2	S	RSD
14.26	14.28	-0.02	0.0004	0.0009	0.03	0.21%
14.29		0.01	0.0001			
14.30		0.02	0.0004			

Table A13. Peak potential value of peak P (Figure 3.16)

Potential (V)	$\bar{X}$	di	di^2	Σdi^2	S	RSD
0.57	0.56	0.01	0.0001	0.0002	0.01	1.78%
0.56		0.0	0.0			
0.55		-0.01	0.0001			

Table A14. Peak current value of peak P (Figure 3.16)

Current, Ax 10^{-6}	$\bar{X}$	di	di^2	Σdi^2	S	RSD
10.84	10.81	0.03	0.0009	0.0014	0.03	0.27%
10.79		-0.02	0.0004			
10.80		-0.01	0.0001			

Table A15. Peak potential value of peak Q (Figure 3.16)

Potential (V)	$\bar{X}$	di	di^2	Σdi^2	S	RSD
0.35	0.35	0.0	0.0	0.0001	0.01	2.85%
0.34		-0.01	0.0001			
0.35		0.0	0.0			

Appendix A

Table A16. Peak current value of peak P (Figure 3.16)

Current, Ax 10^{-6}	$\bar{X}$	di	di^2	Σdi^2	S	RSD
2.46	2.45	0.01	0.0001	0.0009	0.03	1.22%
2.43		-0.02	0.0004			
2.47		0.02	0.0004			

Table A17. Peak potential value of peak a′ (Figure 3.17)

Potential (V)	$\bar{X}$	di	di^2	Σdi^2	S	RSD
0.65	0.65	0.0	0.0	0.0001	0.01	1.53%
0.65		0.0	0.0			
0.64		-0.01	0.0001			

Table A18. Peak potential value of peak a (Figure 3.17)

Potential (V)	$\bar{X}$	di	di^2	Σdi^2	S	RSD
0.41	0.40	0.01	0.0001	0.0002	0.01	2.50%
0.39		-0.01	0.0001			
0.40		0.0	0.0			

Table A19. Calculation of K_m^{app} for GSH (low conc.) (para 3.4.3.2)

Concentration, $molL^{-1}$	1/Concentration , $mol^{-1}L$	Current, A	1/Current, A^{-1}	K_m
0.002	500	0.0000155	64500	0.11 $mmolL^{-1}$
0.001	1000	0.0000140	71400	
0.0005	2000	0.0000132	75800	

Slope = 7.085 $A^{-1}molL^{-1}$

Intercept = 62300 A^{-1}

K_m = Slope/ Intercept

= 7.085/ 62300

= 0.00011 mol L^{-1}

= 0.11 $mmolL^{-1}$

Table A20. Calculation of K_m^{app} for GSH (high conc.) (para 3.4.3.2)

Concentration, $molL^{-1}$	1/Concentration , $mol^{-1}L$	Current, A	1/Current, A^{-1}	K_m
0.05	250	0.0000202	49500	1.66 $mmolL^{-1}$
0.5	333.3333	0.0000179	55900	
0.075	500	0.0000155	64500	

Slope = 58.8 $A^{-1}molL^{-1}$

Intercept = 35400 A^{-1}

K_m = Slope/ Intercept

= 58.8/ 35400

= 0.00166 mol L^{-1}

= 1.66 $mmolL^{-1}$

Table A21. Calculation of K_m^{app} for CDNB (low conc.) (para 3.4.3.2)

Concentration, $molL^{-1}$	1/Concentration , $mol^{-1}L$	Current, A	1/Current, A^{-1}	K_m
0.002	500	0.0000147	68000	0.12 $mmolL^{-1}$
0.001	1000	0.0000133	75200	
0.0005	2000	0.0000124	80600	

Slope = 7.971 $A^{-1}molL^{-1}$

Intercept = 65300 A^{-1}

K_m = Slope/ Intercept

= 7.971/ 65300

= 0.00012 mol L^{-1}

= 0.12 $mmolL^{-1}$

Table A22. Calculation of K_m^{app} for CDNB (high conc.) (para 3.4.3.2)

Concentration, $molL^{-1}$	1/Concentration , $mol^{-1}L$	Current, A	1/Current, A^{-1}	K_m
0.004	250	0.0000196	51000	1.91 $mmolL^{-1}$
0.003	333.3333	0.0000172	58100	
0.002	500	0.0000147	68000	

Slope = 66.77 $A^{-1}molL^{-1}$

Intercept = 34921 A^{-1}

K_m = Slope/ Intercept

= 66.77/ 34921

= 0.00191 mol L^{-1}

= 1.91 $mmolL^{-1}$

Table A23. RSD calculation of K_m^{app} for GSH (Low conc.)

Concentration, $molL^{-1}$ x 10^{-3}	1/Concentration, $mol^{-1}L$ x 10^{2}	Current, A x 10^{-6}	RSD	1/Current, A^{-1} x 10^{4}	RSD
2	5.0	15.5	0.64%	6.45	0.62%
		15.6		6.41	
		15.4		6.49	
1	10	14.0	0.71%	7.14	0.42%
		14.1		7.09	
		14.1		7.09	
0.5	20	13.0	0.15%	7.69	1.45%
		13.4		7.46	
		13.2		7.57	

Appendix A

Table A23.1.

Current, Ax 10^{-6}	$\bar{X}$	di	di^2	Σdi^2	S	RSD
15.5	15.5	0.0	0.0	0.02	0.1	0.64%
15.6		0.1	0.01			
15.4		-0.1	0.01			

Table A23.2.

Current, Ax 10^{-6}	$\bar{X}$	di	di^2	Σdi^2	S	RSD
14.0	14.0	0.0	0.00	0.02	0.1	0.71%
14.1		0.1	0.01			
14.1		0.1	0.01			

Table A23.3.

Current, Ax 10^{-6}	$\bar{X}$	di	di^2	Σdi^2	S	RSD
13.0	13.2	- 0.02	0.0004	0.0008	0.02	0.15%
13.4		0.02	0.0004			
13.2		0.0	0.0			

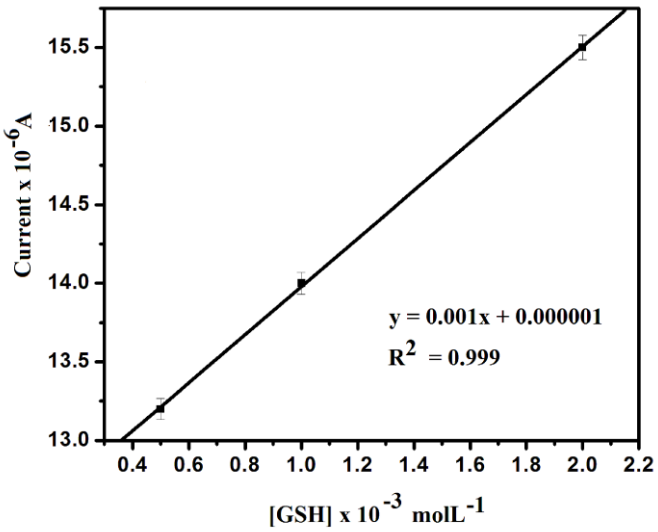

Figure A1.

R^2= 0.999. Sensitivity = Slope = 0.001 A/ M = 1 mA / M

Table A23.4.

1/Current, $A^{-1}x\ 10^4$	$\overline{X}$	di	di^2	Σdi^2	S	RSD
6.45	6.45	0.0	0.0	0.0032	0.04	0.62%
6.41		- 0.04	0.0016			
6.49		0.04	0.0016			

Table A23.5

1/Current, $A^{-1}x\ 10^4$	$\overline{X}$	di	di^2	Σdi^2	S	RSD
7.14	7.10	0.04	0.0016	0.0018	0.03	0.42%
7.09		-0.01	0.0001			
7.09		-0.01	0.0001			

Table A23.6

1/Current, $A^{-1} \times 10^4$	$\bar{X}$	di	di^2	Σdi^2	S	RSD
7.69	7.57	0.12	0.0144	0.0265	0.11	1.45%
7.46		0.11	0.0121			
7.57		0.0	0.0			

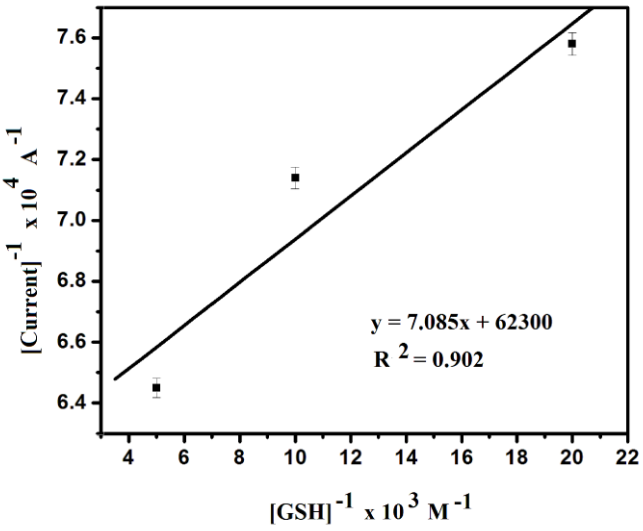

Figure A2.

R^2= 0.902; Slope/intercept = 7.085/62300 = 0.11 $mmolL^{-1}$

Table A24. RSD calculation of K_m^{app} for GSH (high conc.)

Concentration, $molL^{-1} \times 10^{-3}$	1/Concentration, $mol^{-1}L \times 10^2$	Current, A $\times 10^{-6}$	RSD	1/Current, $A^{-1} \times 10^4$	RSD
4	2.5	20.1	0.49%	4.97	0.40%
		20.3		4.92	

		20.2		4.95	
3	3.3	17.8	0.39%	5.61	0.17%
		17.9		5.58	
		17.9		5.58	
2	5.0	15.5	0.64%	6.45	0.62%
		15.6		6.41	
		15.4		6.49	

Table A24.1.

Current, Ax 10^{-6}	$\bar{X}$	di	di^2	Σdi^2	S	RSD
20.1	20.2	-0.1	0.01	0.02	0.1	0.49%
20.3		0.1	0.01			
20.2		0.0	0.0			

Table A24.2.

Current, Ax 10^{-6}	$\bar{X}$	di	di^2	Σdi^2	S	RSD
17.8	17.9	-0.1	0.01	0.01	0.07	0.39%
17.9		0.0	0.0			
17.9		0.0	0.0			

Table 24.3.

Current, Ax 10^{-6}	$\bar{X}$	di	di^2	Σdi^2	S	RSD
15.5	15.5	0.0	0.0	0.02	0.1	0.64%
15.6		0.1	0.01			
15.4		-0.1	0.01			

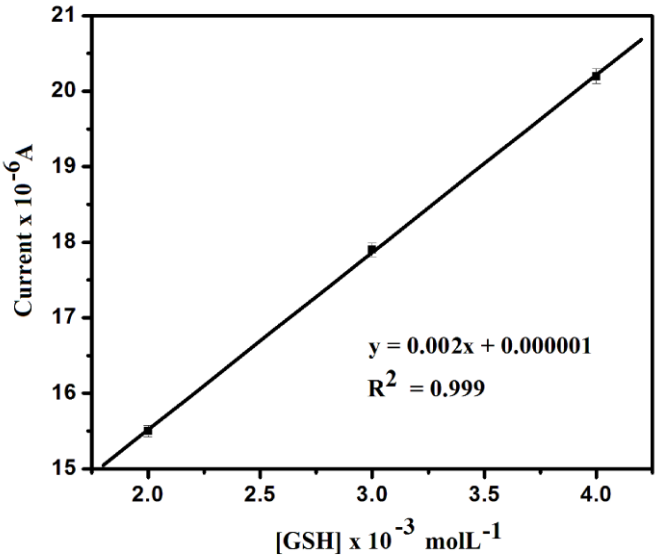

Figure A3.

R^2= 0.999, Sensitivity = Slope = 0.002 A/ M = 2 mA / M

Table 24.4.

1/Current, $A^{-1}x\ 10^4$	$\bar{X}$	di	di^2	Σdi^2	S	RSD
4.97	4.94	0.03	0.0009	0.0014	0.02	0.40%
4.92		-0.02	0.0004			
4.95		0.01	0.0001			

Table 24.5.

1/Current, A $^{-1}$x 10^4	$\bar{X}$	di	di^2	Σdi^2	S	RSD
5.61	5.59	0.02	0.0004	0.0006	0.01	0.17%
5.58		-0.01	0.0001			
5.58		-0.01	0.0001			

Table 24.6.

1/Current, A $^{-1}$x 10^4	$\bar{X}$	di	di^2	Σdi^2	S	RSD
6.45	6.45	0.0	0.0	0.0032	0.04	0.62%
6.41		- 0.04	0.0016			
6.49		0.04	0.0016			

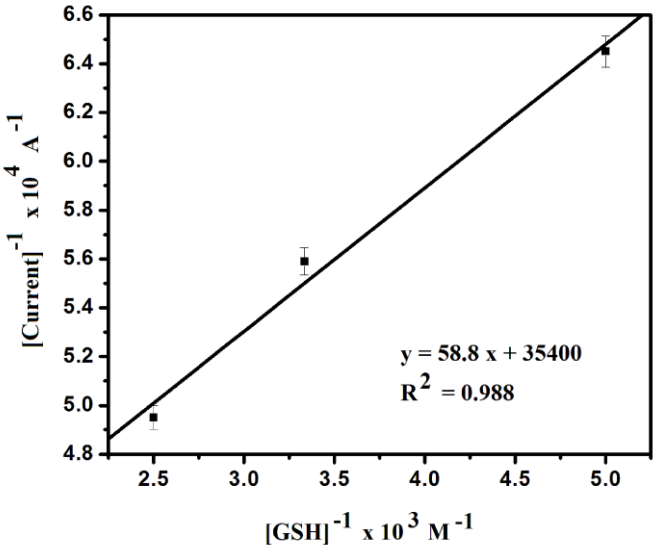

Figure A4.

R^2= 0.988; Slope/intercept = 58.8/35400 = 1.66 $mmolL^{-1}$

Table A25. RSD calculation of K_m^{app} for CDNB (Low conc)

Concentration, $molL^{-1}$ x 10^{-3}	1/Concentration, $mol^{-1}L$ x 10^2	Current, A x 10^{-6}	RSD	1/Current, A^{-1} x 10^4	RSD
2	5.0	14.9	0.68%	6.71	1.03%
		14.6		6.84	
		14.6		6.84	
1	10	13.2	0.75%	7.57	1.33%
		13.5		7.40	
		13.2		7.57	
0.5	20	12.5	0.80%	8.00	0.74%
		12.3		8.13	
		12.4		8.06	

Table A25.1.

Current, Ax 10^{-6}	$\bar{X}$	di	di^2	Σdi^2	S	RSD
14.9	14.7	0.2	0.004	0.024	0.1	0.68%
14.6		-0.1	0.01			
14.6		-0.1	0.01			

Table A25.2.

Current, Ax 10^{-6}	$\bar{X}$	di	di^2	Σdi^2	S	RSD
13.2	13.3	-0.1	0.01	0.06	0.1	0.75%
13.5		0.2	0.04			
13.2		-0.1	0.01			

Table A25.3.

Current, Ax 10^{-6}	$\bar{X}$	di	di^2	Σdi^2	S	RSD
12.5	12.4	0.1	0.01	0.02	0.1	0.80%
12.3		-0.1	0.01			
12.4		0.0	0.0			

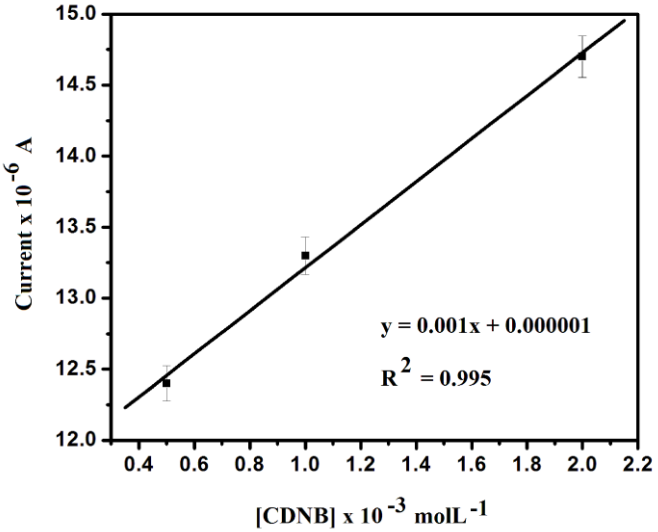

Figure A5.

R^2= 0.995, Sensitivity = Slope = 0.001 A/ M = 1 mA / M

Table A25.4.

1/Current, $A^{-1} \times 10^4$	$\bar{X}$	di	di^2	Σdi^2	S	RSD
6.71	6.79	-0.08	0.0064	0.0114	0.07	1.03%
6.84		0.05	0.0025			
6.84		0.05	0.0025			

Table A25.5.

1/Current, $A^{-1} \times 10^4$	$\bar{X}$	di	di^2	Σdi^2	S	RSD
7.57	7.51	0.06	0.0036	0.0193	0.09	1.33%
7.40		0.11	0.0121			
7.57		0.06	0.0036			

Table A25.6.

1/Current, $A^{-1} \times 10^4$	$\bar{X}$	di	di^2	Σdi^2	S	RSD
8.00	8.06	-0.06	0.0036	0.0085	0.06	0.74%
8.13		0.07	0.0049			
8.06		0.0	0.0			

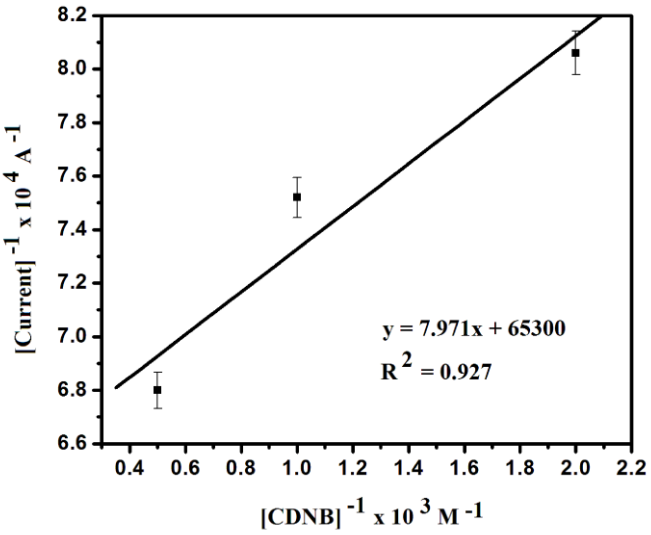

Figure A6.

R^2= 0.927; Slope/intercept = 7.971/65300 = 0.12 mmolL^{-1}

Table A26. RSD calculation of K_m^{app} for CDNB (high conc)

Concentration, molL^{-1} x 10^{-3}	1/Concentration , mol^{-1}L x 10^2	Current, A x 10^{-6}	RSD	1/Current, A^{-1} x 10^4	RSD
4	2.5	19.5	0.51%	5.12	0.39%
		19.6		5.10	
		19.7		5.07	
3	3.3	17.4	0.58%	5.74	0.86%
		17.1		5.84	
		17.3		5.78	
2	5.0	14.9	0.68%	6.71	1.03%
		14.6		6.84	
		14.6		6.84	

Appendix A

Table A26.1.

Current, Ax 10^{-6}	$\bar{X}$	di	di^2	Σdi^2	S	RSD
19.5	19.6	-0.1	0.01	0.02	0.1	0.51%
19.6		0.0	0.0			
19.7		0.1	0.01			

Table A26.2.

Current, Ax 10^{-6}	$\bar{X}$	di	di^2	Σdi^2	S	RSD
17.4	17.2	0.2	0.04	0.06	0.1	0.58%
17.1		-0.1	0.01			
17.3		0.1	0.01			

Table A26.3.

Current, Ax 10^{-6}	$\bar{X}$	di	di^2	Σdi^2	S	RSD
14.9	14.7	0.2	0.004	0.024	0.1	0.68%
14.6		-0.1	0.01			
14.6		-0.1	0.01			

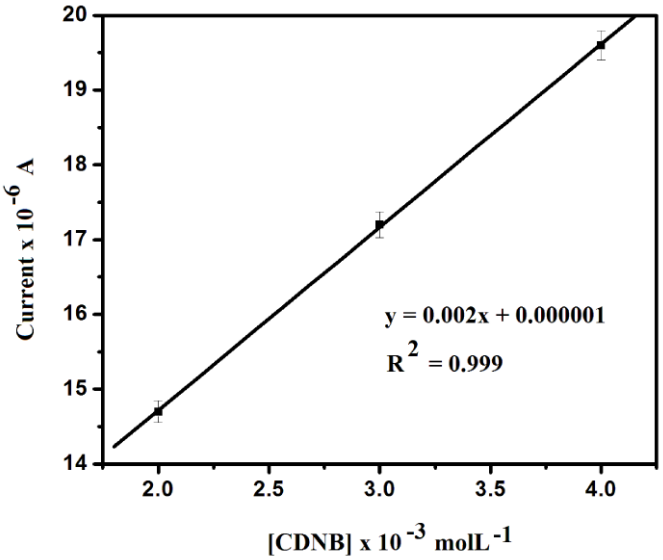

Figure A7.

R^2= 0.999, Sensitivity = Slope = 0.002 A/ M = 2 mA / M

Table A26.4.

1/Current, A $^{-1}$x 10^4	$\overline{X}$	di	di^2	Σdi^2	S	RSD
5.12	5.10	0.02	0.0004	0.0013	0.02	0.39%
5.10		0.0	0.0			
5.07		-0.03	0.0009			

Table A26.5.

1/Current, A $^{-1}$x 10^4	$\overline{X}$	di	di^2	Σdi^2	S	RSD
5.74	5.78	-0.04	0.0016	0.0052	0.05	0.86%
5.84		0.06	0.0036			
5.78		0.0	0.0			

Table A26.6.

1/Current, $A^{-1} \times 10^4$	$\bar{X}$	di	di^2	Σdi^2	S	RSD
6.71	6.79	-0.08	0.0064	0.0114	0.07	1.03%
6.84		0.05	0.0025			
6.84		0.05	0.0025			

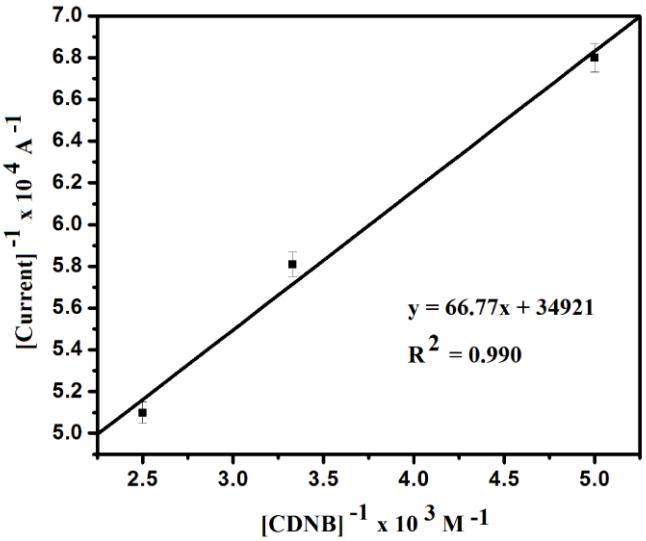

Figure A8.

R^2= 0.990; Slope/intercept = 66.77/34921 = 1.91 $mmolL^{-1}$

Table A27. RSD calculation for method validation study (para 3.4.4.2)

Recovery (%)	$\bar{X}$	di	di^2	Σdi^2	S	RSD
95.16	96.05	-0.89	0.79	2.32	1.52	1.58%
95.74		-0.31	0.09			
97.25		1.2	1.44			

APPENDIX A(II)

Calculations from chapter 4:

Table A28. Peak potential value of peak A (Figure 4.2)

Potential (V)	$\bar{X}$	di	di^2	Σdi^2	S	RSD
0.31	0.30	0.01	0.0001	0.0001	0.01	3.33%
0.30		0.0	0.0			
0.30		0.0	0.0			

Table A29. Peak potential value of peak B (Figure 4.2)

Potential (V)	$\bar{X}$	di	di^2	Σdi^2	S	RSD
0.60	0.60	0.0	0.0	0.0001	0.01	1.66%
0.61		0.01	0.0001			
0.60		0.0	0.01			

Table A30. Peak potential value of peak C (Figure 4.2)

Potential (V)	$\bar{X}$	di	di^2	Σdi^2	S	RSD
0.054	0.054	0.0	0.0	0.000002	0.0014	2.59%
0.053		-0.001	0.000001			
0.055		0.001	0.000001			

Table A31. Peak potential value of peak D (Figure 4.2)

Potential (V)	$\bar{X}$	di	di^2	Σdi^2	S	RSD
0.100	0.100	0.0	0.0	0.000001	0.001	1.0%
0.101		0.001	0.000001			
0.100		0.0	0.0			

Table A32. Method validation study for Fenobucarb (para 4.4.6)

Recovery (%)	$\bar{X}$	di	di^2	Σdi^2	S	RSD
95.5	97.1	1.6	2.56	7.22	2.68	2.76%
99.2		2.1	4.41			
96.6		0.5	0.25			

Table A33. Method validation study for Temephos (para 4.4.6)

Recovery (%)	$\bar{X}$	di	di^2	Σdi^2	S	RSD
91.3	90.1	1.2	1.44	2.89	1.7	1.88%
88.9		-1.2	1.44			
90.2		0.1	0.01			

Table A34. Method validation study for Dimethoate (para 4.4.6)

Recovery (%)	$\bar{X}$	di	di^2	Σdi^2	S	RSD
80.5	83.6	-3.1	9.61	16.22	4.02	4.80%
84.2		0.6	0.36			
86.1		2.5	6.25			

APPENDIX A(III)

Calculations from chapter 5

Table A35. Peak potential value of peak A (Figure 5.5)

Potential (V)	$\bar{X}$	di	di^2	Σdi^2	S	RSD
0.30	0.30	0.0	0.0	0.0001	0.01	3.33%
0.31		0.01	0.0001			
0.30		0.0	0.0			

Table A36. Peak potential value of peak B (Figure 5.5)

Potential (V)	$\bar{X}$	di	di^2	Σdi^2	S	RSD
0.60	0.60	0.0	0.0	0.0002	0.01	1.66%
0.61		0.01	0.0001			
0.59		-0.01	0.0001			

Table A37. Peak potential value of peak C (Figure 5.5)

Potential (V)	$\bar{X}$	di	di^2	Σdi^2	S	RSD
0.051	0.052	- 0.001	0.000001	0.000005	0.002	3.84%
0.052		0.0	0.0			
0.054		0.002	0.000004			

Table A38. Peak potential value of peak D (Figure 5.5)

Potential (V)	$\bar{X}$	di	di^2	Σdi^2	S	RSD
0.101	0.10	0.0	0.0	0.0001	0.01	1.0%
0.102		0.0	0.0			
0.099		-0.01	0.0001			

Calculation of saturated substrate concentration, apparent Michaelis-Menten constant and substrate specificity (para 5.4.5.1)

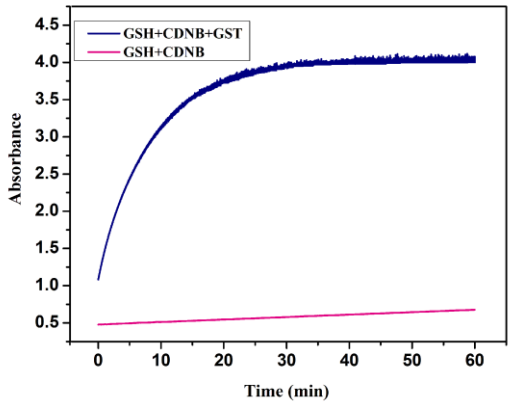

Figure A9. UV-Visible spectroscopic study of both GST catalyzed and uncatalyzed reaction of GSH (2 mmol) and CDNB (2mmol) prepared in P.B and methanol (50%).

Table A39. Calculations for GSH:

[S]	Current
0.05	5.25
0.5	11.18
0.75	13.69
1	14.19
2	14.73
3	14.95
4	15.05

Rate (R) = Saturated substrate concentration / maximum current = 4 mmol/15.05 μA= 0.26 mmolμA^{-1} =R

V =dx/dt = (R x current corresponding to each point)/time (sec)

V = (0.26 mmolμA^{-1} x 5.25 μA)/20 sec = 0.068 mmolsec^{-1}

(0.26 x 11.18)/20 = 0.145

(0.26 x 13.69) / 20 = 0.177

(0.26 x 14.19)/ 20 = 0.184

(0.26 x 14.73) /20 = 0.191

(0.26 x 14.95)/20 = 0.194

(0.26 x 15.05)/ 20 = 0.195

Table A40.

[S]	V
0.05	0.068
0.5	0.145
0.75	0.177
1	0.184
2	0.191
3	0.194
4	0.195

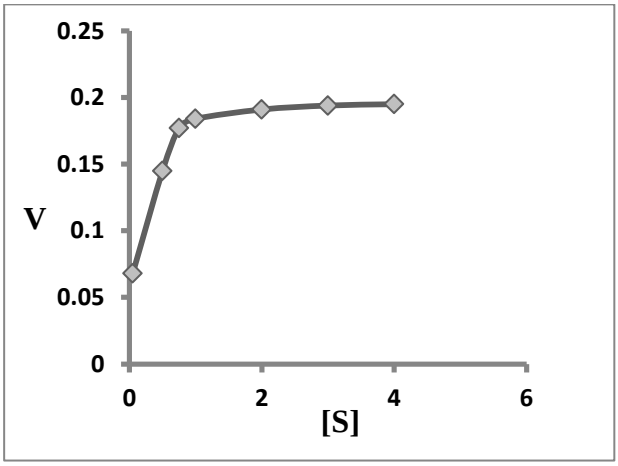

Figure A10.

Table A41. For Lineweaver-Burk Plot:

Conc. mmol	V mmol/sec	1/Conc.	1/V	Arranging the values in ascending order	
0.05	0.068	20	14.70588	1.33333	5.649718
0.5	0.145	2	6.896552	2	6.896552
0.75	0.177	1.33333	5.649718	20	14.70588

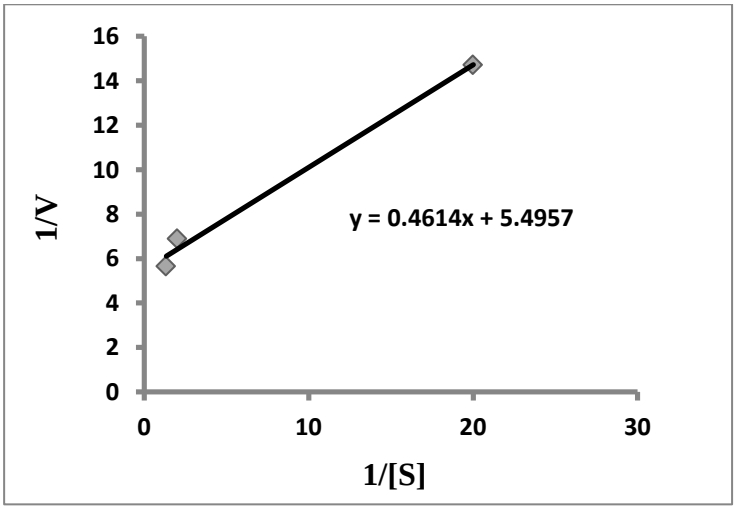

Figure A11.

K_m = 0.461/5.495=0.0838

V_{max} = 0.0838/0.461 = 0.1817 mmol/s

[ET] = (ΔA x 3 x t') /9.6 x t x 10^3

= (0.5 x 3 x 300) /9.6x 1200x 10^3

= 450/ 11520000 = 0.000039 mmol

t' =5min = 300sec

t = 20 min = 1200sec

Determination of K_{cat} :

K_{cat}= V_{max} /[ET]

=0.1817 $mmols^{-1}$/0.000039 mmol = 4658.97 s^{-1}

K_{cat}/K_m = 4658.97/0.1817 = 25641.00

*(9.6=Millimolar extinction coefficient of Glutathione-1-Chloro-2,4-Dinitrobenzene conjugate at 340 nm

3.0 = Total volume (in mL) of assay

Table A42. Calculations for CDNB:

[S]	Current
0.05	3.4
0.5	9.51
0.75	13.46
1	14.7
2	18.02
3	20.15
4	21.21

Saturated substrate concentration / max current = 4 mmol/21.21 μA= 0.18 mmolμA^{-1} =R

V =dx/dt = (R x current corresponding to each point)/time(sec)

V = (0.18 mmolμA^{-1} x 3.5 μA)/20 sec = 0.0315 mmolsec^{-1}

(0.18 x 9.51)/20 = 0.0855

(0.18 x 13.46)/20 = 0.1211

(0.18 x 14.7)/ 20= 0.1323

(0.18x 18.02)/ 20 =0.1621

(0.18 x 20.15)/ 20= 0.1813

(0.18x 21.21)/20= 0.1908

Table A43.

[S]	V
0.05	0.0315
0.5	0.0855
0.75	0.1211
1	0.1323
2	0.1621
3	0.1813
4	0.1908

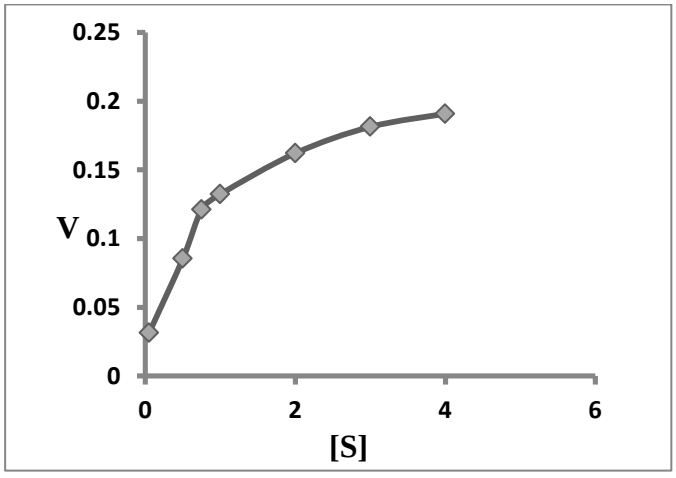

Figure A12.

Table A44. For Lineweaver-Burk Plot:

Conc. mmol	V mmol/sec	1/Conc.	1/V	Arranging the values in ascending order	
0.05	0.0315	20	31.746	1.33333	8.25764
0.5	0.0855	2	11.6959	2	11.6959
0.75	0.1211	1.33333	8.25764	20	31.746

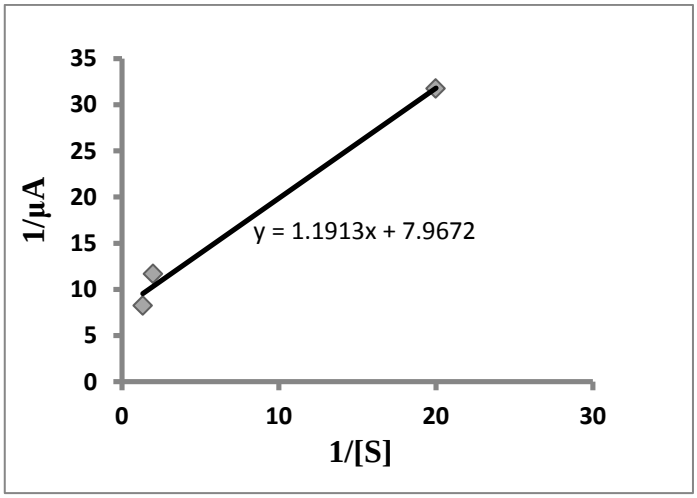

Figure A13.

K_m = 1.191/7.967 = 0.1494

V_{max} = 0.0838/0.461 = 0.1254 mmol/s

[ET] = (ΔA x 3 x t') /9.6 x tx 10^3

= (0.5 x 3 x 300) /9.6x 1200x 10^3

= (450/11520000) mmol

= 0.000039

t' =5 min=300 sec

t = 20 min = 1200 sec

$$K_{cat} = V_{max} / [ET]$$

$$= 0.1254 \text{ mmols}^{-1}/0.000039 \text{ mmol} = 3215.38 \text{ s}^{-1}$$

$$K_{cat}/K_m = 21521.95$$

Table A45. Precision measurement, interassay (para 5.4.5.6)

Current, Ax 10 $^{-6}$	$\bar{X}$	di	di^2	Σdi^2	S	RSD
27.7	28.4	-0.6	0.36	2.67	1.63	5.73%
28.3		-0.1	0.01			
27.8		-0.6	0.36			
29.5		1.1	1.21			
29.2		0.8	0.64			
28.1		-0.3	0.09			

Table A46. Precision measurement, intra state (para 5.4.5.6)

Current, Ax 10 $^{-6}$	$\bar{X}$	di	di^2	Σdi^2	S	RSD
28.4	28.3	0.1	0.01	0.04	0.2	0.70%
28.4		0.1	0.01			
28.4		0.1	0.01			
28.3		0.0	0.0			
28.3		0.0	0.0			

28.3		0.0	0.0			
28.3		0.0	0.0			
28.2		-0.1	0.01			

APPENDIX A(IV)

Calculations from Chapter 6:

Calculation of K_m and V_{max} for GSH-CDNB-GST (without inhibitor):

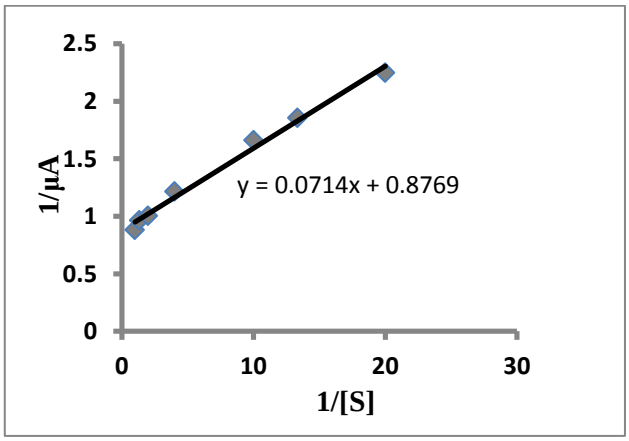

Figure A14.

K_m = slope/intercept= 0.071/0.876 = 0.08

V_{max}= K_m/slope = 0.08/0.071 =1.14

K_i calculation for Fenobucarb:

K_m 60ppb= 0.219/0.875 = 0.2502 V_{max} = 0.2502/0.219 = 1.14

K_m 50ppb= 0.135/0.872 = 0.1548 V_{max} = 0.1548/0.135= 1.14

K_m 40ppb = 0.083/0.875= 0.0948 V_{max} = 0.0948/0.083= 1.14

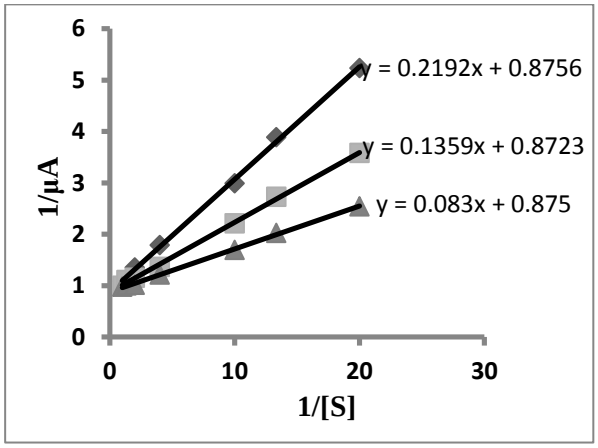

Figure A 15.

K_m (inhibitor) / K_m (without inhibitor) vs [I] = Slope = $1/K_i$

K_m (without inhibitor) = 0.08

$K_{60\ ppb}/K_m = 0.2502/0.08 = 3.12$

$K_{50\ ppb}/K_m = 0.1548/0.08 = 1.93$

$K_{40ppb}/K_m = 0.0948/\ 0.08 = 1.18$

Table A47.

Concentration of fenobucarb	K_m value for each concentration
60 ppb	3.12
50 ppb	1.93
40 ppb	1.18

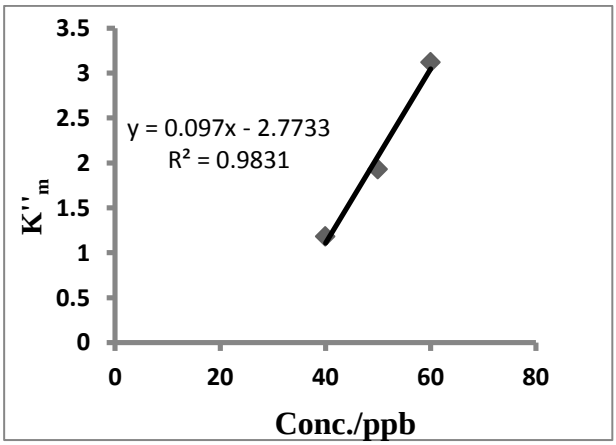

Figure A16

Slope = $1/K_i = 0.097$

Therefore, $K_i = 1/0.097 = 10.30$

K_i calculation for DDT:

K_m 150 ppb = 0.289/0.871 = 0.3318

V_{max} 150 ppb = 0.3318/0.289 = 1.1481

K_m 120 ppb = 0.202/0.870 = 0.2321

V_{max} 120 ppb = 0.2321/0.202 = 1.1494

K_m 100 ppb = 0.123/0.87 = 0.1413

V_{max} 100 ppb = 0.1413/0.123= 1.1494

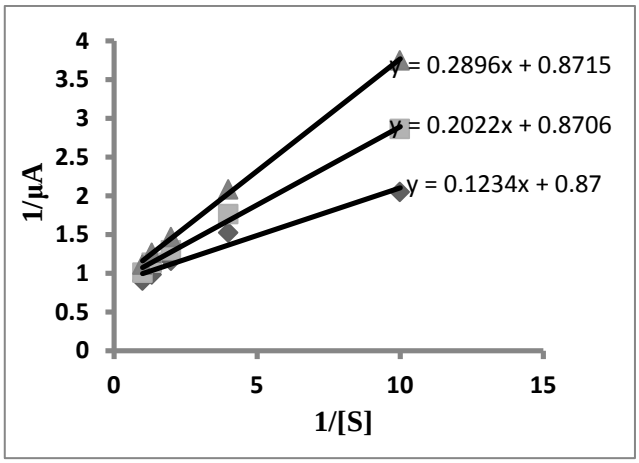

Figure A17.

$K^{//}m$ (inhibitor) / K_m (without inhibitor) vs [I] = Slope = $1/K_i$

K_m (without inhibitor) = 0.08

K_m 150 ppb/K_m = 0.3318/0.08 = 4.1475

K_m 120 ppb/K_m = 0.2321/0.08= 2.9012

K_m 100 ppb/K_m = 0.1413/0.08= 1.7662

Table A48.

Concentration of DDT	K_m value for each concentration
150 ppb	4.1475
120 ppb	2.9012
100 ppb	1.7662

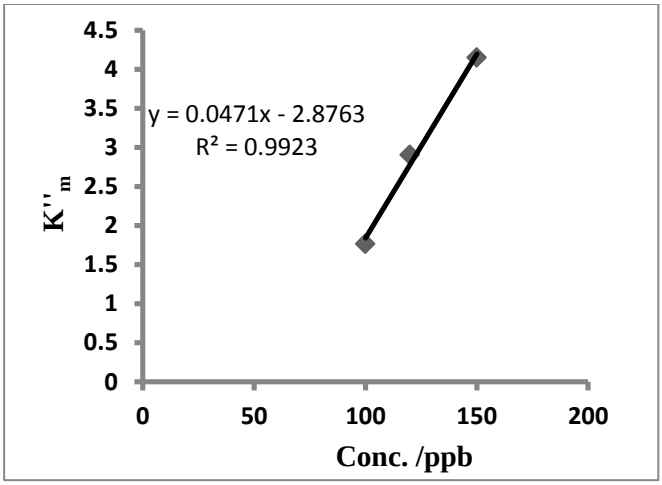

Figure A18.

Slope = $1/K_i = 0.047$

Therefore, $K_i = 1/0.047 = 21.27$

<u>K_i calculation for Cypermethrin:</u>

K_m 60 ppb = 0.246/0.874 = 0.2814

V_{max} 60 ppb = 0.2814/0.246= 1.14

K_m 50 ppb = 0.139/0.871 = 0.1595

V_{max} 50 ppb = 0.1595/0.139 = 1.14

K_m 40 ppb = 0.057/0.87 = 0.0655

V_{max} 40 ppb = 0.0655/0.057 = 1.14

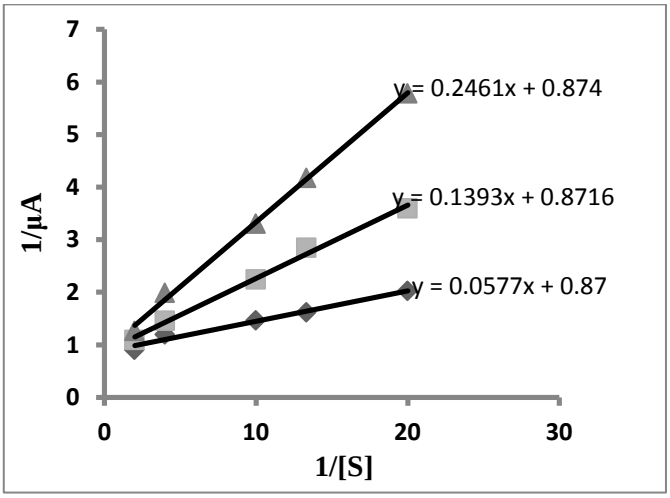

Figure A19.

K''_m (inhibitor) / K_m (without inhibitor) vs [I] = Slope = $1/K_i$

K_m (without inhibitor) = 0.08

K_m 60 ppb/K_m = 0.2814/0.08 = 3.5175

K_m 120 ppb/K_m = 0.1595/0.08 = 1.9937

K_m 100 ppb/K_m = 0.0655/0.08 = 0.8187

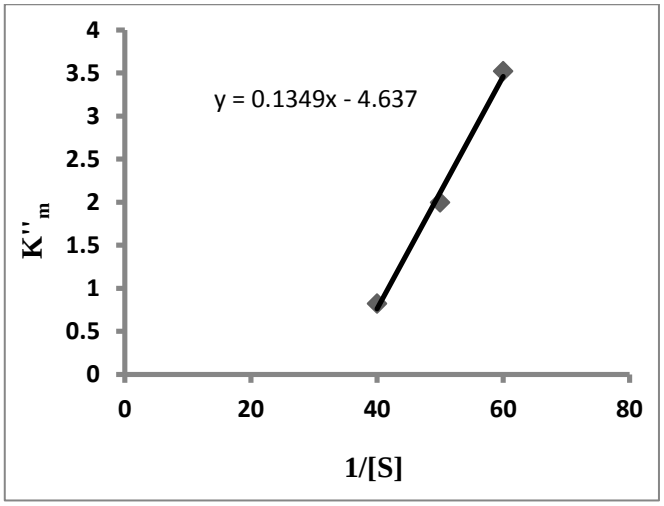

Figure A20.

Slope = $1/K_i = 0.134$

Therefore, $K_i = 1/0.134 = 7.46$

K_i calculation for Temephos:

K_m 60 ppb= 0.104/ 1.278 = 0.0813 V_{max}= 0.0813/0.104= 0.7817

K_m 50ppb = 0.090/1.094 = 0.0822 V_{max} = 0.0822/0.090 = 0.9133

K_m 40 ppb= 0.077/0.948 = 0.0812 V_{max} = 0.0812/0.077 = 1.054

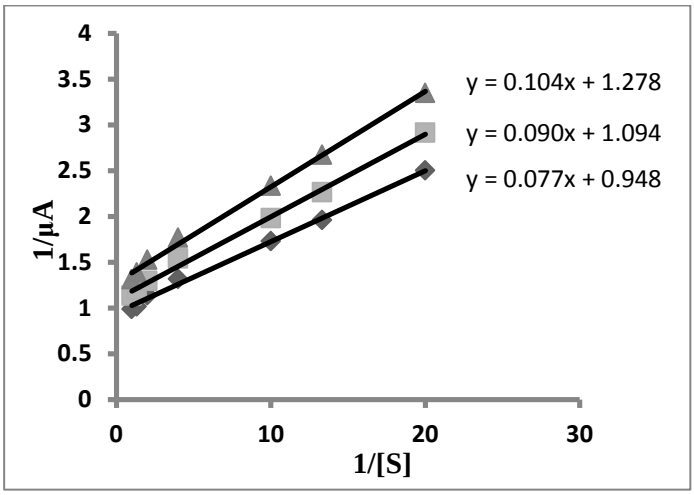

Figure A21.

Table A49.

Concentration of temephos	1/ V_{max} value for each concentration
60 ppb	1.278
50 ppb	1.094
40 ppb	0.948

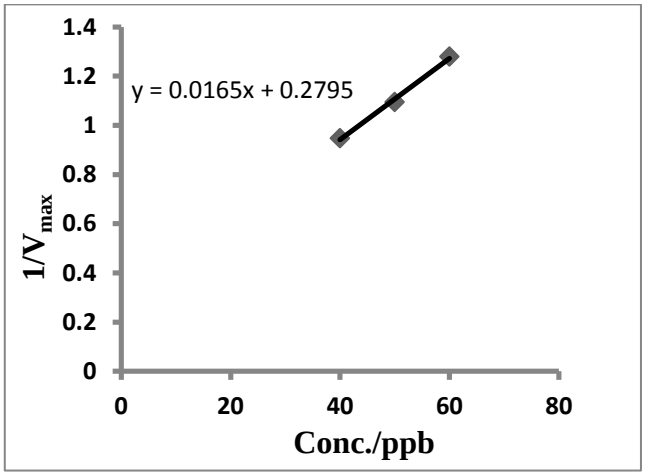

Figure A22.

K_i = 1/(slope x V_{max}) = 1/(0.016 x 1.14) = 54.82

[V_{max} (without inhibitor) = 1.14]

<u>K_i calculation forEthion:</u>

K_m 200 ppb = 0.274/3.246= 0.08 V_{max} 200 ppb= 0.08/0.274 = 0.3080

K_m 150 ppb = 0.195/2.284 = 0.08 V_{max} 150 ppb = 0.08/0.195 = 0.4102

K_m 100 ppb =0.127 /1.569 = 0.08 V_{max} 100 ppb = 0.08/0.127 = 0.6299

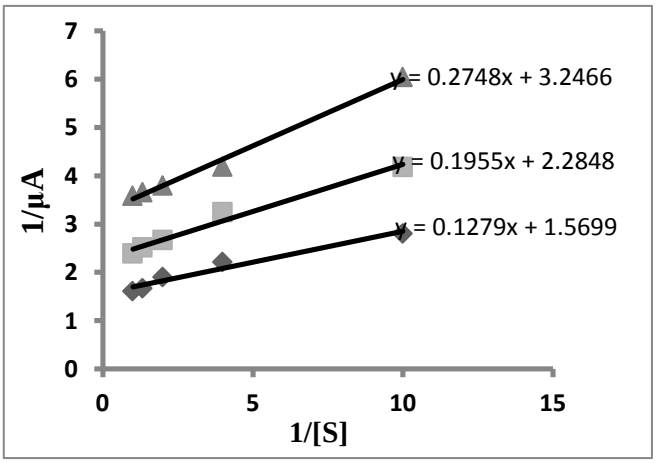

Figure A23.

Table A50.

Concentration of ethion	1/ V_{max} value for each concentration
200 ppb	3.2467
150 ppb	2.4378
100 ppb	1.5875

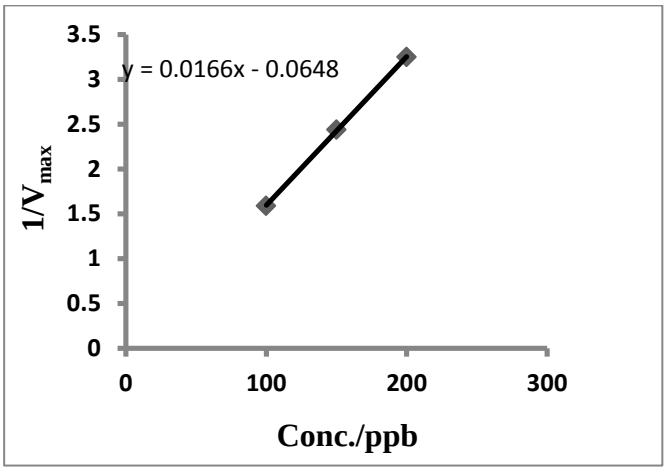

Figure A24.

K_i = 1/(slope x V_{max}) = 1/(0.016 x 1.14) = 54.82

[V_{max} (without inhibitor) = 1.14]

<u>K_i calculation for chlorpyrifos:</u>

K_m 200 ppb = 0.065/0.763 = 0.0851 V_{max} 200 ppb = 0.0851/0.065 = 1.3106

K_m 150 ppb = 0.049/0.569 = 0.0861 V_{max} 150 ppb = 0.0861/0.049 = 1.7571

K_m 100 ppb = 0.030/0.364 = 0.0824 V_{max} 100 ppb = 0.0824/0.030 = 2.7466

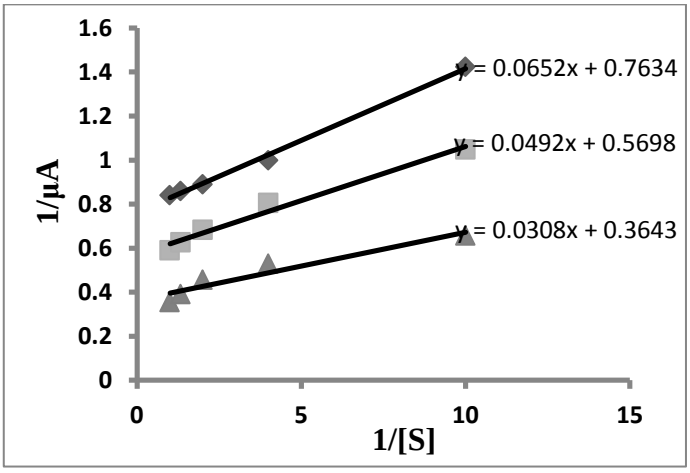

Figure A25.

Table A51.

Concentration of chlorpyrifos	1/ V_{max} value for each concentration
200 ppb	0.763
150 ppb	0.569
100 ppb	0.364

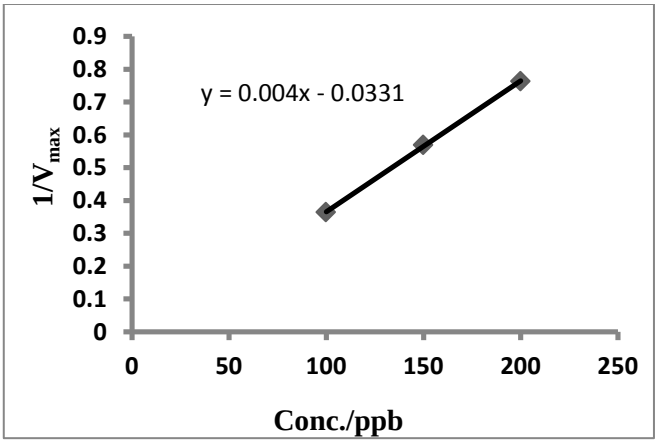

Figure A26.

K_i = 1/(slope x V_{max}) = 1/(0.004 x 1.14) = 219.29

[V_{max} (without inhibitor) = 1.14]

K_i calculation for Dimethoate:

K_m 60ppb = 0.139/0.231= 0.6017 Vmax 60 ppb= 0.6017/0.139 = 4.32

K_m 50ppb= 0.1/0.42 = 0.2380 Vmax 50 ppb = 0.2380/0.1 = 2.38

K_m 40ppb = 0.071/0.564 = 0.1258 Vmax 40 ppb = 0.1258/0.071 = 1.77

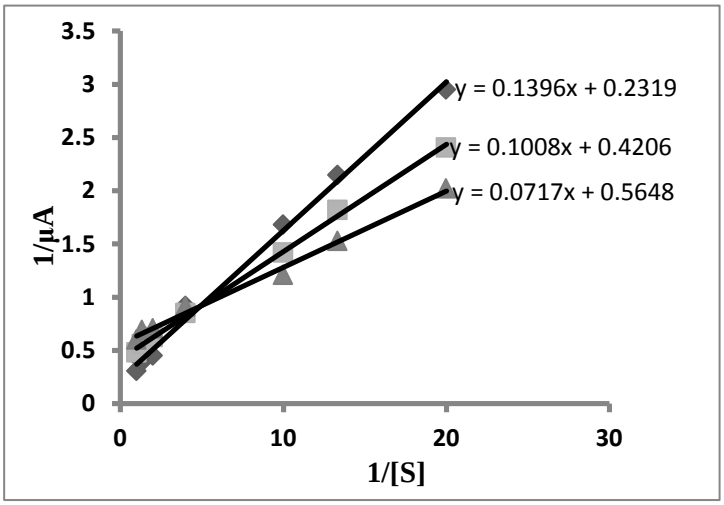

Figure A27.

K_i calculation for Dinocap:

K_m 100ppb = 0.345/0.177 = 1.9491 V_{max} 100ppb = 1.949/0.345 = 5.649

K_m 150 ppb = 0.271/0.372 = 0.728 V_{max} 150 ppb = 0.728/0.271 = 2.686

K_m 200 ppb = 0.208/0.484 = 0.4297 V_{max} 200 ppb = 0.429/0.208 = 2.062

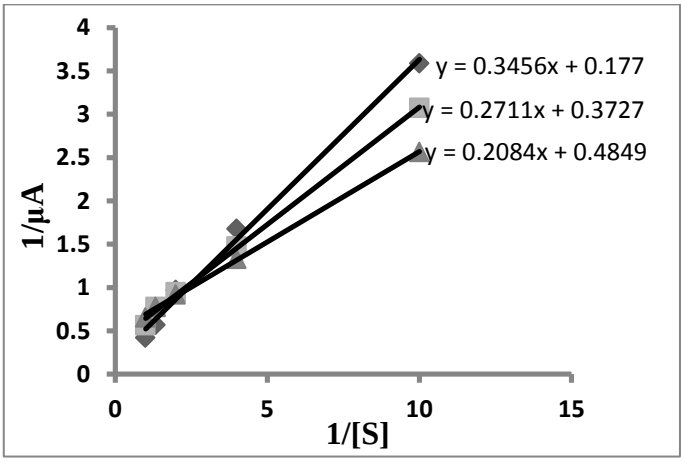

Figure A28.

K_i calculation for carbendazim:

K_m 50 ppb = 0.455/0.645 = 0.7054

V_{max} 50 ppb = 0.7054/0.455 = 1.5503

K_m 40 ppb = 0.236/0.991 = 0.2381

V_{max} 40 ppb = 0.2381/0.236 = 1.008

K_m 30 ppb = 0.100/1.159 = 0.0862

V_{max} 30 ppb = 0.0862/0.100 = 0.862

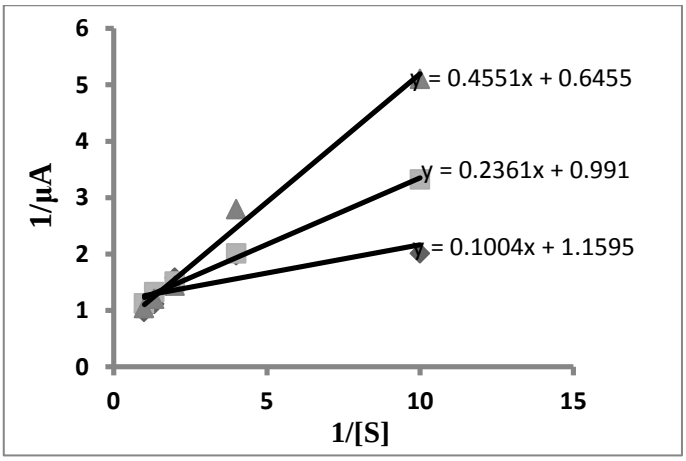

Figure A29.

APPENDIX A(V)

Table for Chapter 7:

Table A52: List of agricultural commodities to which the present method can be applied for the risk management of the selected pesticides.

Pesticide	LOD (ppb)	LOD (mg/kg)	MRL/ERL (mg/kg)	Application to different food commodities	Regulation as per EU database
DDT	40	0.04	0.05 (ERL)	Applicable to all	Reg.(EC) No 149/2008
Dinocap	50	0.05	0.02- 0.1	Teas, coffee beans, cereals, oilseeds, pulses, spices	Reg.(EU) No 1127/2014
Ethion	100	0.1	0.01-5	Teas, Spices(seeds, fruits, roots)	Reg.(Eu) No 310/2011
Chlorpyrifos	60	0.06	0.01-5	Citrus fruits, bananas, onions, teas, spices (seeds, fruits)	Reg. (EU) 2018/686
Carbendazim	2	0.002	0.1-2	Applicable to all	Reg. (EU) No 559/2011
Cypermethrin	2	0.002	0.05-3	Applicable to all	Reg. (EU) No 396/2005

Publications:

- **Borah, H.**, Dutta, R. R., Gogoi, S., and Puzari, P. Influence of methanol, ethanol and cypermethrin on the Glutathione S-tranferase catalyzed reaction of Glutathione with 1-chloro-2,4-dinitrobenzene: A method for detection and quantification of cypermethrin. *Electrochimica Acta,* 205:198-206, 2016.

- **Borah, H.**, Dutta, R. R., Gogoi, S., Medhi, T., and Puzari, P. Glutathione S-transferase catalyzed reaction of glutathione for electrochemical biosensing of temephos, fenobucarb and dimethoate. *Analytical Methods,* 9:4044-4051, 2017.

- **Borah, H.**, Gogoi, S., Kalita, S., and Puzari, P. A broad spectrum amperometric pesticide biosensor based on Glutathione S-transferase immobilized on graphene oxide-gelatin matrix. *Journal of Electroanalytical Chemistry*, 828:116-123, 2018.

- Gogoi, S., **Borah, H.**, Dutta, R. R., and Puzari, P. Evaluation of Diffusion Coefficient of Thiocholine in Enzyme-Loaded Polypyrrole Composite Film through Different Methods and Electrode Polarization. *The Journal of Physical Chemistry B*, 119:4749-4757, 2015.

- Dutta, R. R., **Borah, H.**, Gogoi, S., and Puzari, P. Recent advances in AChE based Electrochemical Biosensors for Pesticide Detection. *Biochemistry Research International* (*submitted).*

- Dutta, R.R., **Borah, H.**, Gogoi, S., and Puzari, P. Low potential thiocholine oxidation on polypyrrole surface and application to organophosphate detection (*submitted).*

Patent:

- "Enhancement of stability of acetylcholinesterase in ethyl acetate through the use of Lipase and L-Serine and hence a method for pesticide biosensing in QuEChERS extract" Application No: 201631008813 A.

Book Chapter

- **Borah, H.**, Dutta, R. R., Gogoi, S., and Puzari, P. Electrochemical biosensing of pesticide residue in produce using Glutathione-S-transferase catalyzed

detoxification reaction. In *Trends and Innovations in Food processing Technology; prospects and challenges (TIFPT 2017)* (*submitted).*

Conference Proceddings:

- **Borah, H.** and Puzari, P. A Simple and Sensitive Electrochemical Biosensor Employing Glutathione S-transferase Enzyme for Detection of Organophosphate and Organocabamate Pesticide. In "*National Seminar on Recent Developments in Chemistry*" page 33, Saint Mary's College, Laitumkhrah, Shillong, Meghalaya, Excel India Publishers, New Delhi, ISBN: 978-93-86724-66-3, 2018.

Conference/Seminar/Workshop attended:

- **Poster presentation** in "International symposium on polymer science and technology" at IACS, Kolkata, India, 23rd-26th January 2015.
- **Poster presentation** in "National conference on Contemporary developments in Chemical sciences" at Tezpur University, India, 23rd-24th November, 2015.
- **Poster presentation** in "104th Indian Science Congress" at S.V. University, Tirupati, India, 3rd-7th January, 2017.
- **Oral presentation** in " National seminar on Recent Developments in Chemistry" at Saint Marry's College, Shillong, India, 12th-13th July, 2017.
- **Poster presentation** in **"**International conference on Emerging trends in Chemical Sciences" at Dibrugarh University, Assam, India, 26th-28th February, 2018.
- **Poster presentation** in "International Conference on Advancement in Science & Technology (ICAST- 2018)" at Visva-Bharati University, Santiniketan, West Bengal, India, 3rd – 4th September, 2018.
- **Workshop on** "Fluoride Nilogon" at Dengaon, Karbi Anglong, 25th March, 2017 by Department of Chemical Sciences, Tezpur University.
- **Workshop on** "Emerging Trends in Chemical Sciences" (Science Academies lecture), 11-13th November, 2016 at Department of Chemical Sciences, Tezpur University.

Electrochimica Acta 205 (2016) 198–206

Contents lists available at ScienceDirect

Electrochimica Acta

journal homepage: www.elsevier.com/locate/electacta

Influence of methanol, ethanol and cypermethrin on the Glutathione S-tranferase catalyzed reaction of Glutathione with 1-chloro-2,4-dinitrobenzene: A method for detection and quantification of cypermethrin

Himadri Borah, Rekha Rani Dutta, Sudarsan Gogoi, Panchanan Puzari*

Department of Chemical Sciences, Tezpur University, Tezpur, Assam 784028, India

ARTICLE INFO

Article history:
Received 16 December 2015
Received in revised form 28 March 2016
Accepted 31 March 2016
Available online 14 April 2016

Keywords:
Glutathione S-transferase
pesticide tolerance
glutathione
cypermethrin
phase II metabolism

ABSTRACT

This article describes application of normal mediatorless cyclic voltammetry and UV-visible spectroscopy to study the Glutathione S-tranferase (GST) catalyzed reaction of reduced glutathione(GSH) with 1-chloro-2,4-dinitrobenzene(CDNB) in two solvents methanol and ethanol, and influence of pyrethroid cypermethrin on it. The course of the reaction between CDNB and GSH in presence of GST differs in the two solvents, viz., methanol and ethanol. Unlike the case when ethanol was used as the solvent, in methanol GSH got transformed to an electro active state under the influence of electrode polarization. This electro active intermediate undergoes oxidation at 0.3 V, sufficiently stable (more than two hours) and reacts with CDNB to form UV active but electro inactive final product. The same electro active intermediate is also formed by non-electrochemical process in presence of CDNB in methanol and the formation is catalyzed by GST. The said reaction is quantitatively affected by cypemethrin. A 25 ppb cypermethrin solution can suppress completely the cyclic voltammetric peak as well as the UVpeak obtained from a 1:1 millimolar mixture of GSH and CDNB in presence of 20 μL (0.02 mg) of GST. Based on this, an electrochemical method for quantification of cypermethrin has been proposed that can detect cypermethrin down to 2 ppb.The work has opened up new possibilities for electrochemical study of detoxification processes carried out by GSH.

1. Introduction

Glutathione S-transferases (GSTs; EC 2.5.1.18) are a multigenic family of cytosolic proteins with multifunctional biological roles, widely distributed throughout the body and found in the liver, kidney, brain, pancreas, testis, heart, lung, small intestine, skeletal muscles, prostate and spleen [1]. The important biological function of GSTs is their catalytic action in detoxification reaction [2]. Over expressions of GST during phase II metabolism or the drug resistance associated with anticancer therapies of human [3,4] and the resistance acquired by certain insects while getting exposed to pesticides [5–7] are the consequence of the detoxification mechanism involving GST. GST catalyzes the formation of thioether conjugates between the endogenous tripeptide glutathione (GSH) and xenobiotic compounds, the major detoxification pathway in insects and human. This detoxification process sometimes creates problem when a drug is considered as a toxicant by our biological system. Overexpression is resulted in which the excessive increase of the GST level is seen. This is observed most of the time during cancer treatment. A primary cause of cancer treatment failure is an acquired or intrinsic resistance to anticancer therapies. Chemo-therapeutic –resistant tumor cell lines have been shown to overexpress GST isozymes. This overexpression leads to an accelerated detoxification of drug substrates and thus an acquired resistance [1]. Based on this, the specific variety of Glutathione S-transferase, GST-P, is used as a marker protein during treatment of many cancers (ovarian, breast, liver, pancreas, colon, lymphomas and non-small cell lung) and high levels are linked to drug resistance even when the selected drug is not a substrate [4].

In insects increased levels of GSTs are observed when they are exposed to organochlorine, organophosphate and pyretrhoid pesticides [5–8]. Thus *in-vitro* study of the GST catalyzed reaction is important not only for development of protocols for quantification of those pesticides but also to understand the

* Corresponding author. Tel.: +91 3712 267007/8/9 + 5061; fax: +91 3712 267005/6.
E-mail address: pancha@tezu.ernet.in (P. Puzari).

http://dx.doi.org/10.1016/j.electacta.2016.03.199
0013-4686/

molecular basis of insecticide resistance that could be an important step in developing strategies to mitigate the resistance problem.

The most commonly applied substrate for *in-vitro* study of the GST catalyzed detoxification reaction of GSH is CDNB. Both spectrophotometric [9] and electrochemical methods have been applied for kinetic and mechanistic study of the reaction and also to quantify pesticides [10]. Compared to the spectroscopic methods, applications of electrochemical methods are not much in literature. Among the electrochemical methods two are commonly applied for the purpose. The first type involves the use of special techniques such as differential pulse voltammetry (DPV) [11] and the second type is the mediator based cyclic voltammetry [12]. To our knowledge, common electrochemical technique like the cyclic voltammetry (CV) technique has not been applied for the purpose perhaps because of the poor sensitivity that might be due to poor solubility of CDNB in phosphate buffer. GSH is soluble in phosphate buffer but CDNB is sparingly soluble in phosphate buffer. So, for a better study the GSH-CDNB reaction, an organic solvent is required. The commonly used solvent is dilute ethanol(5%). But in ethanol the intensity of the signal is found to be poor due to which special technique such as DPV or mediator based techniques have been applied to study the reaction. However such special techniques, though able to improve the signal intensity to some extent, can't help in the study of the mechanism of the reaction as well as the influence of other reactants on it, due to the transient nature of the signal. Thus proper study of the influence of external reagents, particularly the pesticides, to that reaction still remaining difficult. Therefore we aim to find out alternate suitable solvents for the said reaction. As a first choice we have chosen methanol for the purpose. It has been shown in the work that though methanol is very sensitive to electro oxidation at platinum electrode, yet it does not affect the main course reaction i.e., the GST catalyzed reaction between GSH and CDNB. The electro active complex formed between GSH and CDNB was found to be stable for hours. Next, we aimed to study the interaction of cypermethrin, an extensively used pyrethroid class of pesticide, to the reaction. Cypermethrin in different formulations are widely used in agricultural and household pest control in different countries worldwide. Though the toxicity is relatively low in mammals, it is highly toxic for aquatic organism and honey bees [13]. A minimal concentration of pyrethroids [0.25–1.5 mg/kg bw/day] for cypermethrin may affect immune system and central nervous system resulting in cancer and other associated disorders [14]. It has been reported in literature that many insects have the capability to develop tolerance to the pyrethroid pesticides [5]. Therefore we have chosen typical pyrethroid pesticide cypermethrin to study the influence of it on the GST catalyzed detoxification reaction of GSH.

2. Experimental

2.1. Materials and reagents

GST (from equine liver), CDNB, GSH and cypermethrin (analytical standard) were purchased from Sigma–Aldrich. Phosphate buffer (PB) of 0.1 M (pH 6.5) was prepared by mixing KH_2PO_4 and K_2HPO_4 procured from Merck-Germany. The GST solution was prepared in PB (pH 6.5) and stored at −22 °C. GSH stock solution was also prepared in PB (pH 6.5). CDNB solution was prepared in 50% aq. methanol so as to maintain the final percentage of methanol 25%. Distilled methanol was diluted to 50% using ultrapure water from a Millipore Milli-Q system. All the solutions except GST were prepared regularly before experiments.

2.2. Instrumentation

Electrochemical measurements were performed at 32 (±0.05) °C, using a standard electrochemical cell with three-electrode assembly. Cyclic voltammetric experiments were carried out on CHI 660A potentiostate (USA). The working electrode was Pt electrode (3 mm diameter) purchased from CH Instrument. A Pt wire was used as counter electrode and Ag/AgCl refilled with 0.1 M KCl was the reference electrode. KCl solutions were changed before each experiment. It is to be mentioned that non-aqueous Ag/Ag^+ can also be used for the purpose but due to cost effect as well as due to the inconvenience in preparing the refilling Ag^+ solution, we have used the aqueous Ag/AgCl reference electrode. Pt electrode was cleaned by polishing in γ-Al_2O_3 (0.05 μm) until a shining surface was obtained and sonicated for 5–10 minutes using digital ultrasonic cleaner. Cleaning of all electrodes was done before each experiment. Electrodes were then dipped in PB and cycled from −0.1 to 0.1 V until it acquired a steady state baseline. UV-visible spectra were recorded by using UV-2550 spectrophotometer, Shimadzu, Japan. Prior to electrochemical measurement the solution mixtures were mixed thoroughly in vortex shaker and then the measurements were made in static solution condition. During the kinetic study using UV-visible spectrophotometer the solutions were stirred constantly with magnetic needle. The infrared spectra were recorded in a PerkinElmer Frontier MIR-FIR spectrometer.

2.3. Analysis procedure

Cyclic voltammetry and UV-visible spectroscopy were used throughout the study. The total volume of the working solution in the electrochemical cell was 3 mL and prepared by mixing 1.5 mL of 2 millimolar GSH in PB with 1.5 mL of 2 millimolar CDNB in 50% methanol, unless stated otherwise.

2.4. Interference study

The cross reactivity of the various components studied through CV to check whether any interference in the main course reaction was present.

2.5. Optimization

Saturated substrate concentration was determined through Michaelis-Menten plot and apparent Michaelis-Menten constant was obtained from the Lineweaver-Burk plot using equation (1).

$$\frac{1}{i} = \frac{1}{i_{max}} + \frac{k_m^{app}}{i_{max}} \frac{1}{[S]} \quad (1)$$

Optimum methanol percentage was evaluated. Optimum pH for the reaction was maintained at 6.5 based on literature data [9].

2.6. Validation study

A calibration curve was obtained by evaluating the % reduction in CV current maxima relative to a blank caused by cypermethrin of different standard amounts when mixed to the reaction mixture in the electrochemical cell. Cypermethrin stock solution was freshly prepared in methanol and added to the reaction mixture with a micropipette.

Method validation was checked by fortifying tomato samples with known amount of cypermethrin followed by extraction and clean up using QuEChERS [15] and finally reconstituting in methanol and appropriate dilution (50%) before subjecting to CV analysis.

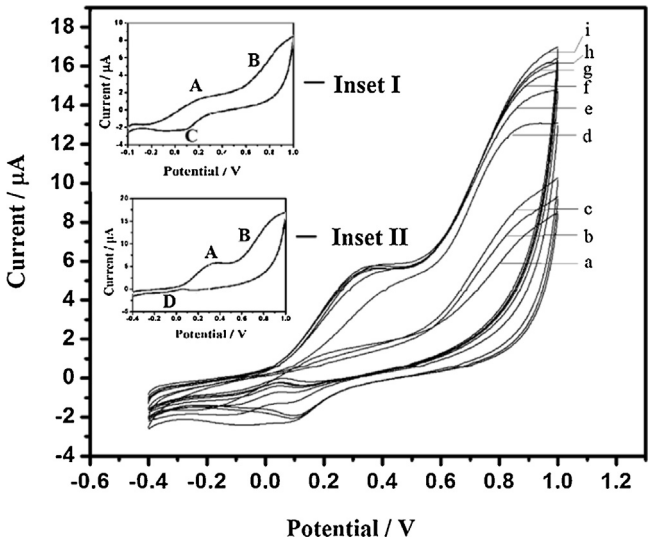

Fig. 1. Cyclic Voltammograms recorded in a 1:1 volume mixture of 2 mM GSH in PB and 2 mM CDNB in 50% aqueous methanol at scan rate 20 mV/s after 30 minutes of mixture preparation. *Inset I*: Fig. 1(a). *Inset II*: Fig. 1(i).

3. Results and discussion

3.1. Cyclic voltammetric study of GSH-CDNB reaction in methanol

In absence of GST, the CV showed moderate intensity oxidation peakA (0.30 V, RSD 0.53%, 5.35 µA, RSD 0.22%) and the peak height remained constant with successive CV run (Fig. 1). Another peak B appeared with onset at 0.60 V and peak maxima at 0.90 V. One low intensity reduction peak (C) appeared at 0.1 V (RSD 0.45%) and disappeared after the third and successive runs. From third run onwards a low intensity oxidation peak (D) appeared at 0.05 V (RSD 0.71%) in the reverse cycle. The peak B is attributed to methanol oxidation (CO_2 formation) [16–19]. The peak A is attributed to oxidation of newly formed complex or intermediate. The reduction wave C is due to adsorption of H_2 at the platinum surface which normally occurs in the potential range from −0.23 to +0.20 V [19]. The oxidation peak at 0.05 V (actually in the region from 0.05 to 0.2 V in all the CVs, peak D) that appears in the reverse cycle is attributed to oxidation of COH produced through dissociation of methanol (Scheme 1). Possibility of hydrogen desorption phenomenon behind this peak is ruled out because, it did not show up in the first three runs when the adsorption waves appeared in the reverse run. And the possibility of CO oxidation is also ruled out because of the fact that CO oxidation normally occurs from 0.41 V onwards [18].

In presence of GST the peak A became more intense (20.67 µA, RSD 0.56%), the peak B and D remains unchanged (Fig. 2A). The CV

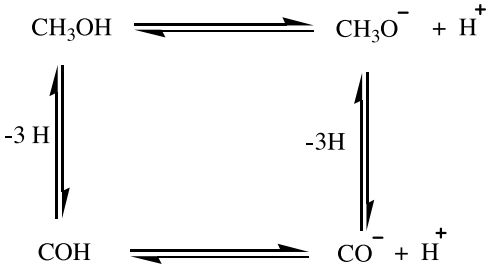

Scheme 1. Probable dissociation pathways for methanol in phosphate buffer medium.

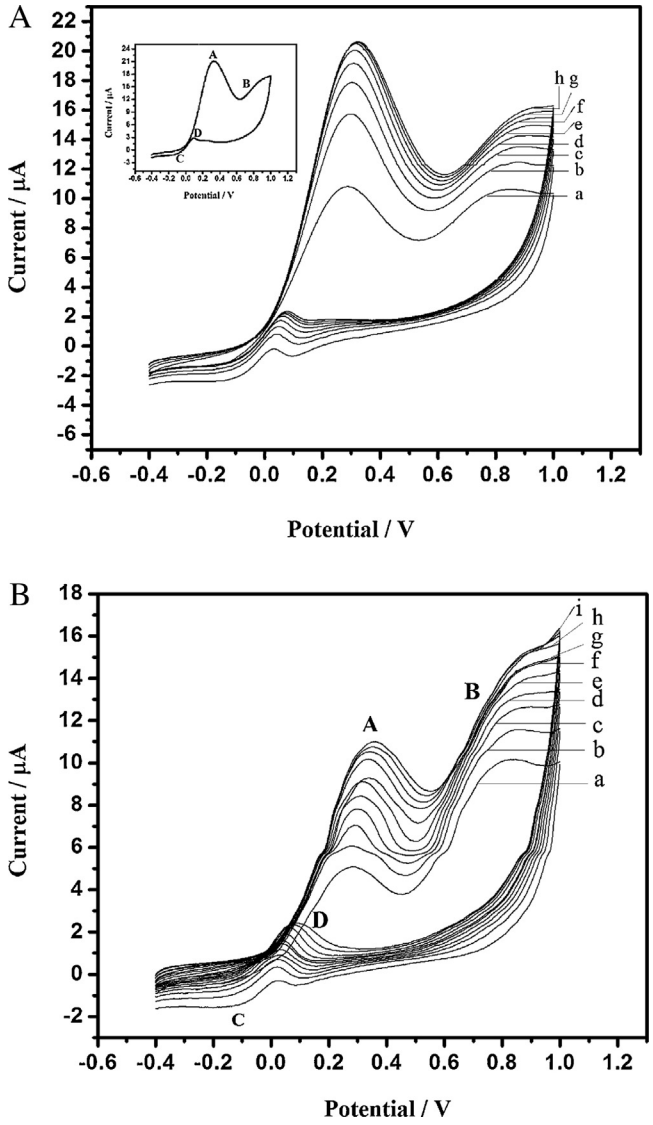

Fig. 2. Cyclic Voltammograms recorded in a 1:1 volume mixture of 2 mM GSH in PB and 2 mM CDNB in 50% aqueous methanol and 20 µL GST (0.02 mg) at scan rate 20 mV/s. A. after 30 minutes incubation. B. in the same mixture after 24 hrs. *Inset*: Fig. 2 A(h).

behavior was partially reproducible on the next day, that is, the peak A appears at same position, but the maximum intensity after several CV runs remained at almost the half height (10.45 µA, RSD 0.62%, Fig. 2B) to that of the previous one (20.67 µA, RSD 0.56%, Fig. 2A). This apparently indicates a two steps reaction with formation of an electro active intermediate and the intermediate formation step is partially reversible.

UV-visible spectroscopic study shows two absorptions, one at the 220 nm (peak M, Fig. 3) and the other at 335 nm (peak N, Fig. 3). The peak at 335 is due to the new complex formed, while that at 220 nm is due to methanol. The peak at 335 nm increases with time which indicates gradual formation of the complex.

3.2. Interference due to cross reactivity of the components under the applied electrochemical condition

3.2.1. Cross reactivity of MeOH and GSH

Shown in Fig. 4A is the CV of GSH and MeOH in absence of GST. The same three peaks obtained during electro oxidation of

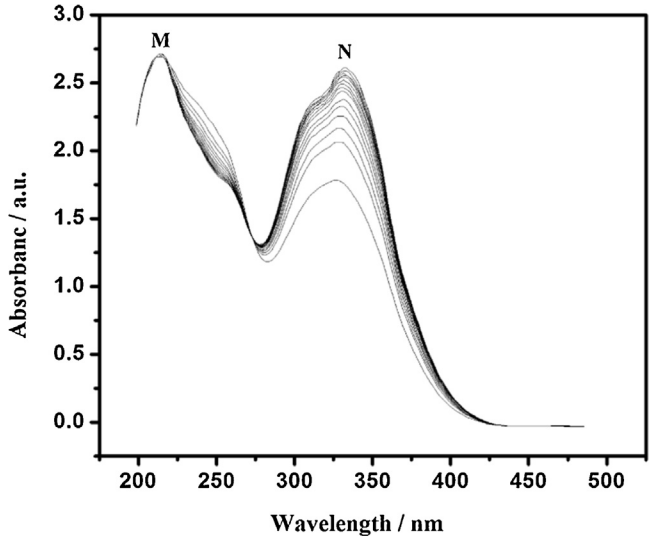

Fig. 3. UV-visible spectra of a mixture of 2 mM each of GSH and CDNB in methanol (50%) with 20 μL GST recorded immediately after preparation.

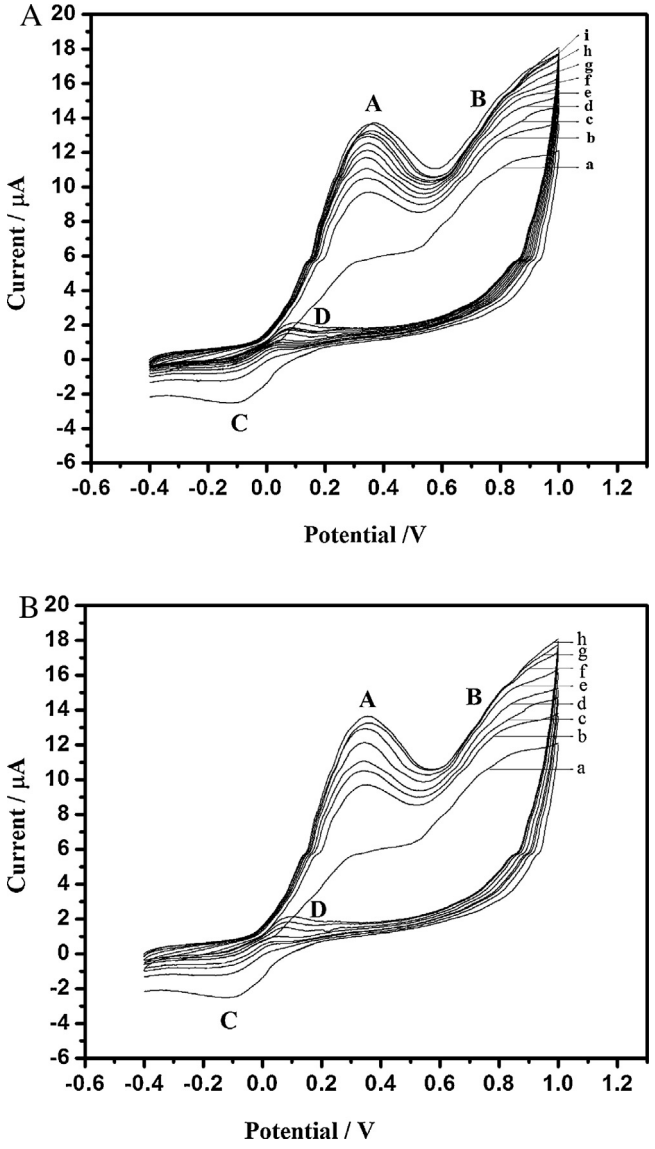

Fig. 4. Cyclic Voltammograms recorded in a mixture of 2 mM GSH in PB and methanol with final concentration 25% at scan rate 20 mV/s. A. in a fresh mixture after 30 minutes of preparation B. in the same mixture on the next day.

GSH-CDNB-GST in methanol obtained in this case also, however with two distinct differences. The height of peak A is much lower than the previous case (12.98 μA in Fig. 4A as compared to 20.67 μA in Fig. 2A) and the reproducibility of the peak height (Fig. 4B) next day was almost 100% (12.95 μA, RSD 0.33%) unlike the previous case where it was close to50%. This infers that methanol-GSH mixture upon electro oxidation produces intermediate complex that is completely reversible. In presence of enzyme with 30 minutes incubation same CV pattern was obtained with slight increase in peak current (15.20 μA in Fig. 5A as compared to 12.98 μA in Fig. 4A) indicating that enzyme catalyzes the reaction with poor catalytic performance. The enzyme catalyzed reaction on the next day was found to be reproducible again with almost same peak intensity (15.20 μA in Fig. 5A; 14.28 μA in Fig. 5B), thus, indicating the involvement of the same reaction path in absence and in presence of the enzyme.

UV-visible spectra of GSH and MeOH mixture showed peak in the UV region (220 nm, peak M) but no peak in the visible region (Fig. 6).

To know whether the electro oxidation has any role on the formation of UV-visible active product in the mixture of GSH, CDNB, MeOH and PB, the CV and UV experiments were performed in the same solution mixture in an alternate sequence. It was found that the CV peak maximum of peak A is affected by electrochemical disturbance when applied initially. When CV was run after completing the UV experiment the CV peak height was nearly double than when CV was run immediately after mixing. But the UV peak height at 335 nm reaches the same level (slowly with time) irrespective of whether disturbed electrochemically or not (Figure not shown).

In ethanol, GSH electro oxidation could not be detected by normal cyclic voltammetry (Fig. 12). In presence of CDNB and GST an UV-visible active, yellow colored complex though formed, the reaction mixture was found to be insensitive to electro oxidation under normal cyclic voltammetric condition.

Plausible mechanism

The observed CV and UV behavior can be explained with the following reaction schemes (Schemes 1 and 2). FTIR (MIR and FIR) spectroscopic study also corroborate this mechanism (data not shown).

In phosphate buffer (PB) solution GSH forms H-bonded complex with $H_2PO_4^-$ ion. Due to remaining in H-bonded state, the SH group of GHS is less reactive in phosphate buffer. In presence of methanol the situation get altered due to PB-methanol interaction and C-O-P bond formation between PB and MeOH; H-bonding network get removed and SH groups are set free.

It is attributed that in PB solution, methanol dissociate into COH and CO^- in much the same way it does in strongly alkaline solution [16] (Scheme 1). The CO^- thus produced interacts with GSH to produce electro active intermediate $[GSH]^{\#}$ (Scheme 2).

Path A can occur under electrochemical process in which GSH is not directly affected by the electrode potential but the CO^- formed from methanol oxidation at higher potential (0.65 V) triggers the reaction of GSH. Evidence of involvement methanol dissociation product (CO^-) in the first step of path A comes from the observation that the peak at 0.3 V appears with very small magnitude initially and increases with successive run. That is, the peak height of peak A (0.3 V) is proportional to the second oxidation at higher potential (from 0. 65 V).

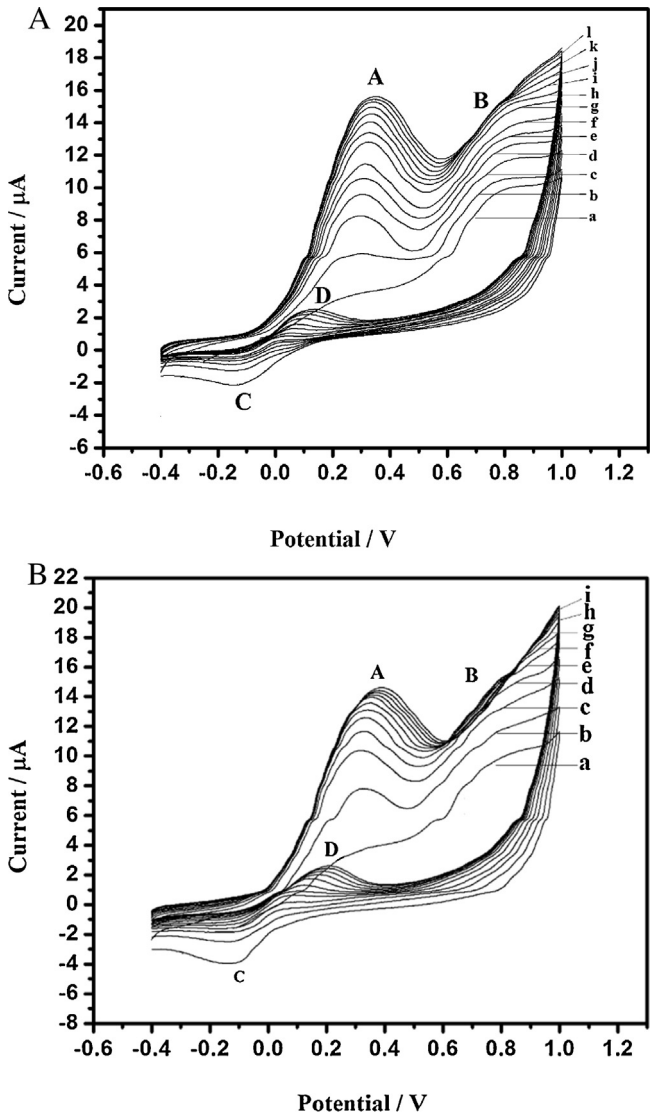

Fig. 5. Cyclic Voltammograms recorded in a mixture of 2 mM GSH in PB and methanol (50%) with 20 μL GST at scan rate 20 mV/s. A. in a fresh mixture after 30 minutes of preparation. B. in the same mixture on the next day.

Path B prefers to occur under non electrochemical process. When electrochemical disturbance is applied, path A outperforms path B. The products form through paths A1, A2, B1 and B2 can occur to a lesser extent through purely non electrochemical process also. This is possible because of the fact that a certain fraction of methanol molecules remain in dissociated form (Scheme 1) even in absence of any electrode polarization.

The peak A (at 0.30 V) is attributed to the oxidation of $[GSH]^{\#}$. The oxidation peak height of this oxidation increases with continuous CV runs up to certain time and then remains constant for more than an hour, after which it decreases slowly. So it is attributed that this oxidation involves a reversible process or a cyclic process in which the reverse step is either non-electrochemical or controlled by the second oxidation at higher potential. $[GHS]^{\#}$ formation through path B is more as compared to the same through path A. It is attributed that GST plays some role in facilitating the interaction between GSH and CO^{-}.

In ethanol, due to lack of PB-ethanol interaction the PB-GSH interaction remains and as a result the SH group becomes less sensitive to electro oxidation. However, GST catalyzed non

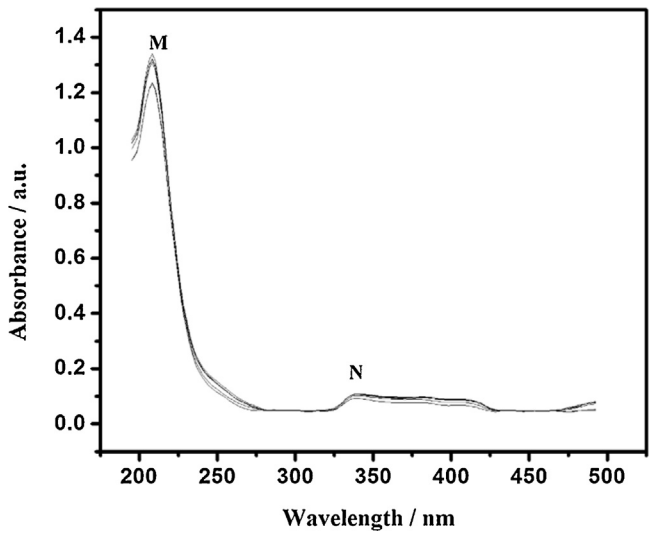

Fig. 6. UV-visible spectra of 2 mM GSH in methanol.

electrochemical reaction between GSH CDNB still occurs leading to the UV active GS-CDNB complex.

3.2.2. Cross reactivity of MeOH with PB

In Fig. 7, curve aa′ and bb′ are the CVs of phosphate buffer methanol mixture respectively at 50% and 25% composition at scan rate 20 mV/s. With higher amount of methanol two oxidation peaks were observed peak P (0.56 V, RSD 0.35% 10.81 μA, RSD 0.18%) and Q (0.35 V, RSD 0.41%, 2.45 μA, RSD 0.27%). The oxidation peak P is attributed to oxidation of methanol (CO_2 formation step). The oxidation peak Q that shows up in the reverse cycle is due to oxidation of CO adsorbed on Pt surface [17]. Another small reduction peak R appeared at 0.02 V is attributed to reduction wave due to adsorbed hydrogen. In a dilute methanol solution the lower oxidation is not seen, the higher oxidation peak appears in a sharper pattern and gets shifted to higher potential. This shifting is attributed to creation of stronger diffusion barrier by the phosphate group created near the electrode surface due to positive

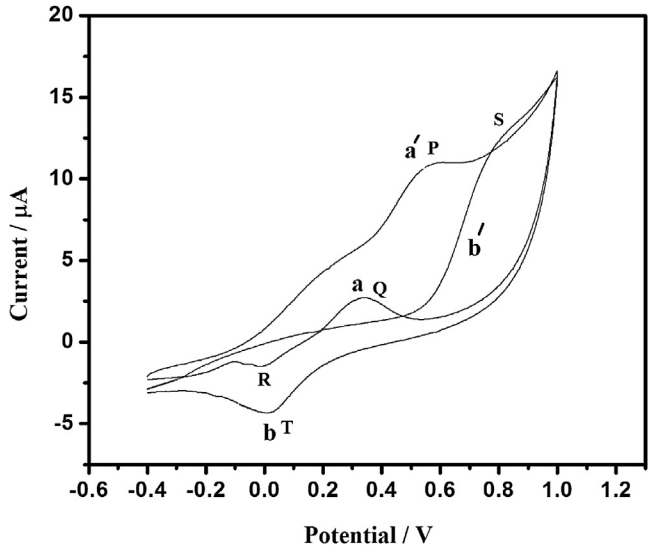

Fig. 7. CVs at scan rate 20 mV/s of PB–MeOH mixture of composition a. 50%. b. 25%.

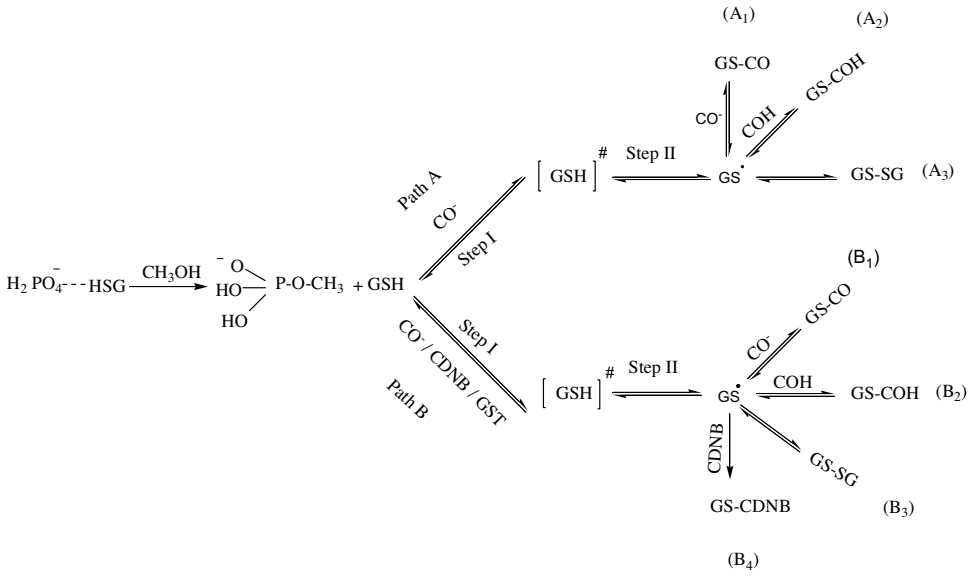

Scheme 2. Various reaction pathways showing 1. the GSH – PB and PB – methanol interactions (the singular path), 2. the electrochemical reaction between GSH and methanol (path A) and 3. the non electrochemical, enzyme catalyzed reaction between GSH and CDNB in methanol (Path B). A_1, A_2, A_3 and B_1, B_2, B_3 are the same reactions occurring through two different routes. B_4 is the irreversible conjugation reaction between GS and CDNB that leads to the formation of the UV active product.

electrode polarization. The low intensity reduction peak T around 0.02Vis due to charging current of H_2 adsorption.

3.2.3. Cross reactivity of CDNB with MeOH

CVs of CDNB methanol mixture are shown in Fig. 8. In methanol, two oxidation peaks were seen, one at 0.65 V in the forward scan and another at 0.4 V in the reverse scan. These are characteristic oxidation peaks of methanol at Pt surface [16–19]. It implies that CDNB does not undergo any redox reaction under the applied experimental condition.

3.2.4. Cross reactivity of GSH with PB

CV of GSH in PB is shown in Fig. 9. The reduction wave at a potential close to 0.1 V is probably due to reduction of oxygen adsorbed on platinum surface. A new oxidation peak of relatively lower intensity appearing from 0.60 V onwards is probably due to oxidation of some components in GSH. Due to poor intensity this oxidation gets masked by the methanol oxidation peak in the same region.

3.3. Optimization

3.3.1. Effect of GST amount

For equimolar mixture of GSH and CDNB, and for incubation time of 30 minutes, peak current was found to vary with GST concentrations. Peak current and hence the enzyme activity showed almost linear increase up to 120 μL (0.12 mg). Beyond 120 μL the reaction starts to be limited by substrate concentration (Fig. 10). Though an amount of 0.12 mg (120 μL) of GST was found to be the maximum enzyme amount for the reaction of GSH and CDNB in 1:1 millimolar ratio, due to the preciousness of the enzyme, an amount of 20 μL (0.02 mg) was used in most of the experiments wherever possible.

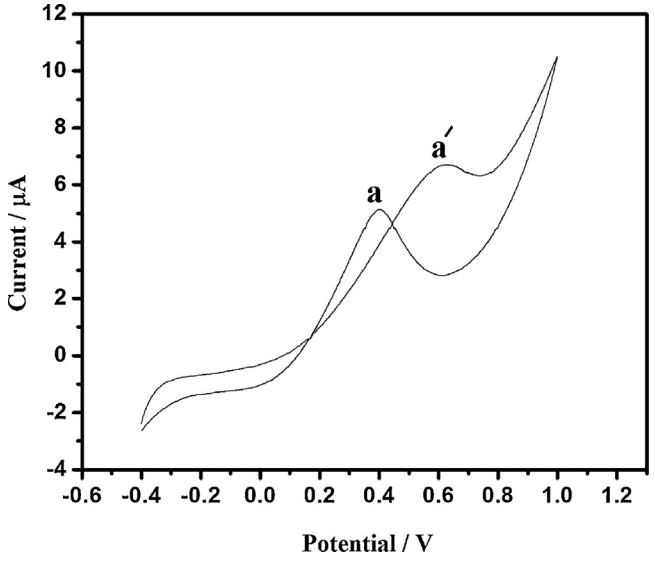

Fig. 8. CV of CDNB in 50% aqueous methanol.

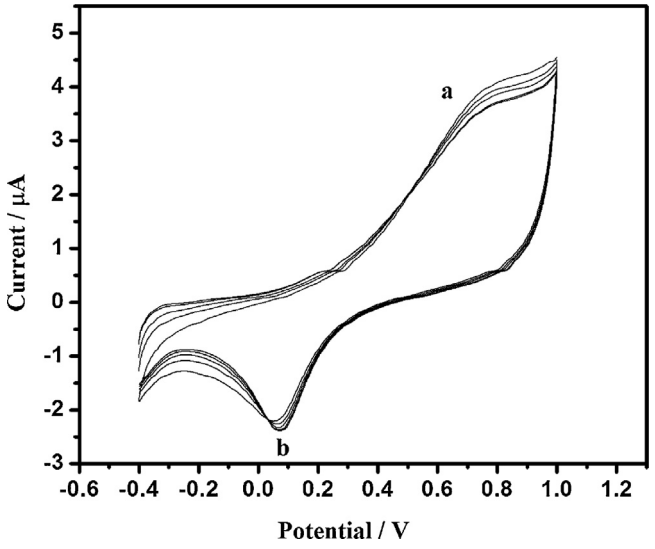

Fig. 9. CV of reduced glutathione (GSH) in PB.

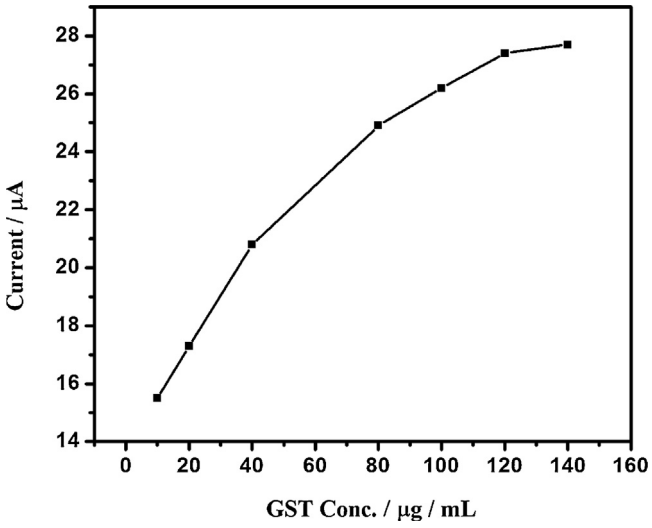

Fig. 10. Variation of peak current of GSH-CDNB reaction (1:1 millimolar) in 25% methanol with GST concentration after 30 min incubation.

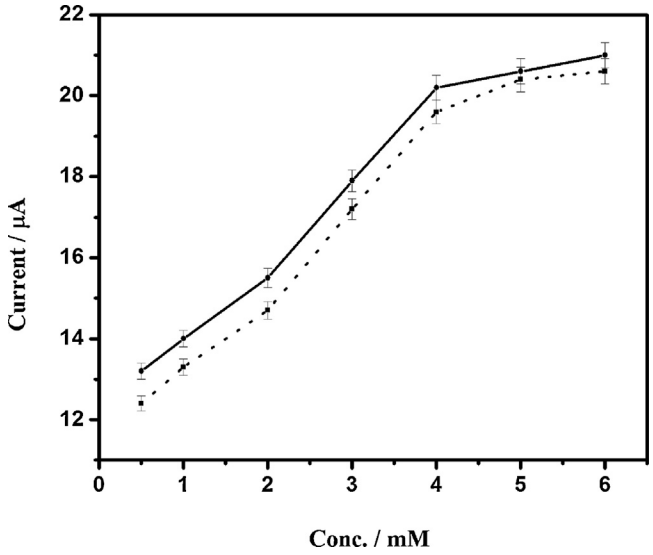

Fig. 11. Dependency of peak current with substrate concentration when 120 μL of GST was used. Solid line for GSH concentrations, dotted line for CDNB concentrations.

3.3.2. Apparent Michealis-Menten constant (K_m^{app})

Effect of both GSH and CDNB concentration on the oxidation peak current was measured. A similar pattern of concentration dependency was observed indicating that both GSH and CDNB act as substrates. This is in agreement with available literature [20]. Slightly lower current value was obtained in case of CDNB probably because of partial passivation of the Ag/AgCl reference electrode. The Michaelis–Menten plots show two different region of linear dependency. The first region is in the low concentration range from 0.5 to 2 millimolar and the second region is from 2 to 4 millimolar. Apparent Michealis-Menten constant obtained through the Line-waever-Burk plots (eqn. (1)) were 0.114 mmolL^{-1} and 0.122 mmolL^{-1} at low concentration and 1.66 mmol L^{-1} and 1.91 mmol L^{-1} at high concentration respectively for GSH and CDNB. The value of (K_m^{app}) reported in literature lies between 0.1 to 1 millimolar [21–24]. The value in the low concentration range is in good agreement with the reported values. Obtaining of the high value in the higher concentration range (2 to 4 millimolar) is assigned to the increasing influence of non-enzymatic reaction under high reactant density. Variation of CV peak current with GSH and CDNB concentrations is shown in Fig. 11.

3.3.3. Optimum methanol composition and effect of ethanol on the reaction

Effect of ethanol on the said reaction was studied using CV (Fig. 12). When methanol was replaced with ethanol (25%) and subjected to CV analysis, no new peak other than the one from 0.6 V onwards was seen (curve e), in spite of the solution getting yellow colored. The peak from 0.6 V onwards was the same obtained in GSH-PB mixture. It indicates that the GSH-CDNB mixture does not produce any electro active species in ethanol under the normal cyclic voltammetric condition. Effect of methanol composition on the peak intensity was studied from 5% composition onwards through CV and found that it varies linearly with composition and reaches maximum at 25% composition. Beyond 25% composition, the increase was not significant. Thus a composition of 25% methanol was taken as the optimum methanol composition.

3.4. Pesticides interaction study

Effect of cypermethrin on the GST catalyzed reaction between GSH and CDNB in methanol was studied. While the reaction was in progress, addition of cypermethrin suppresses the reaction to an extent proportional to cypermethrin amount. Similarly, addition of cypermethrin in the initial mixture suppresses the CV and UV-visible peak to different extent depending on the amount of cypermethrin (Fig. 13). A 25 ppb of cypermethrin in methanol solution was sufficient for complete inhibition of the reaction in a standard 3 mL mixture of 2 mM of GSH and 2 mM of CDNB and 20 μL of the enzyme.

3.5. Quantification of cypermethrin

CV method was used to quantify cypermetrhin. It was observed that when 25 ppb of cypermethrin was mixed initially to the solution mixture and kept for 30 min., then CV was run, the 0.3 V peak almost disappeared. Cypermethrin solutions of concentration lower than 25 ppb, when mixed in the reaction mixture, found to

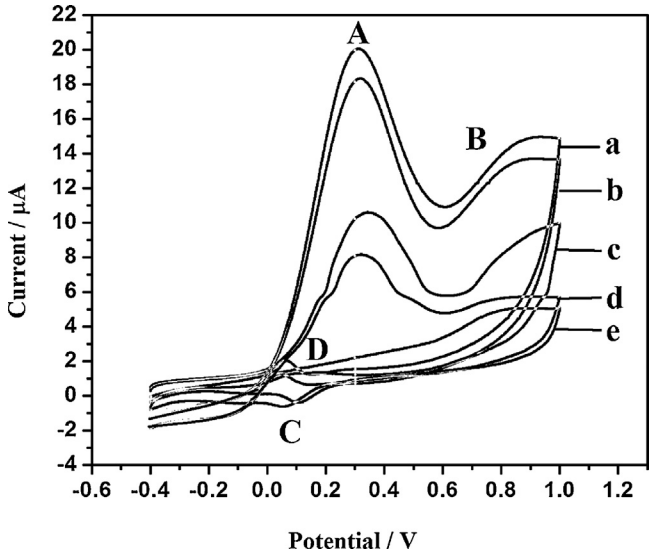

Fig. 12. Cyclic voltammograms showing variation of peak current with methanol concentration (a-d) and effect of ethanol (e). Reaction mixture contains 2 mM GSH, 2 mM CDNB and 20 μL GST. Methanol concentrations (a) 50% (b) 25% (c) 10% (d) 5% and ethanol concentration 25% (e).

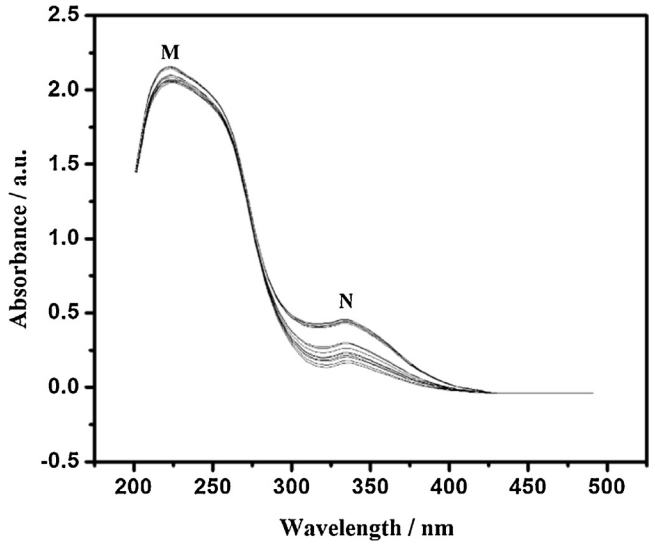

Fig. 13. UV-visible spectra recorded in a solution mixture of GSH (1 mmol), CDNB (1 mmol), GST (20 μL) and PB-MeOH (25%) in presence of 25 ppb cypermethrin.

suppress the peak current up to different extent which was proportional to concentration of cypermethrin. Based on this observation, a calibration curve for cypermethin was obtained by plotting percentage inhibition i.e., percent reduction in peak current versus cypermethrin concentration up to 25 ppb and was found to be linear. Limit of detection is considered as the ppb of the pesticide required for 10% inhibition and found to be 2 ppb (Fig. 14).

For determining the percentage inhibition two solution mixtures containing GSH-CDNB-MeOH, PB and GST of exactly same composition were prepared, one of which served as the blank. The other was treated with fixed amount of cypermethrin and the difference in CV peak current in the two were noted, which was converted to percentage inhibition.

It is obvious from the UV-visible spectroscopic study that visible spectroscopy can also be applied to quantify cypermethrin taking the GST catalyzed GSH-CDNB reaction. However, in the present work our interest was to explore the feasibility of electrochemical detection, so the spectroscopic method was not tried for.

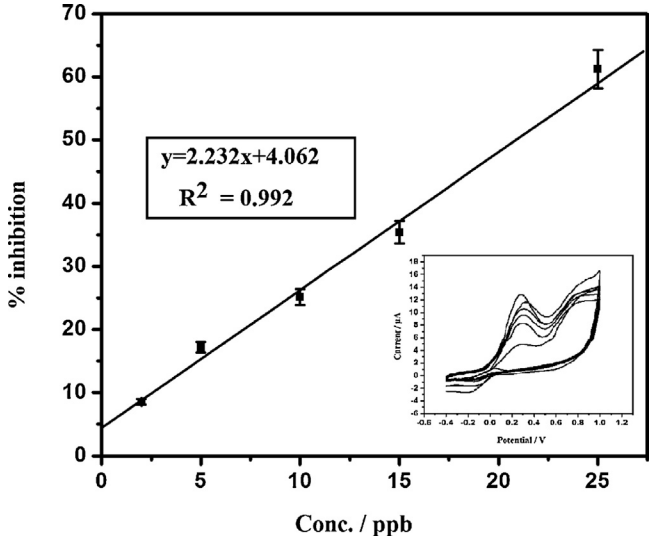

Fig. 14. Calibration curve for cypermethrin. Inset: variation of CV peak current with ppb of cypermethrin.

3.6. Method validation study

For validation study, cypermethrin from spiked samples were extracted and cleaned up using modern extraction technique QuEChERS.

10 gram of chopped vegetable (tomato) was spiked with 5 mL of 60 ppb cypermethrin solution (prepared in acetonitrile) and then homogenized. 5 mL of acetonitrile was added and shaken in vortex shaker for 5 minutes. Then 4 gram of $MgSO_4 \cdot H_2O$ and 1 gram of NaCl was added, shaken for 5 minutes. Then 1 gram of sodium citrate dihydrade and 0.5 g of sodium hydrogen citrate sesquihydrate were added. The mixture was shaken vigorously for 10 seconds and then sonicated for 5 minutes and then centrifuged for 10 minutes at 2000 rpm. 5 mL of the supernatant was taken and treated with 125 mg of PSA (primary secondary amine) and 750 mg of $MgSO_4$ $4H_2O$, shaken for few seconds and then sonicated for 5 minute and centrifuged again. Then supernatant clean liquid was collected in 50 mL round bottom flask and evaporated to dryness at 40 °C and 200 mbar in rotavapor. The dry residue was reconstituted in mixture of 4 mL methanol and 1 mL dichloromethane and evaporated again to about 1 mL diluted to 5 mL by adding extra methanol. To 1 mLof this solution was added 1 mL each of of 3 millimolar GSH and CDNB and 20 μL GST. % inhibition in peak current calculated and pesticide amount determined with the help of the calibration curve. The whole process was repeated thrice to get triplicate results. The recovery was found to be 96% (RSD 6.5%).

4. Conclusion

Through the application of normal cyclic voltammetric method we have studied the reaction between GSH and CDNB in methanol and ethanol and shown that the reaction follows two different paths in the two solvents. Unlike the case when ethanol is used as the solvent, in methanol GSH get transformed to an electro active intermediate state under the influence of applied electric potential. This electro active intermediate undergoes oxidation at 0.3 V, sufficiently stable (more than one hour) and reacts with CDNB to form UV active final product. The same electro active intermediate is also formed by non-electrochemical process in presence of CDNB and the formation is catalyzed by GST.

Influence of different components of the reaction mixture on the electrochemical response has been evaluated. Optimum GST amount, methanol concentration, saturated substrate concentration and apparent Michaelis-Menten constant for the enzymatic reaction have been determined.

We have also studied the influence of typical pyrethriod pesticide cypermethrin on the said reaction and found that cypermethrin has negative influence on the reaction. Application of the phenomena for quantifying cypermethin through cyclic voltammetric method has been demonstrated. Cypermethrin was detected down to 2 ppb by using normal cyclic voltammetric method. The quantification method has been validated through spiked sample and using QuEChERS extraction/clean up method.

Acknowledgement

One of the authors Dr. P. Puzari would like to thank the Ministry of Food Processing Industries, Govt of India for the financial grant through the project No. SERB/MOFPI/0005/2014.

Appendix A. Supplementary data

Supplementary data associated with this article can be found, in the online version, at http://dx.doi.org/10.1016/j.electacta.2016.03.199.

References

[1] P. Jancova, P. Anzenbacher, E. Anzenbacherova, Phase II drug metabolizing enzyme, Biomed. Pap. Med. Fac. Univ. Palacky Olomouc Czech Repub. 154 (2010) 103–116.

[2] W.H. Habig, M.J. Pabst, W.B. Jakoby, Glutathione S-Transferases. The first enzymatic step in mercapturic acid formation, J. Biol. Chem. 249 (1974) 7130–7139.

[3] C.C. Mcllwain, D.M. Townsend, K.D. Tew, Glutathione *S*-transferase polymorphisms: cancer incidence and therapy, Oncogene 25 (2006) 1639–1648.

[4] D.M. Townsend, K.D. Tew, The role of glutathione S-transferasein anti-cancer drug resistance, Oncogene 22 (2003) 7369–7375.

[5] L. Kostaropoulos, A.I. Papadopoulos, A. Metaxakis, E. Boukouvala, E. Papadopoulou-Mourkidou, Glutathione S-transferase in the defence against pyrethroids in insects, Insect Biochem. Mol. Biol. 31 (2001) 313–319.

[6] T.D. Waite, H. Huang, B. Inceoglu, J.A. Christiansen, R.D. McAbee, B.D. Hammock, A.J. Cornel, Proceedings and Papers of the Seventy-Third Annual Conference of the Mosquito and Vector Control Association of California 73 (2005) 131–136.

[7] N. Lumjuan, S. Rajatileka, D. Changsom, J. Wicheer, P. Leelapat, L. Prapanthadara, P. Somboon, G. Lycett, H. Ranson, The role of the *Aedesaegypti* Epsilon glutathione transferases in conferring resistance to DDT and pyrethroid insecticides, Insect Biochem. Mol. Biol. 41 (2011) 203–209.

[8] J.G. Vontas, A.A. Enayati, G.J. Small, J. Hemingway, A Simple Biochemical Assay for Glutathione *S*-Transferase Activity and Its Possible Field Application for Screening Glutathione *S*-Transferase-Based Insecticide Resistance, Pestic. Biochem. Physiol. 68 (2000) 184–192.

[9] J.W. Choi, Y.K. Kim, B.K. Oh, S.Y. Song, W.H. Lee, Optical biosensor for simultaneous detection of captan and organophosphorus compounds, Biosens. Bioelectron. 18 (2003) 591–597.

[10] J.W. Choi, Y.K. Kim, S.Y. Song, I.H. Lee, W.H. Lee, Optical biosensor consisting of glutathione-S-transferase for detection of captan, Biosens. Bioelectron. 18 (2003) 1461–1466.

[11] T.I.S. Oliveira, M. Oliveira, S. Viswanathan, M.F. Barroso, L. Barreiros, O.C. Nunes, J.A. Rodrigues, P. Lima-Neto, S.E. Mazzetto, S. Morais, C.D. Matos, Molinate quantification in environmental water by a glutathione-S-transferase based biosensor, Talanta 106 (2013) 249–254.

[12] R.P. Sing, Y.J. Kim, B.K. Oh, J.W. Choi, Glutathione-s-transferase based electrochemical biosensor for the detection of captan, Electrochem. Commun. 11 (2009) 181–185.

[13] S. Saha, A. Kaviraj, Acute toxicity of synthetic pyrethroidcypermethrin to some freshwater organisms, Bull Environ. Contam. Toxicol. 80 (2008) 49–52.

[14] A. Kaushik, P.R. Solanki, A.A. Ansari, B.D. Malhotra, S. Ahmed, Iron oxide-chitosan hybrid nanobiocomposite based nucleic acid sensor for pyrethroid detection, Biochem. Eng. J. 46 (2009) 132–140.

[15] M. Asensio-Ramos, J. Hernandez-Borges, L.M. Ravelo-Perez, M.A. Rodriguez-Deelgado, Evaluation of a modified QuEChERS method for the extraction of pesticides from agricultural, ornamental and forestall solis, Anal. Bioanal. Chem. 396 (2010) 2307–2319.

[16] V.S. Bagotzky, Y.B. Vassilev, Mechanism of electro-oxidation of methanol on the platinum electrode, Electrochim. Acta. 12 (1967) 1323–1343.

[17] R. Chetty, W. Xia, S. Kundu, M. Bron, T. Reinecke, W. Schuhmann, M. Muhler, Effect of Reduction Temperature on the Preparation and Characterization of Pt-Ru Nanoparticles on Multiwalled Carbon Nanotubes, Langmuir 25 (2009) 3853–3860.

[18] E. Herrero, W. Chrzanowski, A. Wieckowski, Dual Path Mechanism in Methanol Electrooxidation on a Platinum Electrode, J. Phys. Chem. 99 (1995) 10423–10424.

[19] C. Zhou, H. Wang, F. Peng, J. Liang, H. Yu, J. Yang, MnO_2/CNT Supported Pt and Pt-RuNanocatalysts for Direct Methanol Fuel Cells, Langmuir 25 (2009) 7711–7717.

[20] T.A. Enache, A.M. Oliveira-Brett, Electrochemical evaluation of glutathione S-transferase kinetic parameters, Bioelectrochemistry 101 (2015) 46–51.

[21] P.A. Adams, C.N.T. Sikakana, Factors affecting the inactivation of human placental glutathione *S*-transferase π: The kinetic mechanism and pH-dependence of solvational and 1-chloro-2,4-dinitrobenzene-mediated inactivation of the enzyme, Biochem. Pharmacol. 39 (1990) 1883–1889.

[22] A. Grammou, C. Papadimitriou, P.E. Samaras, E. Vasara, A.I. Papadopoulos, Effect of municipal waste water effluent upon the expression of Glutathione S-transferaseisoenzymes of brine shrimp *Artemia*, Chemosphere 84 (2011) 105–109.

[23] S.M. Valles, O.P. Perera, C.A. Strong, Purification biochemical characterization, and cDNA cloning of a glutathione *S*-transferase from the red imported fire ant, *Solenopsisinvicta*, Insect Biochem. Mol. Biol. 33 (2003) 981–988.

[24] I. Zibaee, A.R. Bandani, S. Haghani, A. Zibaee, Partial characterization of Glutathione S-Transferase in two populations of the sunn pest, *eurygasterintegricepsputon* (Heteroptera: Scutellaridae), Mun. Ent. Zool. 4 (2009) 564–571.

Analytical Methods

PAPER

View Article Online
View Journal | View Issue

Cite this: *Anal. Methods*, 2017, **9**, 4044

Glutathione-*S*-transferase-catalyzed reaction of glutathione for electrochemical biosensing of temephos, fenobucarb and dimethoate†

Himadri Borah,[a] Rekha Rani Dutta,[a] Sudarshan Gogoi,[a] Tapas Medhi[b] and Panchanan Puzari*[a]

Received 17th May 2017
Accepted 9th June 2017

DOI: 10.1039/c7ay01258f

rsc.li/methods

This study describes a sensitive bio-electrochemical detection method for extensively used toxic organothiophosphate pesticides temephos and dimethoate, and organocarbamate fenobucarb, by employing a simple mediatorless cyclic voltammetric technique. The sensing scheme is based on the inhibition of the catalytic activity of glutathione-*s*-transferase using these pesticides during the course of the conjugation reaction between reduced glutathione and 1-chloro-2,4-dinitrobenzene, resulting in a reduction in the oxidation peak current of the activated glutathione oxidation. The types of inhibition of these three pesticides were studied. Fenobucarb showed competitive inhibition with a K_i value of 10.30 mM, temephos showed non-competitive inhibition with a K_i value of 54.82 mM and dimethoate exhibited a mixed type of inhibition. Calibration curves for all the three pesticides were obtained with detection limits down to 2, 4 and 5 ppb for fenobucarb, temephos, and dimethoate, respectively. The method was validated with a spiked tomato sample using the standard solid-phase extraction clean-up method. The method is a promising new tool for analysis of water-insoluble organophosphate and organocarbamate pesticides.

1. Introduction

Development of easy, field-deployable, and highly sensitive analytical techniques for detection of pesticide content in environmental and food samples is a research area of high demand at the present time owing to the alarming adverse effects of those pesticides on human health and the environment.[1–10] Among the analytical techniques, enzyme inhibition-based electrochemical biosensing techniques are extensively used due to the advantages of high sensitivity, reliability, fast response, and the feasibility of integration into a miniaturized sensor device.[11–17] Currently, different enzymes are being used for development of bioanalytical techniques as well as biosensors for different classes of pesticides, such as acetylcholinesterase and choline oxidase for organophosphates and organocarbamates,[18–29] chicken liver esterase and organophosphate hydrolase for organophosphates,[14,18,30,31] and tyrosinase for phenolic pesticides.[32–44] Owing to the class specificity of enzyme action on one hand and the availability of diverse classes of pesticides in the market on the other hand, it is quite challenging to come up with different enzyme or bio-receptor molecules for each class. As an effort towards that direction, attempts have been made to use the cytosolic enzyme glutathione-*s*-transferase (GST) for pesticide biosensing, with the presumption that since it is a detoxification catalyst capable of binding with several hydrophobic compounds,[35–40] it may bind with the pesticides also, thus affecting the catalytic action of itself and thereby triggering a biochemical signal. The GST-based detoxification reactions rely on the catalysis of the conjugation between a xenobiotic and reduced glutathione (GSH) forming a conjugate compound, which in turn is further metabolized inside our body or excreted in a subsequent step.[41–45] Different substrates are in use for the *in vitro* study of the GST-catalyzed conjugation with GSH, and the most commonly used one among them is 1-chloro-2,4-dinitrobenzene (CDNB).[46,47] Conjugation of GSH with CDNB produces a yellow colored complex that absorbs at 335 nm.[48] The presence of certain pesticides in the reaction mixture dampens the UV peak through binding with GST, thereby decreasing its catalytic action towards the conjugation reaction. Based on this phenomenon, few workers have developed UV-visible spectroscopic detection protocol for pesticides.[48,49] Some others have used the direct reaction between GSH and pesticides for developing a detection protocol for the latter.[50] Yet another group has developed electrochemical protocols for pesticide biosensing utilizing the reaction. Ravindra P. Singh

[a]*Department of Chemical Sciences, Tezpur University, Tezpur, Assam, India-784028. E-mail: pancha@tezu.ernet.in; Fax: +91 3712 267005; +91 3712 267006; Tel: +91 3712 267007 ext. 5061; +91 3712 267008 ext. 5061; +91 3712 267009 ext. 5061*

[b]*Department of Molecular Biology and Biotechnology, Tezpur University, Tezpur, Assam, India-784028*

† Electronic supplementary information (ESI) available. See DOI: 10.1039/c7ay01258f

et al., (2009) proposed an electrochemical detection method for the fungicide captan using a bioelectrode fabricated through immobilization of GST a on (3-aminopropyl)triethoxysilane (APTES) self-assembled gold nanoparticle substrate. The electrochemical signal was enhanced through the use of the mediator $[Fe(CN)_6]^+$.[51] T. I. S. Oliveira *et al.* (2013) developed a GST-based bioelectrode for molinate quantification in water using the same fabrication procedure but utilizing a glassy carbon substrate instead of Au nanoparticles.[52] The correlation of the current signal with the amount of inhibition and hence with the pesticide concentration was established through differential pulse voltammetric (DPV) technique. However, monitoring of the mentioned reaction through simple electrochemical techniques such as cyclic voltammetry without any mediator was not reported earlier probably due to the solubility issue of CDNB.

In a recent study, we have shown that the GST-catalyzed reaction between GSH and CDNB as well as the influence of pesticides on the said reaction can be studied through a normal, mediator-less cyclic voltammetric technique, if 25% methanol is used as the electrolyte instead of phosphate buffer. We have demonstrated the detection of pyrethroid pesticide cypermethrin using this method.[53] In the present study, we have extended the method for the detection of organothiophosphate (OTP) and organocarbamate (OC) classes of pesticides, considering the commonly used organothiophosphate temephos, dimethoate and organocarbamate fenobucarb. Inhibition kinetics of the three pesticides was also studied and the method has been validated through the analysis of tomato samples spiked with those pesticides.

It was found that the method works well in case of those three targeted pesticides. This new method is a promising new tool for pesticide analysis because the detection protocol involves the use of 25% methanol, which makes bioanalysis of real samples more feasible.

2. Experimental

2.1. Materials and reagents

GST (from equine liver), CDNB, GSH, temephos, fenobucarb and dimethoate (analytical standard) were purchased from Sigma-Aldrich. Phosphate buffer (PB) of 0.1 M (pH 6.5) was prepared by mixing KH_2PO_4 and K_2HPO_4 procured from Merck-Germany. Methanol, dichloromethane (DCM) and acetonitrile were of analytical reagent grade and purchased from Merck chemicals. Bondesil-NH_2 and carbon SPE bulk sorbent were purchased from Agilent technologies. The GST solution was prepared in PB containing 0.1 M KCl at pH 6.5 as the supporting electrolyte and stored at −22 °C. The GSH stock solution was also prepared in PB (pH 6.5). The CDNB solution was prepared in 50% aqueous methanol so as to maintain the final percentage of methanol as 25%. Distilled methanol was diluted to 50% using ultra-pure water from a Millipore Milli-Q system. The stock solutions of fenobucarb, temephos and dimethoate were prepared in methanol and diluted to the appropriate concentration for further experimental use. All the solutions except GST were prepared regularly before experiments.

2.2. Instrumentation

Electrochemical measurements were performed at 30(±0.05) °C, using a standard electrochemical cell with three-electrode assembly. Cyclic voltammetric experiments were carried out on PAR 273-A potentiostat/galvanostat. The working electrode was Pt electrode (3 mm diameter). A Pt wire was used as the counter electrode and Ag/AgCl refilled with 0.1 M KCl was the reference electrode. KCl solutions were changed before each experiment. It should be mentioned that non-aqueous Ag/Ag^+ can also be used for the purpose, but due to cost effect as well as due to the inconvenience in preparing the refilling Ag^+ solution, we have used the aqueous Ag/AgCl reference electrode. The Pt electrode was cleaned by polishing in γ-Al_2O_3 (0.05 μm), until a shining surface was obtained, and sonicated for 5–10 minutes using a digital ultrasonic cleaner. Cleaning of all electrodes was done before each experiment. Electrodes were then dipped in PB and cycled from −0.1 to 0.1 V until a steady-state baseline was obtained. UV-visible spectra were recorded using the UV-2550 spectrophotometer, Shimadzu, Japan. Prior to electrochemical measurement, the solution mixtures were mixed thoroughly in a vortex shaker and then the measurements were made in a static solution condition. During the kinetic study using the UV-visible spectrophotometer, the solutions were stirred constantly using a magnetic needle.

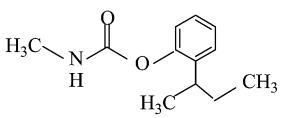

Fenobucarb

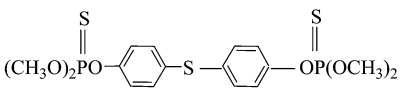

Temephos

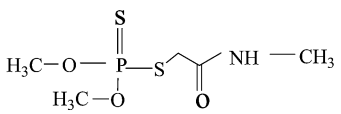

Dimethoate

2.3 Analysis procedure

2.3.1 Cyclic voltammetry measurements. The total volume of the working solution in the electrochemical cell was 3 mL, which was prepared by mixing 1.5 mL of 2 mM GSH in PB with 1.5 mL of 2 mM CDNB in 50% methanol, unless stated otherwise. The Pt electrode was employed in the CV measurements with the potential range from – 0.4 V to 1 V at a scan rate of 20 mV s^{-1}.

2.3.2 UV-visible spectroscopic study. For absorbance measurements of the GSH–CDNB–GST mixture, 0.5 mmol each of GSH and CDNB solutions were prepared in a quartz cuvette along with 20 μL GST solution at room temperature 30(±0.05) °C.

2.4 Validation study

The method was validated by fortifying tomato samples with known amounts of fenobucarb, temephos and dimethoate separately, followed by extraction and clean-up using solid-phase extraction technique. Finally, the contents were added to 25% methanol before subjecting to CV analysis.

3. Results and discussion

3.1 Cyclic voltammetric study of GSH–CDNB reaction in methanol and effect of pesticides on it

Fig. 1 shows the cyclic voltammetric behavior of the GSH–CDNB reaction catalyzed by GST in the absence of pesticides. The CV produces an intense oxidation peak with the peak maxima at 0.30 V (peak A, current 18.5 μA, RSD 0.62%) that gradually increases with successive CV runs and becomes stable after 20 minutes. Another peak appeared from 0.6 V onwards (peak B, current 10.8 μA, RSD 0.47%), which was due to methanol oxidation, and the one at 0.3 V was attributed to the oxidation of the newly formed complex or intermediate. A low-intensity oxidation peak C that appeared at 0.05 V (RSD 0.21%) in the reverse cycle is attributed to the oxidation of: COH produced through the dissociation of methanol. A low-intensity reduction peak (D) appeared at 0.1 V (RSD 0.35%), which is due to adsorption of H_2 at the platinum surface, which normally shows up in the potential range from −0.23 to +0.20 V.

3.2 Pesticides interaction study

Fig. 2 shows the effect of pesticides on the CV peak at 0.3 V.

Curve b in Fig. 2 shows the CV of the reaction mixture in presence of 100 μL of 25 ppb fenobucarb solution after 30 minutes of incubation. With the addition of increasing amounts of pesticide solution to the mixture and with an incubation time of 30 minutes, the CV peak currents at 0.3 V were further reduced. Similar results were obtained in case of other two pesticides too. The catalytic activity of GST towards GSH–CDNB conjugation reaction was inhibited after exposure to all the three pesticides.

3.3 UV-visible study

The UV-visible spectroscopic method is used to corroborate the results of CV analysis. UV-visible spectra recorded two absorptions: one at 250 nm and the other at 335 nm (curve a, Fig. 3). Addition of these pesticides to the initial mixture suppresses the UV-visible peak to different extents depending on the amount of the pesticide (curve b, Fig. 3). It was also observed that the amount of inhibition was different for different pesticides (Fig. 4).

The peak at 335 nm is due to the new complex or intermediate formed after conjugation, while that at 250 nm is due to methanol. The peak at 335 nm increases with time, which indicates gradual formation of the complex. We found that the 335 nm peak intensity decreased with the increasing pesticide concentration. Concentrations of 50, 30 and 25 ppb of fenobucarb, temephos and dimethoate, respectively, in methanol solution are sufficient for complete inhibition of the reaction in

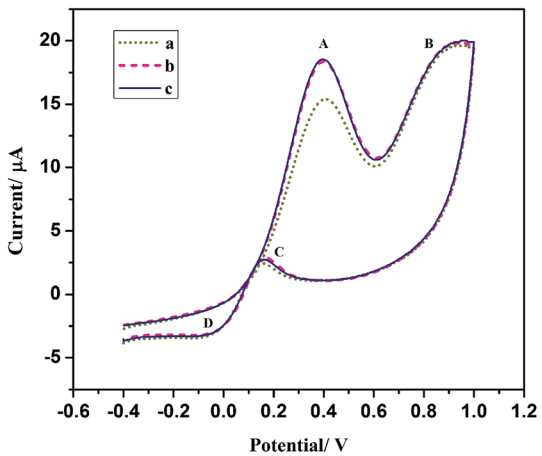

Fig. 1 Cyclic voltammograms recorded in a 1 : 1 volume mixture of 2 mM GSH in PB and 2 mM CDNB in 50% aqueous methanol in presence of 20 μL GST (0.02 mg) at a scan rate of 20 mV s^{-1}. Curve a through curve c is recorded at 15, 20 and 25 minutes, respectively.

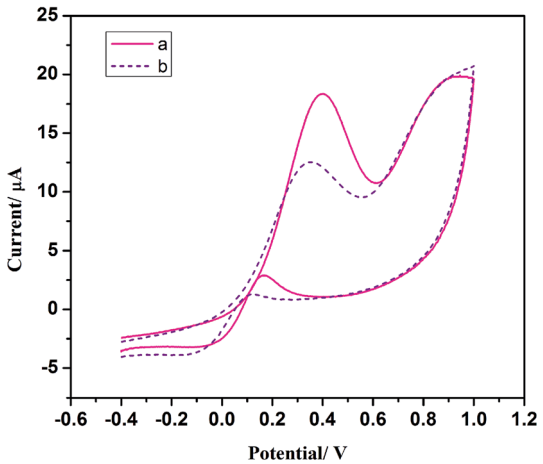

Fig. 2 Cyclic voltammograms recorded in a mixture of 2 mM GSH in PB and 2 mM CDNB in methanol (50%) in presence of 20 μL GST at a scan rate of 20 mV s^{-1}. Curve a, in absence of pesticide; curve b, in presence of 100 μL of 25 ppb fenobucarb.

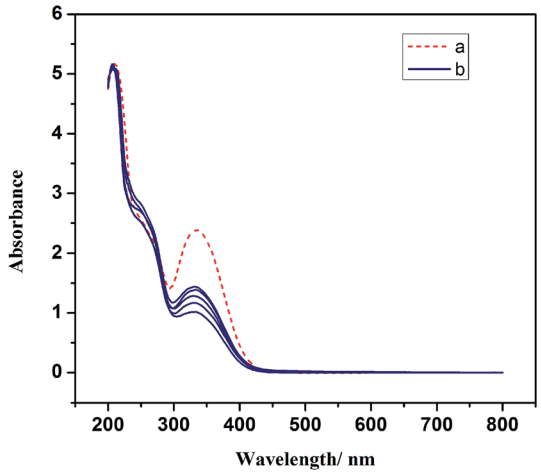

Fig. 3 UV-visible spectra recorded in a solution mixture of GSH (0.5 mmol), CDNB (0.5 mmol), GST (20 μL) and PB–MeOH (25%) in absence of temephos (curve a) and in presence of different concentrations of temephos (curve b).

a standard 3 mL mixture of 2 mM of GSH and 2 mM of CDNB in the presence of 20 μL of GST.

3.4 Optimization of kinetic parameters

To obtain better performance with respect to electrochemical signals from the reaction, we optimized the experimental parameters such as the saturated substrate and enzyme concentrations, the maximum incubation time of the reaction and the maximum inhibition time of the pesticides. The saturated substrate concentration determined through the Michaelis–Menten plot was found to be 2 mM in respect of both CDNB and GSH.[53] Optimized GST amount was determined to be 0.02 mg mL^{-1}, and the maximum incubation time of the reaction was found to be 20 minutes. The maximum inhibition time

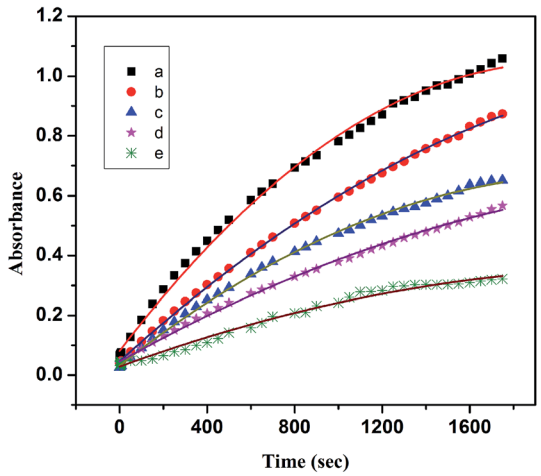

Fig. 4 UV-visible study of the inhibition by the three pesticides through time *versus* absorbance curve. Curve a, enzymatic reaction mixture in the absence of pesticides; curves b–d, enzymatic reaction mixture in the presence of 25 ppb of dimethoate, temephos and fenobucarb, respectively; curve e, inhibition by 50 ppb of fenobucarb solution. The reaction mixture was prepared by mixing 0.5 mmol GSH in PB (pH 6.5) with 0.5 mmol CDNB in 50% MeOH along with 20 μL GST.

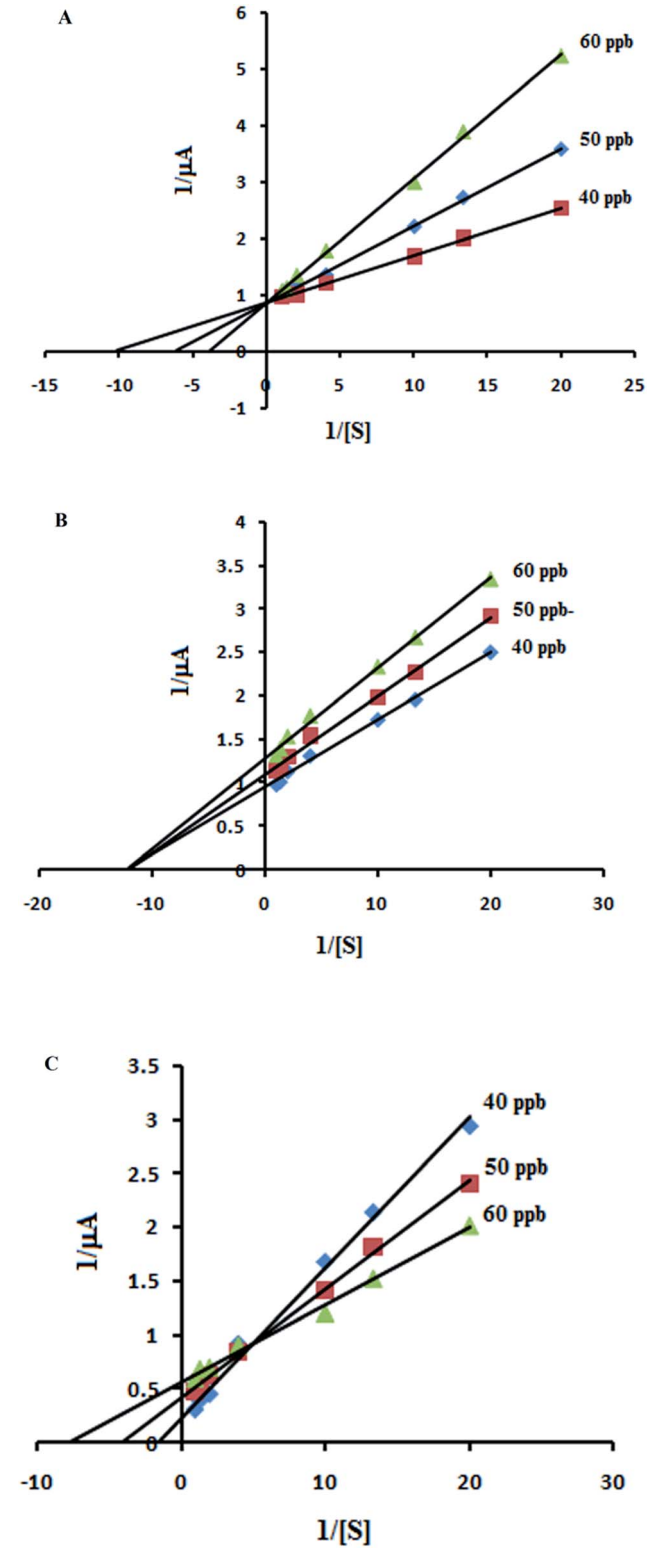

Fig. 5 Lineweaver–Burk plots showing the effect of different concentrations of fenobucarb (5A), temephos (5B) and dimethoate (5C) on the kinetics of GST-catalyzed GSH–CDNB reaction.

was found to vary with pesticides and their concentrations. With the upper limit of pesticide concentration the inhibition was maximum near zero minutes, and the time *versus* absorbance plot in the UV-visible spectra runs almost parallel to the time axis, while in case of lower concentrations of the pesticides the plot runs below the reference (no pesticide mixture) curve in a divergent manner and becomes parallel to the reference curve at about 20 minutes, that is, at the equilibrium time of the GSH–CDNB reaction (Fig. 4). This indicates a fast inhibition (near zero minutes) by the pesticides. However, since peak current comparison is to be done at 20 minutes, which is the incubation time of the reaction, a time of 20 minutes was considered as the maximum inhibition time in this study. The pH value for the reaction was maintained at 6.5 based on literature data.[49]

Fig. 4 shows real-time UV-visible spectroscopic monitoring of the inhibition of the catalytic activity of GST by the three pesticides. It is seen that the inhibitory power of the three pesticides follow the order fenobucarb > temephos > dimethoate.

3.5 Kinetics of inhibition

Enzyme inhibitors may interact with enzymes and/or enzyme–substrate complexes in several different ways to make the activity of an enzyme futile to carry out an enzyme-catalyzed reaction. For each mode of inhibition, it is possible to calculate a dissociation constant, K_i, for the inhibitor that reflects the potential interaction between the enzyme and the inhibitor. It can be said that K_i for an inhibitor is analogous to K_m for a substrate; a smaller K_i value exhibits stronger binding of an inhibitor to an enzyme, whereas a larger K_i value shows weaker binding.

Taking fenobucarb, temephos and dimethoate as the effectors, we probed the effects of these compounds on the activity of GST enzyme while catalyzing the conjugation of GSH to CDNB through the double-reciprocal Lineweaver–Burk plots. Fenobucarb is found to be a competitive inhibitor since increasing the fenobucarb concentration results in a family of lines with a common intercept on the $1/v$ axis and hence a constant V_{max} but with increasing K_m (Fig. 5A). In this type of inhibition, because of their molecular similarity, the inhibitor competes with the substrate for an active site on the enzyme. As a result, the rate of catalysis depends on the relative concentrations of the inhibitor and the substrate. In the presence of a competitive inhibitor, the V_{max} for an enzyme should be the same as that for the uninhibited case. However, the apparent K_m should be larger in the presence of the inhibitor (K_m^{app}). The equilibrium constant for the inhibitor binding with the free enzyme, K_i, was obtained from a plot of K_m^{app}/K_m *versus* the inhibitor concentration $[I_0]$, which is linear, and the slope of the line gave a K_i value of 10.30 mM in this case (Table 1).

The kinetic behaviour of temephos showed a non-competitive mechanism. The Lineweaver–Burk plots yielded a family of straight lines with different slopes and with a common intercept on the *x*-axis. The results are shown in Fig. 5B, indicating that temephos can decrease the apparent value of V_{max} with no effect on K_m. Therefore, it is a non-competitive inhibitor in which the inhibitor does not compete for the same binding site. A non-competitive inhibitor usually binds at a location other than the active site but is able to change the conformation of the active site in such a way that the enzyme is no longer in the optimal arrangement to efficiently catalyze the reaction. The V'_{max} for an enzyme in the presence of a non-competitive inhibitor is less than the one observed under uninhibited conditions, V_{max}. The magnitude of this decrease reflects the strength of the interaction between the enzyme and the inhibitor. However, there is no change in the K_m. The value of the inhibition constant can be obtained from a plot of the vertical intercept $(1/V'_{max})$ *versus* the inhibitor concentration $[I_0]$. The slope of $(1/V'_{max})$ *vs.* $[I_0]$ gives K_i, which is linear and found to be 54.82 mM.

The other major type of inhibition occurs when the inhibitor is capable of binding to both the free enzyme and the enzyme–substrate complex. Herein, dimethoate shows this type of inhibition. In this case, the inhibitor can bind to both E and ES, but with different affinities. It is not possible to calculate a single K_i value for this type of inhibition as the dissociation constant for binding the free enzyme may differ from the dissociation constant for binding the enzyme–substrate complex.

3.6 Quantification of fenobucarb, temephos and dimethoate

The CV method was used to quantify the three pesticides. It was observed that when 50 ppb, 30 ppb and 25 ppb of fenobucarb, temephos, and dimethoate, respectively, were initially mixed with the solution mixture and kept for 20 min., the CV peak at 0.30 V almost disappeared. Fenobucarb, temephos,

Table 1 Kinetic parameters of GST-catalyzed GSH–CDNB reaction in absence and presence of inhibitors

Name of the pesticide (inhibitors)	V_{max}	K_m	K_i (mM)
GSH–CDNB reaction	1.14 (RSD 0.61%)	0.08 (RSD 0.49%)	
Fenobucarb	1.14 (RSD 0.48%)	(i) 0.25 (RSD 0.66%) (60 ppb) (ii) 0.15 (RSD 0.26%) (50 ppb) (iii) 0.09 (RSD 0.79%) (40 ppb)	10.30
Temephos	(i) 0.78 (RSD 0.16%) (60 ppb) (ii) 0.91 (RSD 0.32%) (50 ppb) (iii) 1.05 (RSD 0.43%) (40 ppb)	0.08 (RSD 0.34%)	54.82
Dimethoate	(i) 1.77 (RSD 0.82%) (60 ppb) (ii) 2.38 (RSD 0.77%) (50 ppb) (iii) 4.32 (RSD 0.72%) (40 ppb)	(i) 0.12 (RSD 0.95%) (60 ppb) (ii) 0.23 (RSD 0.68%) (50 ppb) (iii) 0.60 (RSD 0.85%) (40 ppb)	—

and dimethoate solutions of concentrations lower than 50 ppb, 30 ppb and 25 ppb, respectively, when mixed in separate reaction mixtures, were found to suppress the peak current to different extents that were proportional to the concentrations of the pesticides. Based on these observations, calibration curves obtained by plotting the percentage of inhibition, that is, the percentage of reduction in peak current *versus* pesticide concentration, were found to be linear. For determining the concentration based on peak current reduction, two solution mixtures containing GSH–CDNB–MeOH, PB and GST of the exact same composition were prepared, one of which served as the blank. The other was treated with a fixed amount of pesticide, and the difference in CV peak current between the two was noted, which was converted into the percentage of inhibition.

The percentage of inhibition of the biocatalyst was calculated using eqn (1):

$$\text{Inhibition}(\%) = \frac{I_0 - I_i}{I_0} \times 100 \quad (1)$$

where I_o and I_i are the CV peak currents obtained from the mixture before and after mixing pesticides. Triplicate measurements were made at each concentration of the three pesticides. Detection limits were determined by the lowest analyte concentration at which a measurable electrochemical change took place. The limit of detection is considered as the amount of the pesticide in parts per billion required for 10% inhibition and was found to be 2, 4 and 5 ppb for fenobucarb, temephos and dimethoate, respectively (Fig. 6). The linear ranges for the three pesticides are found to be 2–50 ppb ($y = 1.065x + 9.374$; $R^2 = 0.995$), 4–30 ppb ($y = 1.026x + 6.553$; $R^2 = 0.984$) and 5–25 ppb ($y = 0.980x + 5.484$; $R^2 = 0.993$).

3.7 Method validation

The method was validated by the solid-phase extraction method.

Chopped vegetable (tomato) weighing 10 grams was spiked with 5 mL of 50 ppb fenobucarb solution (prepared in acetonitrile) and then homogenized. Then, 5 mL of acetonitrile was added and shaken in a vortex shaker for 5 minutes, sonicated for 5 minutes and then centrifuged for 10 minutes at 2000 rpm. Following this, 5 mL of the supernatant was separated out and passed through a pre-conditioned (acetonitrile–hexane mixture in a 3 : 1 ratio) column of size 14 mm × 160 mm and packed with 5 g each of bondesil-NH_2 and carbon SPE bulk sorbent. The solution passing through the column was collected in a 50 mL round-bottom flask and evaporated to dryness at 40 °C and 200 mbar in the Rotavapor. The dry residue was reconstituted in a mixture of 4 mL methanol and 1 mL dichloromethane and evaporated again to about 1 mL and then diluted to 5 mL by adding more methanol solution. To 1 mL of this solution, 1 mL each of 3 mM GSH and CDNB, and 20 μL GST was added. The percentage of inhibition in peak current was calculated and the amount of pesticide was determined with the help of the calibration curve. The entire process was repeated thrice to get triplicate results. The recovery was found to be 97% (RSD 3.5%).

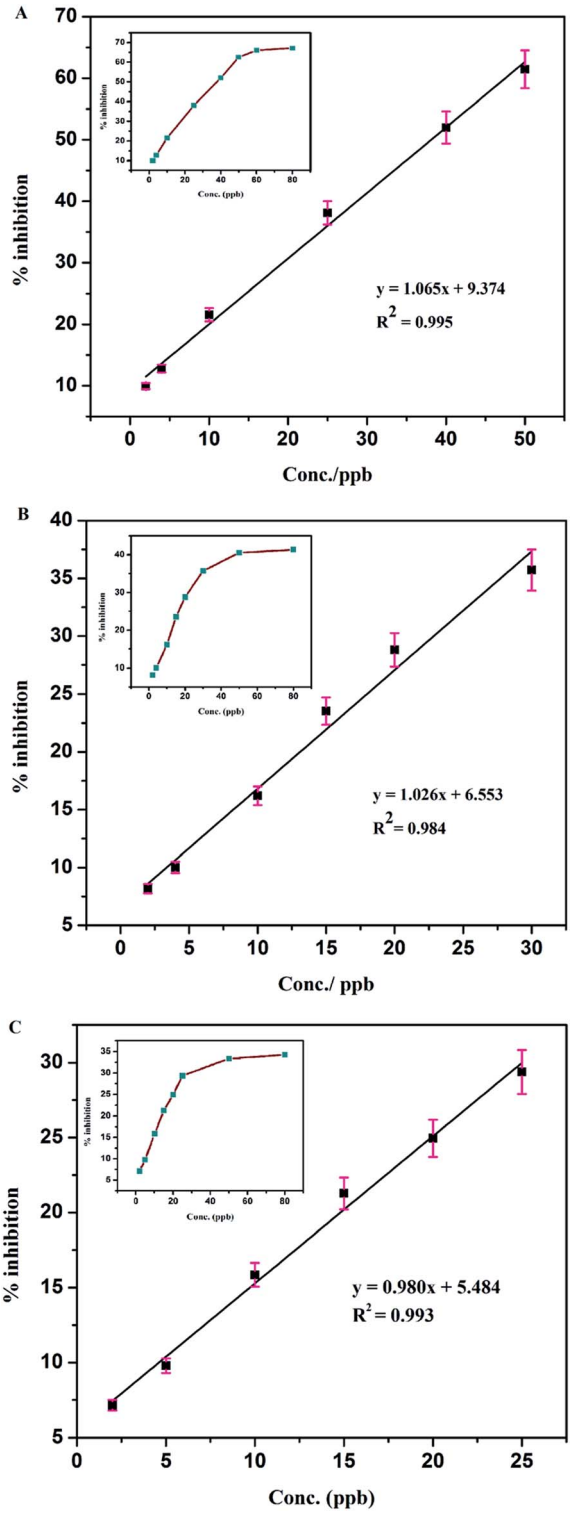

Fig. 6 Calibration curves for the three pesticides studied: (A) fenobucarb, (B) temephos and (C) dimethoate.

The same procedure for validation study was applied for temephos and dimethoate also. Recovery for temephos and dimethoate was found to be 90% (RSD 1.75%) and 83% (RSD 3.12%), respectively.

4. Conclusion

In this study, we have applied the recently developed[53] bioelectrochemical method for detection and quantification of organocarbamate and organothiophosphate pesticides taking fenobucarb, temephos and dimethoate as typical examples. The method uses the GST-catalyzed *in vitro* detoxification reaction between glutathione and 1-chloro-2,4-dinitrobenzene as the benchmark reaction and methanol as the electrolyte. The study proved that the newly developed method is effective for detection and quantification of three classes of pesticides: the pyrethroid, the organocarbamate and the organothiophosphate class. The effectiveness of the method to the former class was demonstrated in our previous study,[53] while the effectiveness of the latter classes is evident from the present study. Organocarbamate fenobucarb shows higher binding affinity to GST (with K_i value 10.35) than temephos (K_i value 54.82). It was also observed that inhibition of GST activity by different members of the same group differs. This is attributed to the structural influence on binding site selectivity and/or on the kinetics. Thus, temephos showed non-competitive inhibition, whereas dimethoate showed a mixed type of inhibition although both belong to the same organothiophosphate group. This shows the possibility of a theoretical study of the inhibitor-enzyme's binding site correlation, a study that is being carried out in our laboratory. Both fenobucarb and temephos are water-insoluble pesticides. Successful application of the method to detect these two water-insoluble pesticides as well as its applicability to different classes of pesticides has proved the versatility of the method. Moreover, since methanol is used as the medium during analysis, the method becomes more practicable because, now the bioanalysis of pesticide is no longer restricted only to the laboratory test samples prepared in a buffer medium or to much diluted field samples. Detection limits of the selected pesticides obtained by the present method are within the range of other reported methods (ref. 54–67 of Table T_1 in ESI†).

Acknowledgements

One of the authors Dr P. Puzari gratefully acknowledges the Ministry of Food Processing Industries (MOFI), Govt. of India for the financial support through project No. SERB/MOFPI/0005/2014.

References

1 T. M. G. Selva and T. R. L. C. Paixão, *New J. Chem.*, 2016, **40**, 2514–2520.
2 P. Fantke and R. Juraske, *Environ. Sci. Technol.*, 2013, **47**, 3548–3562.
3 K. Buonasera, G. Pezzotti, V. Scognamiglio, A. Tibuzzi and M. T. Giardi, *J. Agric. Food Chem.*, 2010, **58**, 5982–5990.
4 T. Yang, Z. Zhang, B. Zhao, R. Hou, A. Kinchla, J. M. Clark and L. He, *Anal. Chem.*, 2016, **88**, 5243–5250.
5 Y. He, B. Xu, W. Li and H. Yu, *J. Agric. Food Chem.*, 2015, **63**, 2930–2934.
6 D. A. Duford, Y. Xi and E. D. Salin, *Anal. Chem.*, 2013, **85**, 7834–7841.
7 Y. Hu, W. Pinkham, L. A. French Jr, D. Frankel and J. F. Vetelino, *Sens. Actuators, B*, 2005, **108**, 910–916.
8 G. H. Yao, R. P. Liang, C. F. Huang, Y. Wang and J. D. Qiu, *Anal. Chem.*, 2013, **85**, 11944–11951.
9 M. Liang, K. Fan, Y. Pan, H. Jiang, F. Wang, D. Yang, D. Lu, J. Feng, J. Zhao, L. Yang and X. Yan, *Anal. Chem.*, 2013, **85**, 308–312.
10 X. Wang, X. Qiao, Y. Ma, T. Zhao and Z. Xu, *J. Agric. Food Chem.*, 2013, **61**, 3821–3827.
11 Q. Zhou, L. Yang, G. Wang and Y. Yang, *Biosens. Bioelectron.*, 2013, **49**, 25–31.
12 K. Dutta, D. Bhattacharyay, A. Mukherjee, S. J. Setford, A. P. F. Turner and P. Sarkar, *Ecotoxicol. Environ. Saf.*, 2008, **69**, 556–561.
13 V. Vamvakaki and N. A. Chaniotakis, *Biosens. Bioelectron.*, 2007, **22**, 2848–2853.
14 M. Trojanowicz, *Electroanalysis*, 2002, **14**, 1311–1328.
15 Z. Zheng, X. Li, Z. Dai, S. Liu and Z. Tang, *J. Mater. Chem.*, 2011, **21**, 16955–16962.
16 F. Arduini, F. Ricci, C. S. Tuta, D. Moscone, A. Amine and G. Palleschi, *Anal. Chim. Acta*, 2006, **580**, 155–162.
17 S. Viswanathan, H. Radecka and J. Radecki, *Biosens. Bioelectron.*, 2009, **24**, 2772–2777.
18 S. Liu, L. Yuan, X. Yue, Z. Zheng and Z. Tang, *Adv. Powder Technol.*, 2008, **19**, 419–441.
19 A. N. Ivanov, L. V. Lukachova, G. A. Evtugyn, E. E. Karyakina, S. G. Kiseleva, H. C. Budnikov, A. V. Orlov, G. P. Karpacheva and A. A. Karyakin, *Bioelectrochemistry*, 2002, **55**, 75–77.
20 H. D. Cancar, S. Soylemez, Y. Akpinar, M. Kesik, S. Göker, G. Gunbas, M. Volkan and L. Toppare, *ACS Appl. Mater. Interfaces*, 2016, **8**, 8058–8067.
21 H. Zhao, X. Ji, B. Wang, N. Wang, X. Li, R. Ni and J. Ren, *Biosens. Bioelectron.*, 2015, **65**, 23–30.
22 X. Sun and X. Wang, *Biosens. Bioelectron.*, 2010, **25**, 2611–2614.
23 T. J. Lin, K. T. Huang and C. Y. Liu, *Biosens. Bioelectron.*, 2006, **22**, 513–518.
24 F. Arduini, A. Amine, D. Moscone and G. Palleschi, *Microchim. Acta*, 2010, **170**, 193–214.
25 B. Kaur and R. Srivastava, *New J. Chem.*, 2015, **39**, 6899–6906.
26 D. N. Kumar, S. A. Alex, N. Chandrasekaran and A. Mukherjee, *RSC Adv.*, 2016, **6**, 64769–64777.
27 Y. Zheng, Z. Liu, H. Zhan, J. Li and C. Zhang, *Anal. Methods*, 2016, **8**, 5288–5295.
28 S. Upadhyay, G. R. Rao, M. K. Sharma, B. K. Bhattacharya, V. K. Rao and R. Vijayaraghavan, *Biosens. Bioelectron.*, 2009, **25**, 832–838.
29 Y. Lin, F. Lu and J. Wang, *Electroanalysis*, 2004, **16**, 1–2.
30 Y. H. Zheng, T. C. Hua, D. W. Sun, J. J. Xiao, F. Xu and F. F. Wang, *J. Food Eng.*, 2006, **74**, 24–29.
31 M. Stoytcheva, R. Zlatev, Z. Velkova, B. Valdez, M. Ovalle and L. Petkov, *Electrochim. Acta*, 2009, **54**, 1721–1727.
32 C. C. M. Martinez, F. Pino, S. Kurbanoglu, L. Rivas, S. A. Ozkanb and A. Merkoçi, *J. Mater. Chem. B*, 2014, **2**, 2233–2239.

33 A. Gutés, F. Céspedes, S. Alegret and M. del Valle, *Biosens. Bioelectron.*, 2005, **20**, 1668–1673.
34 G. A. Melo, M. M. Shimizu and P. Mazzafera, *Phytochemistry*, 2006, **67**, 277–285.
35 W. B. Jakoby, *Adv. Enzymol. Relat. Area. Mol. Biol.*, 1978, **46**, 383–414.
36 P. G. Board and M. W. Anders, *Chem. Res. Toxicol.*, 2007, **20**, 149–154.
37 L. O. Hansson, M. Widersten and B. Mannervik, *Biochemistry*, 1997, **36**, 11252–11260.
38 E. M. Materon, P. J. Huang, A. Wong, A. A. P. Ferreira, M. D. P. T. Sotomayor and J. Liu, *Biosens. Bioelectron.*, 2014, **58**, 232–236.
39 D. Balchin, S. H. Stoychev and H. W. Dirr, *Biochemistry*, 2013, **52**, 9394–9402.
40 T. Olsen, L. Ellerbeck, T. Fisher, A. Callaghan and M. Crane, *Environ. Toxicol. Chem.*, 2001, **20**, 1725–1732.
41 L. F. Chasseaud, *Adv. Cancer Res.*, 1979, **29**, 175–274.
42 P. Jancova, P. Anzenbacher and E. Anzenbacherova, *Biomed. Pap. Med. Fac. Univ. Palacky Olomouc Czech Repub.*, 2010, **154**, 103–116.
43 J. Yin, Y. Kwon, D. Kim, D. Lee, G. Kim, Y. Hu, J. H. Ryu and J. Yoon, *J. Am. Chem. Soc.*, 2014, **136**, 5351–5358.
44 B. Shi, R. Stevenson, D. J. Campopiano and M. F. Greaney, *J. Am. Chem. Soc.*, 2006, **128**, 8459–8467.
45 P. Kapoli, I. A. Axarli, D. Platis, M. Fragoulaki, M. Paine, J. Hemingway, J. Vontas and N. E. Labrou, *Biosens. Bioelectron.*, 2008, **24**, 498–503.
46 W. H. Habig, M. J. Pabst and W. B. Jakoby, *J. Biol. Chem.*, 1974, **249**, 7130–7139.
47 J. Zhang, A. Shibata, M. Ito, S. Shuto, Y. Ito, B. Mannervik, H. Abe and R. Morgenstern, *J. Am. Chem. Soc.*, 2011, **133**, 14109–14119.
48 J. W. Choi, Y. K. Kim, S. Y. Song, I. Lee and W. H. Lee, *Biosens. Bioelectron.*, 2003, **18**, 1461–1466.
49 J. W. Choi, Y. K. Kim, B. K. Oh, S. Y. Song and W. H. Lee, *Biosens. Bioelectron.*, 2003, **18**, 591–597.
50 V. G. Andreou and Y. D. Clonis, *Anal. Chim. Acta*, 2002, **460**, 151–161.
51 R. P. Singh, Y. J. Kim, B. K. Oh and J. W. Choi, *Electrochem. Commun.*, 2009, **11**, 181–185.
52 T. I. S. Oliveira, M. Oliveira, S. Viswanathan, M. F. Barroso, L. Barreiros, O. C. Nunes, J. A. Rodrigues, P. L. Neto, S. E. Mazzetto, S. Morais and C. D. Matos, *Talanta*, 2013, **106**, 249–254.
53 H. Borah, R. R. Dutta, S. Gogoi and P. Puzari, *Electrochim. Acta*, 2016, **205**, 198–206.
54 M. G. Sales, M. Carmo, V. F. Vaz, C. D. Matos, S. A. A. Almeida, M. F. Barroso and H. A. O. Ferreira, *Int. J. Environ. Anal. Chem.*, 2008, **88**, 37–49.
55 K. H. Park, J. H. Choi, A. M. Abd El-Aty, M. M. Rahman, J. Jang, A. Y. Ko, K. S. Kwon, H. R. Park, H. S. Kim and J. H. Shim, *Food Chem.*, 2013, **138**, 2306–2311.
56 T. D. Nguyen, E. M. Han, M. S. Seo, S. R. Kim, M. Y. Yun, D. M. Lee and G. H. Lee, *Anal. Chim. Acta*, 2008, **619**, 67–74.
57 A. Laganh, G. D'Ascenzo, G. Fago and A. Marino, *Chromatographia*, 1997, **46**, 256–264.
58 S. Lacorte and D. Barcelo, *Anal. Chim. Acta*, 1994, **296**, 223–234.
59 C. Blasco, P. Vazquez-Roig, M. Onghena, A. Masia and Y. Picó, *J. Chromatogr. A*, 2011, **1218**, 4892–4901.
60 S. Lacorte and D. Barcelo, *J. Chromatogr. A*, 1995, **712**, 103–112.
61 D. Du, M. Wang, J. Cai and A. Zhang, *Sens. Actuators, B*, 2010, **146**, 337–341.
62 X. Huang, D. Du, X. Gong, J. Cai, H. Tu, X. Xu and A. Zhang, *Electroanalysis*, 2008, **20**, 402–409.
63 Y. Yang, M. Guo, M. Yang, Z. Wang, G. Shen and R. Yu, *Int. J. Environ. Anal. Chem.*, 2005, **85**, 163–175.
64 P. R. Solanki, N. Prabhakar, M. K. Pandey and B. D. Malhotra, *Biomed. Microdevices*, 2008, **10**, 757–767.
65 A. Kaushik, P. R. Solanki, A. A. Ansari, B. D. Malhotra and S. Ahmad, *Biochem. Eng. J.*, 2009, **46**, 132–140.
66 H. J. Lee, G. Shan, K. C. Ahn, E. K. Park, T. Watanabe, S. J. Gee and B. D. Hammock, *J. Agric. Food Chem.*, 2004, **52**, 1039–1043.
67 A. Gupta, N. Prabhakar, R. Singh, A. Kaushik and B. D. Malhotra, *Thin Solid Films*, 2010, **519**, 1122–1127.

Journal of Electroanalytical Chemistry 828 (2018) 116–123

Contents lists available at ScienceDirect

Journal of Electroanalytical Chemistry

journal homepage: www.elsevier.com/locate/jelechem

A broad spectrum amperometric pesticide biosensor based on glutathione *S*-transferase immobilized on graphene oxide-gelatin matrix

Himadri Borah, Sudarshan Gogoi, Shyamali Kalita, Panchanan Puzari*

Department of Chemical Sciences, Tezpur University, Tezpur, Assam 784028, India

ARTICLE INFO

Keywords:
GST
CDNB
Pesticide biosensors
Substrate specificity
Dinocap
Competitive inhibitor

ABSTRACT

In this work we have fabricated a glutathione-*S*-transferase based amperometric biosensor for pesticides by immobilizing the enzyme on platinum electrode using graphene oxide-gelatin matrix, evaluated various biosensor parameters, applied the same for detection and quantification of four different classes of pesticides and validated the biosensor results with GC–MS analysis. The enzyme immobilization was confirmed through scanning electron microscopy, electrochemical impedance spectroscopy, cyclic voltammetry and chronoamperometry. The apparent Michaelis-Menten constant for the immobilized glutathione-*S*-transferase in the said matrix was found to be 0.083 mmol L^{-1} and 0.15 mmol L^{-1} respectively for glutathione and 1-Chloro-2,4-dinitrobenzene. Substrate specificity found to be $2.56 \times 10^7\ s^{-1}\ M^{-1}$ for glutathione and $2.15 \times 10^7\ s^{-1}\ M^{-1}$ for 1-Chloro-2,4-dinitrobenzene. Pesticide analysis was done in 25% methanol solution. The biosensor is a promising new tool for pesticide analysis as it can be applied for analysis of a broad spectrum of pesticides covering at least six different classes namely - benzamidazole, organochlorine, organothiophosphate, organocarbamate, polyphenol and pyrethroid.

1. Introduction

In recent time development of robust field deployable analytical equipment with high sensitivity, fast response, and reusability for pesticides and other environmental pollutants in less than micro molar amount gaining significant research importance [1,2]. The demand for such newer analytical techniques arising due to the drawbacks associated with the traditional analytical techniques such as gas chromatography–mass spectrometry (GC–MS), High performance liquid chromatography (HPLC), liquid chromatography-mass spectrometry (LC-MS) etc. These techniques, though reliable, require expensive and high maintenance instruments, time consuming sample pre-treatment, and highly expert technicians, thus making them unsuitable for field deployment as well as routine analysis [3,4]. Different newer techniques have been developed such as enzyme inhibition based electrochemical biosensors [5,6], Enzyme linked immunosorbent assays [7,8], surface plasmon resonance [9,10] and quantum dots [11,12]. Among these newer techniques the enzyme inhibition based electrochemical biosensors are extensively studied due to their capabilities of detection in nano-molar quantity, fast response, reliability and miniaturization feasibility. In such sensors the enzyme is immobilized on to the surface of a solid electrode with suitable support matrix.

Immobilization matrix plays a crucial role in the functioning of such biosensors. Different immobilization matrices have been used for immobilization of enzymes such as conducting polymers [13,14], carbon nanotubes [15,16], graphene oxide [17,18], silica sol-gel [19,20] and clay material [21]. Graphene oxide has been attracting the attention of researchers at present time. They have excellent conductivity and biocompatibility [22,23].

Though many enzyme biosensors have been developed for pesticide detection there still remains some limitations in their practical utilization. Two obvious limitations are 1. their class specificity and 2. inability to operate in organic solvents. The enzymes used in pesticide biosensors are class specific, e.g., organophosphate hydrolase for organophosphates [24,25], acetylcholinesterase for organophosphates and organocarbamates [26,27], tyrosinase for phenolic classes [28]. On the other hand the inhibition based enzyme biosensors cannot operate in organic solvents [29]. Few workers have reported the use of 5% acetonitrile as the solvent but this causes excessive dilution of the sample and also affects the reusability of the biosensor [30]. Attempting to address these two problems, in a recent work we have shown that the enzyme glutathione-*S*-transferase (GST) can be used for electrochemical biosensing of pesticides in a moderately high concentration (25%) of methanol [31]. In the present work we have shown that the detection protocol can be used to fabricate biosensor probes through immobilization of GST in graphene oxide and can be used for detection of

* Corresponding author.
E-mail address: pancha@tezu.ernet.in (P. Puzari).

https://doi.org/10.1016/j.jelechem.2018.09.047
Received 15 May 2018; Received in revised form 20 September 2018; Accepted 25 September 2018
Available online 27 September 2018
1572-6657/

a wide varieties of pesticide classes. To our knowledge this is for the first time that the enzyme GST has been immobilized using graphene oxide matrix for electrochemical biosensor application. Advantages of the immobilized GST biosensor over the free enzyme technique is obvious from the facts that 1. it is reusable for 8–10 consecutive measurements thus offering cost efficiency and 2. it can be used in chronoamperometric mode, thus showing the feasibility of real time monitoring application. The biosensor can be applied to detect a broad spectrum of pesticides covering at least six different classes namely - benzamidazole, organochlorine, organothiophosphate, organocarbamate, polyphenol and pyrethroid. Typical pesticides selected from each class and their allowed MRL values as per regulations of the European Union [32] are - carbendazim (0.1–2 mg/kg), DDT (0.05 mg/kg), ethion (0.01–5 mg/kg) and chlorpyrifos (0.01–5 mg/kg), fenobucarb (0.01 mg/kg)[1], Dinocap (0.02–0.1 mg/kg) and cypermethrin (0.05–2 mg/kg). Application to pyrethroids (cypermethrin) and organocarbamates (fenobucarb) were demonstrated in our earlier work [31,33]. Herein we have demonstrated the application of the method to the remaining four classes.

2. Experimental

2.1. Materials and reagents

GST (from equine liver, EC 2.5.1.18), 1-Chloro-2,4-dinitrobenzene (CDNB), glutathione reduced (GSH) and graphite powder (analytical standard) were purchased from Sigma–Aldrich. KH_2PO_4, K_2HPO_4, $NaNO_3$, $KMnO_4$, HCl, H_2SO_4 and methanol is of analytical reagent grade and purchased from Merck chemicals. DDT and Dinocap procured from Dr. Ehrenstorfer; ethion, carbendazim and chlorpyrifos from PESTANAL-Sigma.

The GST solution was prepared in phosphate buffer saline (PBS) of pH 6.5 and stored at −22 °C. GSH stock solution was prepared in phosphate buffer (PB) of pH 6.5. CDNB solution was prepared in 50% aq. methanol so as to maintain the final percentage of methanol 25%. Distilled methanol was diluted to 50% using ultra-pure water from a Millipore Milli-Q system. The stock solutions of pesticides were prepared in methanol and diluted to the appropriate concentration for further use. All the solutions except GST were prepared regularly before experiments.

2.2. Instrumentation

Electrochemical measurements and impedance analysis were performed at 30 (± 0.05)°C, using Biologic SP-300 potentiostat-galvanostat with a three-electrode cell setup comprised of Pt electrode (3 mm), Pt wire counter electrode and Ag/AgCl reference electrode. The infrared spectra were recorded in a Perkin Elmer Frontier MIR-FIR spectrometer. The X-ray diffraction (XRD) study was carried out at room temperature (ca. 298 K) using D8 Focus (Bruker AXS, Germany) in the range of 2θ = 5°–70°. Agilent7890A Gas Chromatogram was used for GC–MS analysis. The scanning electron microscopic (SEM) analysis was conducted on JSM-6390LV (Jeol, Japan) with an energy dispersive X-ray detector.

2.3. Synthesis of graphene oxide

Graphene oxide (GO) was synthesized using modified Hummers method [34]. In brief, graphite powder (0.5 g) and $NaNO_3$ (0.5 g) were mixed with 23 mL of H_2SO_4 (98%) in a conical flask and kept stirring over an ice bath (0–5 °C) for 4 h. 3.0 g of potassium permanganate was added to it slowly under stirred, ice cold condition. Continued the stirring for 1 h after which the ice bath was removed. Next, heated the mixture up to 35 °C and stirred for another 1 h. The mixture was then diluted through very slow addition of 46 mL of water under stirring condition which led to an increase of temperature up to 95^0C. Kept at this temperature for 2 h. Then the mixture was cooled down to room temperature and then added 100 mL distilled water under stirring and continued the stirring for 1 h. The solution was finally treated with 10 mL of 30% H_2O_2 so as to obtain a bright yellow color. Then allowed to stay undisturbed for 3–4 h, whereby solid particles settled at the bottom. The supernatant water was poured to filter. The resulting mixture was washed repeatedly by centrifugation with 5% HCl and then with deionized (DI) water several times until it forms gel like substance (pH - neutral). After centrifugation, the gel like substance was vacuum dried at 60 °C for more than 6 h to get GO powder.

2.4. Biosensor preparation

The platinum working electrode was cleaned at first by polishing with aqueous slurry of alumina followed by treatment with piranha solution (1:3 (v/v) 30% H_2O_2 and concentrated H_2SO_4) and finally rinsing with copious amounts of deionized water. GO-gelatin mixture was prepared by sonicating a suspension of 2.0 mg of GO in 1.0 mL of 5% gelatin solution (prepared by warming the gelatin-water mixture up to 60 °C) for 10 min. 20 μL of the homogeneous GO-gelatin mixture was drop casted at the tip of the cleaned platinum electrode keeping the electrode vertical and allowed to be dried in ambient air for 1 h. Then 20 μL of GST solutions (0.02 mg) was added to it and allowed to stay at room temperature for 2 h. Finally 20 μL of glutaraldehyde (35% in water) was added to it and kept the electrode at room temperature in the same vertical position until the film appeared dry (for approximately 4 h). The prepared sensor was stored at 4 °C when not in use.

2.5. Analysis procedure

2.5.1. Electrochemical measurements

Cyclic voltammetric (CV) measurements were done in the potential range from −0.4 V to 1 V, at scan rate 20 mV/s. Chronoamperometric (CA) analysis was done by setting the parameters as E_0 = 0.0 V applied for 30 s, E_1 = 0.30 V applied for 100 s.

Cleaning of all electrodes was done before each experiment. Platinum electrode was cleaned by polishing in γ-Al_2O_3 (0.05 μM) until a shiny surface was obtained and sonicated for 5–10 min using digital ultrasonic cleaner. Electrodes were then dipped in PB and cycled from −0.1 to 0.1 V until it acquired a steady state baseline. Prior to electrochemical measurement the solution mixtures were mixed thoroughly and then the measurements were done in static solution condition. The total volume of the working solution in the electrochemical cell was 3 mL and prepared by mixing 1.5 mL of 2 millimolar GSH in PB with 1.5 mL of 2 millimolar CDNB in 50% methanol, unless stated otherwise.

2.5.2. Gas chromatographic measurements

A gas chromatogram with auto injector system was used for pesticide analysis. Ultra pure helium was used as the carrier gas at constant flow rate of 1.0 mL/min. The injector and detector temperatures were set at 250 °C. The oven temperature was programmed as follows: initial 80 °C hold 5 min and then programmed from 80 to 250 °C at 15 °C/min and hold for 20 min. The total time for one GC run was 36 min. and injected volume was 1 μL each time through auto injection mode.

3. Results and discussion

3.1. Characterization

X-ray diffraction spectra (Fig. 1), of GO showed peak at 2θ = 10.36° which is very close to the reported XRD pattern of GO corresponding to (001) crystal plane. Fourier transform infrared (FTIR) spectrum shows

[1] Default MRL of Reg. (EC) 396/2005. Currently not approved by the European Union.

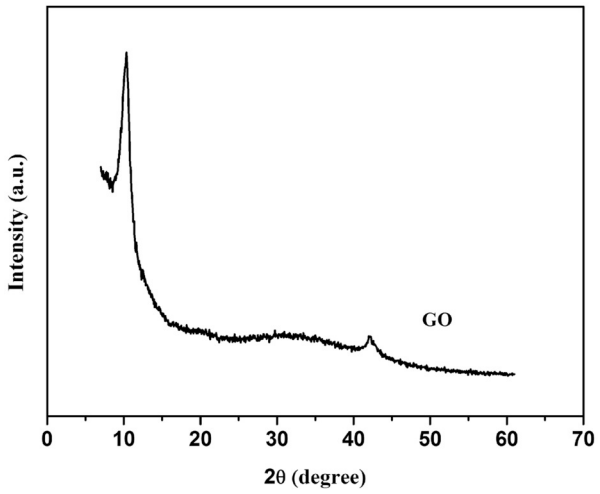

Fig. 1. X-ray diffraction pattern of synthesized graphene oxide.

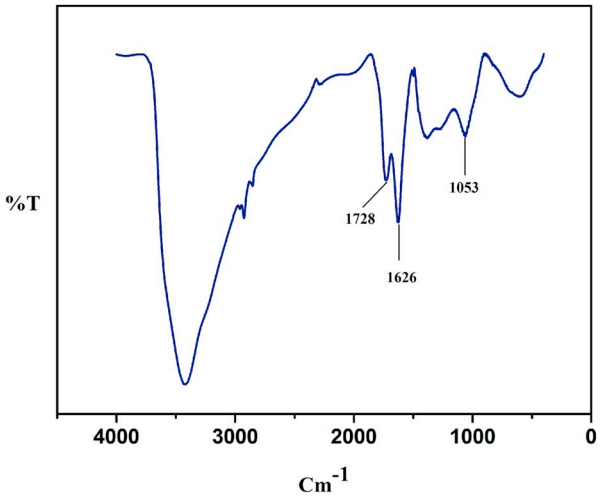

Fig. 2. Fourier transform infrared spectrum of synthesized graphene oxide.

(Fig. 2) the presence of O—H stretching vibrations (3429 cm^{-1}), C═O stretching vibration (1728 cm^{-1}), C═C vibrations of unoxidized sp^2 CC bonds (1626 cm^{-1}), and C—O vibrations (1053 cm^{-1}) which are characteristic peaks of GO as per literature [35].

Morphology of the fabricated electrode was studied by SEM analysis. SEM images of graphene oxide, gelatin - glutaraldehyde - graphene oxide composite film (GO/Gel/Glut) and GST immobilized composite film (GO/Gel/GST/Glut) are shown in Fig. 3. SEM images clearly shows the flake type morphology of GO (Fig. 3a) and the well dispersed thread shaped enzyme units (Fig. 3c) within the matrix.

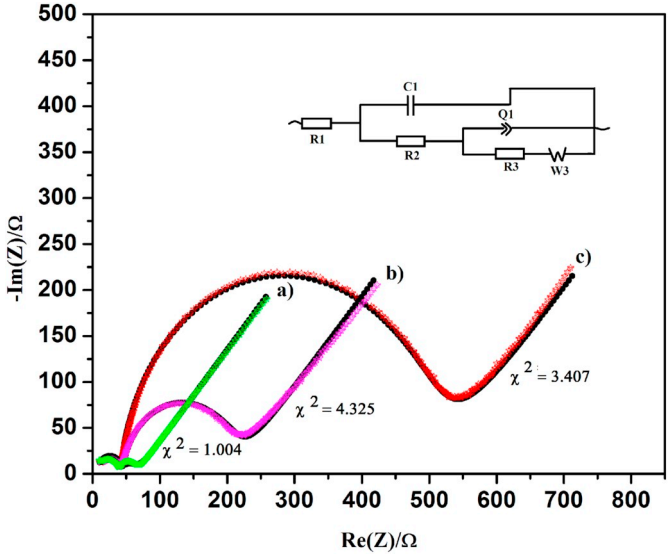

Fig. 4. Nyquist plot of a) bare Pt electrode b) Pt/GO/Gel/Glut and c) Pt/GO/Gel/GST/Glut in 0.1 M KCl containing 0.5 mM $K_3[Fe(CN)_6]$ and 0.5 mM $K_4[Fe(CN)_6]$. Black solid lines represent experimental data and colored lines represent theoretical data. Inset: Best fit circuit model for evaluation of the parameters. Complete list of parameters are provided in the supporting information (Table ST1).

3.2. Electrochemical impedance measurements

Electrochemical impedance spectroscopy (EIS) is an effective tool to characterize electrode modifications by studying the interfacial properties. Fig. 4 shows the typical Nyquist plots obtained for bare Pt, Pt/GO/Gel/Glut, and Pt/GO/Gel/GST/Glut in 0.1 M KCl with equimolar (0.5 mM) $Fe(CN)_6^{3-/4-}$ mixture, when the working frequency range was 1 Hz to 7 MHz and the applied potential was 0.3 V. Theoretical fitting was done by applying Levenberg-Marquard algorithm using 'ZFit-Bio-Logic' software. Charge transfer resistance R_{ct} found to be 27.29 Ω for bare Pt electrode (curve a), 164.2 Ω for Pt/GO/Gel/Glut modified electrode (curve b) and 460.3 Ω for Pt/GO/Gel/GST/Glut modified electrode (curve c). As expected, R_{ct} increased when Pt electrode was coated with GO-gelatin mixture. It increased further when GST was loaded. This increase in the R_{ct} value is due to the fact that most biological molecules (including enzymes) are poor electrical conductors and hence cause hindrance to the electron transfer. This is the direct evidence of successful immobilization of GST on the electrode surface.

3.3. Cyclic voltammetric behavior

Fig. 5 shows the cyclic voltammetric behavior of the GSH-CDNB reaction with GST immobilized Pt working electrode in absence (curve

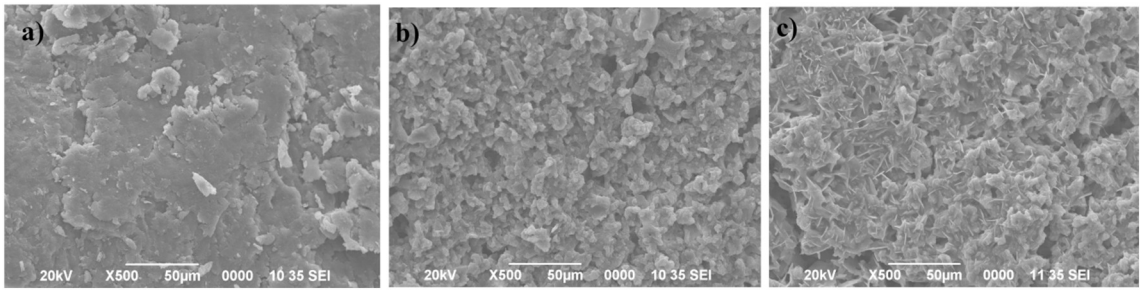

Fig. 3. SEM images of (a) graphene oxide (b) graphene oxide-gelatin-glutaraldehyde composite film (c) GST immobilized graphene oxide-gelatin-glutaraldehyde composite film.

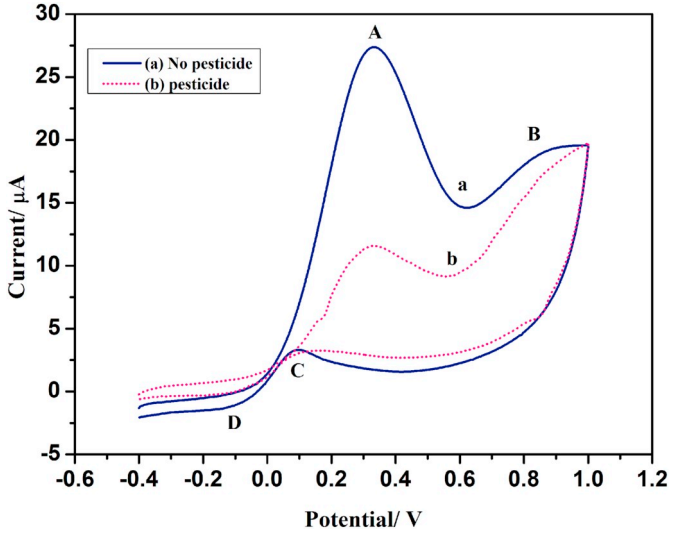

Fig. 5. Cyclic voltammograms recorded in a 1:1 volume mixture of 2 mM GSH in PB and 2 mM CDNB in 50% aqueous methanol in presence of Pt/GO/Gel/GST/Glut electrode at scan rate 20 mV/s. Curve 'a' obtained before inhibition and 'b' after inhibition.

'a') and in presence (curve 'b') of pesticides. The CV produces intense oxidation peak with peak maxima at 0.30 V (peak A, current 27.5 μA, RSD 0.82%) that gradually increases with successive CV runs and get stable after few runs. Another peak appeared from 0.60 V onwards (peak B, current 29.6 μA, RSD 0.97%). The peak from 0.60 V onwards is due to methanol oxidation, the one at 0.30 V is attributed to oxidation of newly formed complex or intermediate. A low intensity oxidation peak C appeared at 0.05 V (RSD 0.31%) in the reverse cycle is attributed to oxidation of: COH produced through dissociation of methanol. Low intensity reduction peak (D) appeared at 0.10 V (RSD 0.55%) is due to adsorption of H_2 at the platinum surface which normally shows up in the potential range from −0.23 to +0.20 V [36]. In presence of pesticides the intensity of peak A decreases (curve 'b').

3.4. Chronoamperometric study

Inhibition was studied by two step procedure, measuring the chronoamperometric responses before and after immersing the sensor probe (Pt/GO/Gel/GST/Glut) in pesticide solution. Typical chronoamperometric sensing responses are shown in Fig. 6. Curve 'a' is the initial response of the sensor to 2 mmol GSH-CDNB solution and curve 'b' is the response after incubating the sensor in 50 ppb chlorpyrifos solution for 10 min. Fig. 6 clearly indicates that, as a result of inhibition, amperometric response of the biosensor decreases. During successive analysis the sensor was reactivated using PB solution.

3.5. Sensor operational parameters

Sensor operational parameters such as apparent Michaelis-Menten constants, saturated substrate concentration, optimum pH, optimum inhibition time, intra and interstate precession, reusability and storage stability were determined.

3.5.1. Saturated substrate concentration

The saturated substrate concentration for both GSH and CDNB were determined through the Michaelis–Menten plot (Fig. 7) measuring the variation of amperometric response with substrate concentration in CA mode. Concentration of one substrate was kept constant at 2 mmol while varying the concentration of the other in the full range. The saturated substrate concentration for both the substrates was found to be 4 mmol L^{-1}. The apparent Michaelis–Menten constant, K_m^{app} was

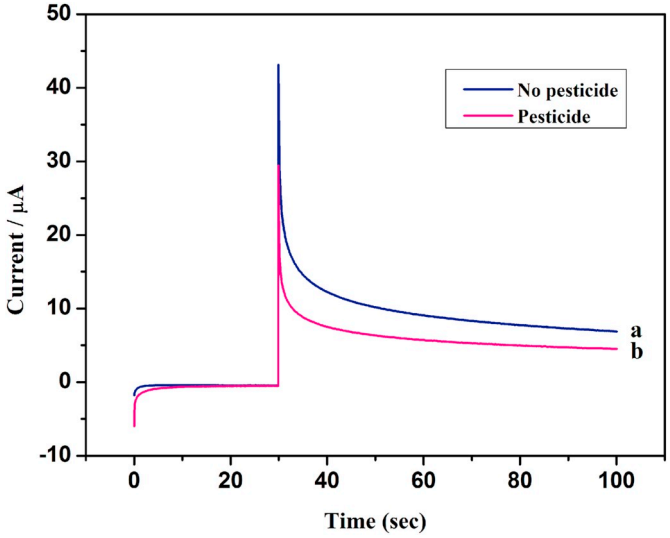

Fig. 6. Chronoamperometric responses of the biosensor towards 1:1 GSH-CDNB solution (a) in absence of inhibitor and (b) in presence of inhibitor.

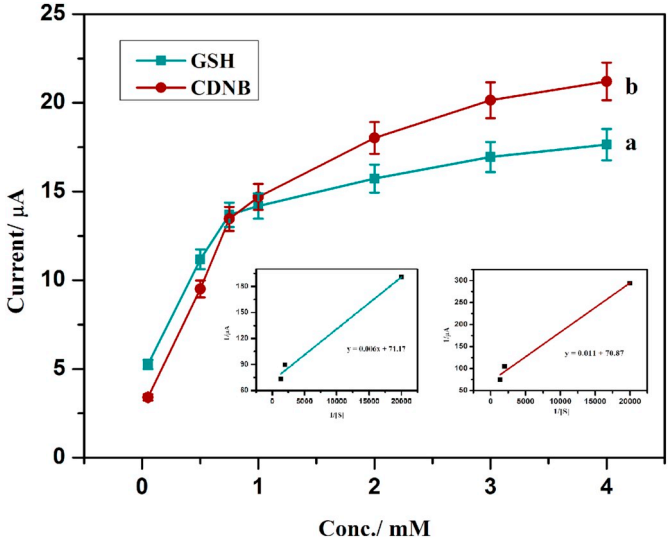

Fig. 7. Variation of sensor response with substrate concentration with 0.02 mg of immobilized enzyme. Inset: Lineweaver-Burk plot for determination of K_m^{app} for both GSH and CDNB.

evaluated through the Lineweaver-Burk plot (Eq. (1)) and found to be 0.083 mmol L^{-1} for GSH and 0.15 mmol L^{-1} for CDNB. The observed value of K_m^{app} for GSH is lower than that reported in our previous study in which the enzyme was in the free state [31]. The K_m^{app} value for CDNB on the other hand found to be 0.15 mmol L^{-1}, which is almost similar to the previously reported value. Lowering of K_m^{app} value of GSH in the immobilized state indicates stronger binding of it with the enzyme in the immobilized state. Stronger binding of GHS over CDNB is also obvious from the substrate specificity values. Substrate specificity found to be $2.56 \times 10^7\ s^{-1}\ M^{-1}$ and $2.15 \times 10^7\ s^{-1}\ M^{-1}$ respectively for GSH and CDNB as substrate. The values indicate that GST has higher affinity for GSH than CDNB as substrate. Detail procedure used for calculation of substrate specificity is given in the supporting information.

$$\frac{1}{i} = \frac{1}{i_{max}} + \frac{k_m^{app}}{i_{max}} \frac{1}{[S]} \quad (1)$$

3.5.2. Effect of pH

The pH dependence of the enzyme electrode over the pH range 6.0–8.0was studied through cyclic voltammetry. Fig. S1 shows the cyclic voltammetric response of the sensor towards 2 mM GSH and CDNB at different solution pH. The maximum peak current was obtained at pH 8.0.

3.5.3. Incubation time

The effect of inhibition time on the degree of inhibition was studied for the five pesticides taking a 100 ppb solution of each (Fig. S2). Maximum inhibition time of each pesticide was found to be 20 min. The percentage inhibition of the biocatalyst was calculated using Eq. (2).

$$Inhibition(\%) = \frac{I_0 - I_i}{I_0} \times 100 \quad (2)$$

where I_o and I_i are the CV peak currents obtained from the mixture before and after mixing pesticides.

3.5.4. Enzyme reactivation studies

For reactivation of the inhibited enzyme, the inhibited sensor was immersed in a solution of phosphate buffer (0.1 M) of pH 6.5 for 10 min. When the inhibition is less than 10%, 95–98% reactivation occurred. But when the percent inhibition is beyond 10%, reactivation efficiency decreased significantly. Reactivation efficiency was calculated by using Eq. (3) [16].

$$Reactivation(\%) = \frac{(I_a - I_s)}{(I_0 - I_s)} \times 100 \quad (3)$$

where I_0 is the maximum peak current of the sensor in 2.0 mM each of GSH and CDNB, I_s is the peak current after inhibition and I_a is the same after reactivation.

3.5.5. Enzyme leaching test

One of the main problems associated with biosensor's use is leaching out of the bioreceptor from the electrode to the solution matrix, which affects the reproducibility of the analysis. A successful immobilizing material should thus not only stabilize the enzyme, but also restrain the enzyme from leaching out to the test solution. Experiment was performed to check if any trace amount of enzyme can leach out from the immobilization matrix during electrochemical treatment of the sensor. This was done by performing several blank CV runs with the sensor, taking PB as the electrolyte followed by subjecting the same electrolyte to the assay procedure developed by Habig et al. [37] preparing CDNB in 50% methanol (the final methanol concentration in the assay was 25%). Absence of enzyme leakage was confirmed through the observation that no increase in UV–vis absorption at 335 nm occurred as compared to the blank for a period of 30 min.

3.5.6. Precision measurement

Inter-assay precision of the sensor was determined by measuring the CV response of six different fabrications when run in solution mixture comprised of 2 mmol each of GSH and CDNB. The relative standard deviation (RSD) of the measurements was calculated. A value of 5.53% was obtained which indicates a good reproducibility of the fabrication process.

The intra state precision was determined by evaluating the RSD of sensor response for eight continuous CV runs with a single fabrication, using equimolar GSH-CDNB solution. The RSD was found to be 0.42%, which indicates that the sensor response has acceptable precision for consecutive measurements of GSH-CDNB reaction.

3.5.7. Storage and operational stability

To study the storage stability, a freshly prepared sensor after initial treatment kept at −20 °C for 30 days. No significant loss in enzyme activity was found at the end of 30 days. We observed that the stored sensor when subjected to continuous analysis at the end of the stored period (30 days) gave stable value up to 8–10 measurements.

3.6. Quantification of pesticides

CV method was used to quantify all the five pesticides. It was observed that when 50 ppb, 200 ppb, 150 ppb, 300 ppb and 400 ppb each of carbendazim, chlorpyrifos, DDT, Dinocap and ethion respectively was mixed initially to six different solution mixtures and kept for 20 min., the CV peak at 0.30 V almost disappeared. Concentrations of these pesticides lower than the aforementioned ones when mixed in separate reaction mixtures, found to suppress the peak current up to the extent proportional to the concentration. Based on this observation, calibration curves were obtained by plotting percentage inhibition versus pesticide concentration and was found to be linear. For determining the concentration based on peak current reduction, two solution mixtures containing GSH-CDNB-MeOH and PB of exactly same composition were prepared, one of which served as the blank. Triplicate measurements were made at each concentration of the five pesticides. Limit of detection is considered as the ppb of the pesticide required for 10% inhibition and found to be 2, 60, 40, 50 and 100 ppb respectively for carbendazim, chlorpyrifos, DDT, Dinocap and ethion. The linear ranges for the five pesticides are found to be 2–50 ppb ($y = 1.158x + 9.1113$; $R^2 = 0.998$) for carbendazim, 60–200 ppb ($y = 0.492x - 21.14$; $R^2 = 0.998$) for chlorpyrifos, 40–150 ppb ($y = 0.412x - 2.810$; $R^2 = 0.989$) for DDT, 50–300 ppb ($y = 0.248x - 8.577$; $R^2 = 0.999$) for Dinocap and 100–400 ppb ($y = 0.154x - 6.598$; $R^2 = 0.995$) for ethion. Fig. S3 shows the various calibration curves.

Comparison of the LODs with the MRL values of those pesticides infers that the method can be applied for checking the MRLs of DDT, carbendazim and cypermethrin in all kinds of food and agricultural commodities covered by the EU database. However, as regard to Dinocap, ethion and chlorpyrifos analysis is concerned, the method can be applied in select cases only. Table ST2 lists few examples of

Table 1
Comparison of the performance of the present biosensor with other reported biosensors.

Pesticides	Method of detection	Limit of detction (LOD)	Linear range	Ref.
Carbendazim	DNA Aptamer based biosensor immobilized on gold surface	0.0082 ppb	0.01 ppb–10 ppb	[38]
	GST biosensor using graphene oxide	2 ppb	2–50 ppb	This work
Chlorpyrifos	Acetylcholinesterase (AChE) immobilized on Fc-F hydrogel support	1.00 ppb	1.75–263 ppb	[39]
	GST biosensor using graphene oxide	60 ppb	60–200 ppb	This work
DDT	Surface plasmon resonance (SPR) based immunosensor	0.015 ppb	Not reported	[40]
	Gold nanoparticles (GNPs) based immunoassay	27 ppb	27–1000 ppb	[41]
	GST biosensor using graphene oxide	40 ppb	40–150 ppb	This work
Dinocap	GST biosensor using graphene oxide	50 ppb	50–300 ppb	This work
	No other biosensing method reported so far.	–	–	–
Ethion	Butyrylcholinesterase biosensor based on multi-walled carbon nanotube–polyvinyl chloride (MWNT–PVC) composite	22 ppb	22–330 ppb	42
	GST biosensor using graphene oxide	100 ppb	100–400 ppb	This work

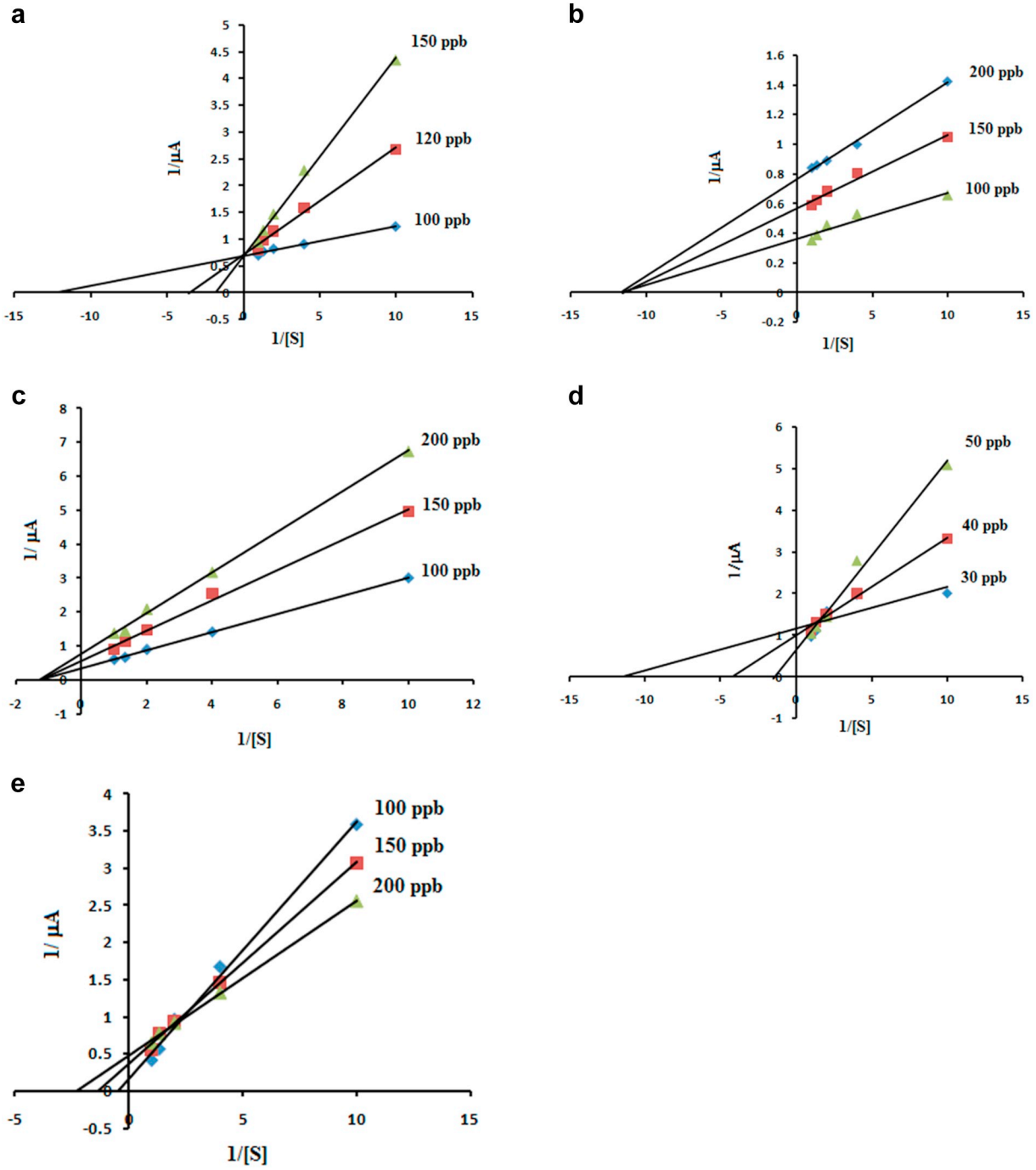

Fig. 8. Lineweaver–Burk plots showing the effect of different concentrations of (a) DDT (b) Chlorpyrifos (c) Ethion (d) Carbendazim and (e) Dinocap on the kinetics of GST-catalyzed GSH–CDNB reaction.

commodities to which the method can be applied for risk management of the selected pesticides.

Table 1 shows a comparison of the performance of the present biosensor with few other biosensors reported in literature. Although the present method offers slightly higher LODs as compared to other biosensors such as DNA aptamer based biosensors and acetylcholinesterase (AChE) based biosensors, yet the method is able to meet the required sensitivity for residue analysis of the selected pesticides in majority of the agricultural commodities as per the EU guidelines.

3.7. Kinetics of inhibition

Enzyme inhibitors may interact with enzymes and/or enzyme–substrate complexes in several different ways to make the activity of an enzyme futile to carry out an enzyme-catalyzed reaction. In most cases, it is possible to calculate the inhibitor dissociation constant, K_i, that reflects the potential interaction between the enzyme and the inhibitor, using the Lineweaver-Burk plot. K_i of an inhibitor is analogous to the K_m of a substrate; a smaller K_i value indicates a stronger binding of an inhibitor to an enzyme, whereas a larger K_i value infers weaker binding. Inhibition characteristics of the five pesticides towards GST catalytic activity were studied in the perspective of GHS-CDNB reaction. K_i values were determined through the double-reciprocal Lineweaver-Burk plots.

DDT was found to be a competitive inhibitor since an increase in its concentration results in a family of Lineweaver-Burk lines with a

common intercept on the 1/v axis and hence a constant V_{max} but an increased K_m (Fig. 8a, Table ST3). The equilibrium constant for the inhibitor binding with the free enzyme, K_i, was obtained from a plot of K_m^{app}/K_m versus the inhibitor concentration [I_0], which was linear. The slope of the line gave a K_i value of 21.27 mM.

The kinetic behavior of chlorpyrifos and ethion showed a non-competitive mechanism. The Lineweaver–Burk plots yielded a family of straight lines with different slopes and with a common intercept on the x-axis (Fig. 8b and c). As expected for non-competitive inhibitor, the V'_{max} in the presence of the inhibitor is less than the same under uninhibited conditions, V_{max}. The value of the inhibition constant was obtained from a plot of the vertical intercept ($1/V'_{max}$) versus the inhibitor concentration [I_0]. The slope of ($1/V'_{max}$) vs. [I_0] gave a linear line with K_i values 219.29 mM for chlorpyrifos and 54.82 mM for ethion.

The other major type of inhibition is mixed inhibition in which the inhibitor is capable of binding to both the free enzyme and the enzyme–substrate complex. Herein, carbendazim and Dinocap show this type of inhibition (Fig. 8d and e). From the figures it is clear that in case of carbendazim the enzyme inhibitor binding constant (k_{ia}) is higher than the enzyme- substrate-inhibitor binding constant (K_{ib}) but the reverse is true in case of Dinocap. It is not possible to calculate a single K_i value for this type of inhibition from the Lineweaver–Burk plots.

3.8. Validation study

Biosensor results were validated by performing a two steps validation experiment. In the first step the recovery of the applied sample pretreatment process was determined by preparing a GC calibration curve for the pesticide, taking solutions of analytical standard sample of ethion. Then the recovery from a spiked potato samples were determined. In the second step the same fortified solution extract was subjected to bioanalysis and the results were compared with recovery values obtained through GC–MS. The concentration range for the GC calibration curve was from 100 ppb to 1000 ppb and the analytical solution for both GC–MS and bioanalysis was prepared by fortifying potato samples with 300 ppb of ethion. The stepwise solid phase extraction procedure was as follows: chopped vegetable (potato) weighing 10 g was spiked with 5 mL of 300 ppb ethion solution (prepared in acetonitrile) and then homogenized. Then, 5 mL of acetonitrile was added and shaken in a vortex shaker for 5 min, sonicated for 5 min and then centrifuged for 10 min at 2000 rpm. Then the supernatant was separated out and passed through a pre-conditioned (acetonitrile–hexane mixture in a 3:1 ratio) column of size 14 mm × 160 mm and packed with 5 g each of bondesil-NH_2 and carbon SPE bulk sorbent. The solution passing out through the column was collected in a 50 mL round-bottom flask and evaporated to dryness at 40 °C and 200 mbar in a rotary evaporator. The dry residue was reconstituted in a mixture of 4 mL methanol and 1 mL dichloromethane and evaporated again to about 1 mL and then diluted to 5 mL by adding more methanol solution. To 1 mL of this solution, 1 mL each of 2 mM GSH and CDNB, and placed in the electrochemical cell with the biosensor probe. The percentage of inhibition in peak current was calculated and the amount of pesticide was determined with the help of the calibration curve and considering the dilution factor. The entire process was repeated thrice to get triplicate results.

Recovery for ethion from potato samples was found to be 88.2% (RSD 4.6%, n = 5) in the GC analysis and, 88.6% (RSD 5.8%, n = 5) in bioanalysis using the fabricated biosensor probe. Close resemblance of the bioanalysis results with the GC results infers that the bioanalysis method if perfect and highly reliable. The gas chromatograms of ethion under the specified analytical parameters are shown in supporting information (Figs. S4 and S5).

4. Conclusion

We have shown for the first time that the enzyme GST can be immobilized on platinum electrode using graphene oxide and gelatin matrix to fabricate an enzyme electrode that can act as sensor probe with a broad spectrum applicability. The sensor can be applied to detect amperometrically at least six different classes of pesticides. The reproducibility of sensor results were confirmed through GC–MS analysis. We have also reported for the first time the catalytic perfection as well as substrate specificity of the enzyme GST towards the two substrate CDNB and GSH. We have also studied the inhibition characteristics of different classes of pesticides towards the enzymatic reaction between GST and CDNB. The trend of inhibition appears to be competitive for organochlorines, non-competitive for organothiophosphates and mixed type for phenolic and benzimidazole classes.

Acknowledgement

One of the authors Ms. Himadri Borah thanks the National Tea Research Foundation, Tea Board of India, Kolkata, for financial support through the project No. NTRF: 191(2016). Mr. Sudarshan Gogoi thanks the UGC, Govt. of India for providing NET-JRF No. 124401 of 2014.

Appendix A. Supplementary data

Supplementary data to this article can be found online at https://doi.org/10.1016/j.jelechem.2018.09.047.

References

[1] D. Liu, W. Chen, J. Wei, X. Li, Z. Wang, X. Jiang, A highly sensitive, dual-readout assay based on gold nanoparticles for organophosphorus and carbamate pesticides, Anal. Chem. 84 (2012) 4185–4191.
[2] M. Xu, Y. Gao, X.X. Han, B. Zhao, Detection of pesticide residues in food using surface-enhanced Raman spectroscopy: a review, J. Agric. Food Chem. 65 (2017) 6719–6726.
[3] M. Kesik, F.E. Kanik, J. Turan, M. Kolb, S. Timur, M. Bahadir, L. Toppare, An acetylcholinesterase biosensor based on a conducting polymer using multiwalled carbon nanotubes for amperometric detection of organophosphorous pesticides, Sensors Actuators B Chem. 205 (2014) 39–49.
[4] Q. Lang, L. Han, C. Hou, F. Wang, A. Liu, A sensitive acetylcholinesterase biosensor based on gold nanorods modified electrode for detection of organophosphate pesticide, Talanta 156–157 (2016) 34–41.
[5] K. Buonasera, G. Pezzotti, V. Scognamiglio, A. Tibuzzi, M.T. Giardi, New platform of biosensors for prescreening of pesticide residues to support laboratory analyses, J. Agric. Food Chem. 58 (2010) 5982–5990.
[6] C.S. Pundir, N. Chauhan, Acetylcholinesterase inhibition-based biosensors for pesticide determination: a review, Anal. Biochem. 429 (2012) 19–31.
[7] Y. Song, M. Liu, S. Wang, Surface plasmon resonance sensor for phosmet of agricultural products at the ppt detection level, J. Agric. Food Chem. 61 (2013) 2625–2630.
[8] X.X. Jiang, H.Y. Shi, N. Wu, M.H. Wang, Development of an enzyme-linked immunosorbent assay for diniconazole in agricultural samples, Food Chem. 125 (2011) 1385–1389.
[9] H. Moriwaki, K. Yamada, H. Nakanishi, Evaluation of the interaction between pesticides and a cell membrane model by surface plasmon resonance spectroscopy analysis, J. Agric. Food Chem. 65 (2017) 5390–5396.
[10] S. Chand, B.D. Gupta, Surface plasmon resonance based fiber-optic sensor for the detection of pesticide, Sensors Actuators B Chem. 123 (2007) 661–666.
[11] E. Zor, E. Morales-Narvaez, A. Zamora-Galvez, H. Bingol, M. Ersoz, A. Merkoci, Graphene quantum dots-based photoluminescent sensor: a multifunctional composite for pesticide detection, ACS Appl. Mater. Interfaces 7 (2015) 20272–20279.
[12] D. Sahoo, A. Mandal, T. Mitra, K. Chakraborty, M. Bardhan, A.K. Dasgupta, Nanosensing of pesticides by zinc oxide quantum dot: an optical and electrochemical approach for the detection of pesticides in water, J. Agric. Food Chem. 66 (2018) 414–423.
[13] R.R. Dutta, P. Puzari, Amperometric biosensing of organophosphate and organocarbamate pesticides utilizing polypyrrole entrapped acetylcholinesterase electrode, Biosens. Bioelectron. 52 (2014) 166–172.
[14] S. Soylemez, F.E. Kanik, M. Ileri, S.O. Hacioglu, L. Toppare, Development of a novel biosensor based on a conducting polymer, Talanta 118 (2014) 84–89.
[15] I. Cesarino, F.C. Moraes, M.R.V. Lanza, S.A.S. Machado, Electrochemical detection of carbamate pesticides in fruit and vegetables with a biosensor based on acetylcholinesterase immobilised on a composite of polyaniline-carbon nanotubes, Food Chem. 135 (2012) 873–879.
[16] S. Viswanathan, H. Radecka, J. Radecki, Electrochemical biosensor for pesticides

based on acetylcholinesterase immobilized on polyaniline deposited on vertically assembled carbon nanotubes wrapped with ssDNA, Biosens. Bioelectron. 24 (2009) 2772–2777.
[17] H. Zhao, X. Ji, B. Wang, N. Wang, X. Li, R. Ni, J. Ren, An ultra-sensitive acetylcholinesterase biosensor based on reduced graphene oxide-Au nanoparticles-β-cyclodextrin/Prussian blue chitosan nanocomposites for organophosphorus pesticides detection, Biosens. Bioelectron. 65 (2015) 23–30.
[18] Y. Li, L. Shi, G. Han, Y. Xiao, W. Zhou, Electrochemical biosensing of carbaryl based on acetylcholinesterase immobilized onto electrochemically inducing porous graphene oxide network, Sensors Actuators B Chem. 238 (2017) 945–953.
[19] P. Raghu, B.E.K. Swamy, T.M. Reddy, B.N. Chandrashekar, K. Reddaiah, Sol–gel immobilized biosensor for the detection of organophosphorous pesticides: a voltammetric method, Bioelectrochemistry 83 (2012) 19–24.
[20] P. Raghu, T.M. Reddy, K. Reddaiah, B.E. Swamy, M. Sreedhar, Acetylcholinesterase based biosensor for monitoring of Malathion and Acephate in food samples: a voltammetric study, Food Chem. 142 (2014) 188–196.
[21] H.L. Tcheumi, I.K. Tonlea, E. Ngameni, A. Walcarius, Electrochemical analysis of methylparathion pesticide by a gemini surfactant-intercalated clay-modified electrode, Talanta 81 (2010) 972–979.
[22] Y. Yang, A.M. Asiri, D. Du, Y. Lin, Acetylcholinesterase biosensor based on a gold nanoparticle–polypyrrole–reduced graphene oxide nanocomposite modified electrode for the amperometric detection of organophosphorus pesticides, Analyst 139 (2014) 3055–3060.
[23] H.F. Cui, W.W. Wu, M.M. Li, X. Song, Y. Lv, T.T. Zhang, A highly stable acetylcholinesterase biosensor based on chitosan-TiO2-graphene nanocomposites for detection of organophosphate pesticides, Biosens. Bioelectron. 99 (2018) 223–229.
[24] X. Ji, J. Zheng, J. Xu, V.K. Rastogi, T.C. Cheng, J.J. DeFrank, R.M. Leblanc, (CdSe) ZnS quantum dots and organophosphorus hydrolase bioconjugate as biosensors for detection of paraoxon, J. Phys. Chem. B 109 (2005) 3793–3799.
[25] J.H. Lee, J.Y. Park, K. Min, H.J. Cha, S.S. Choi, Y.J. Yoo, A novel organophosphorus hydrolase-based biosensor using mesoporous carbons and carbon black for the detection of organophosphate nerve agents, Biosens. Bioelectron. 25 (2010) 1566–1570.
[26] T. Liu, H. Su, X. Qu, P. Ju, L. Cui, S. Ai, Acetylcholinesterase biosensor based on 3-carboxyphenylboronic acid/reduced graphene oxide-gold nanocomposites modified electrode for amperometric detection of organophosphorus and carbamate pesticides, Sensors Actuators B Chem. 160 (2011) 1255–1261.
[27] L. Zhou, X. Zhang, L. Ma, J. Gao, Y. Jiang, Acetylcholinesterase/chitosan-transition metal carbides nanocomposites-based biosensor for the organophosphate pesticides detection, Biochem. Eng. J. 128 (2017) 243–249.
[28] A. Gutés, F. Cespedes, S. Alegretb, M.D. Valle, Determination of phenolic compounds by a polyphenol oxidase amperometric biosensor and artificial neural network analysis, Biosens. Bioelectron. 20 (2005) 1668–1673.
[29] T. Montesinos, S. Pérez-Munguia, F. Valdez, J.L. Marty, Disposable cholinesterase biosensor for the detection of pesticides in water-miscible organic solvents, Anal. Chim. Acta 431 (2001) 231–237.
[30] G. Valdés-Ramírez, M. Cortina, M.T. Ramírez-Silva, J.L. Marty, Acetylcholinesterase-based biosensors for quantification of carbofuran, carbaryl, methylparaoxon, and dichlorvos in 5% acetonitrile, Anal. Bioanal. Chem. 392 (2008) 699–707.
[31] H. Borah, R.R. Dutta, S. Gogoi, P. Puzari, Influence of methanol, ethanol and cypermethrin on the Glutathione *S*-tranferase catalyzed reaction of Glutathione with 1-chloro-2,4-dinitrobenzene: a method for detection and quantification of cypermethrin, Electrochim. Acta 205 (2016) 198–206.
[32] EU, Pesticide database, http://ec.europa.eu/food/plant/pesticides/ (Official Journal of the European Union, Reg. (EU) No 559/2011; (EC) No 149/2008; (EU) No 310/2011; (EU) 2018/686; (EC) No 396/2005; (EU) 2017/626).
[33] H. Borah, R.R. Dutta, S. Gogoi, T. Medhi, P. Puzari, Glutathione-*S*-transferase catalyzed reaction of glutathione for electrochemical biosensing of temephos, fenobucarb and dimethoate, Anal. Methods 9 (2017) 4044–4051.
[34] B. Paulcham, G. Arthi, B.D. Lignesh, A simple approach to stepwise synthesis of graphene oxide nanomaterial, J. Nanomed. Nanotechnol. 6 (2015), https://doi.org/10.4172/2157-7439.1000253.
[35] Z. Li, I.A. Kinloch, R.J. Young, The role of interlayer adhesion in graphene oxide upon its reinforcement of nanocomposites, Phil. Trans. R. Soc. A 374 (2016), https://doi.org/10.1098/rsta.2015.0283.
[36] C. Zhou, H. Wang, F. Peng, J. Liang, H. Yu, J. Yang, MnO_2/CNT supported Pt and Pt-Ru nanocatalysts for direct methanol fuel cells, Langmuir 25 (2009) 7711–7717.
[37] W.H. Habig, M.J. Pabst, W.B. Jakoby, Glutathione *S*-transferases the first enzymatic step in mercapturic acid formation, J. Biol. Chem. 249 (1974) 7130–7139.
[38] S. Eissa, M. Zourob, Selection and characterization of DNA aptamers for electrochemical biosensing of carbendazim, Anal. Chem. 89 (2017) 3138–3145.
[39] N. Xia, Y. Zhang, K. Chang, X. Gai, Y. Jing, S. Li, L. Liu, G. Qu, Ferrocene-phenylalanine hydrogels for immobilization of acetylcholinesterase and detection of chlorpyrifos, J. Electroanal. Chem. 746 (2015) 68–74.
[40] E. Mauriz, A. Calle, J.J. Manclus, A. Montoya, A. Hildebrandt, D. Barcelo, L.M. Lechuga, Optical immunosensor for fast and sensitive detection of DDT and related compounds in river water samples, Biosens. Bioelectron. 22 (2007) 1410–1418.
[41] M. Lisa, R.S. Chouhan, A.C. Vinayaka, H.K. Manonmani, M.S. Thakur, Gold nanoparticles based dipstick immunoassay for the rapid detection of dichlorodiphenyltrichloroethane: an organochlorine pesticide, Biosens. Bioelectron. 25 (2009) 224–227.
[42] E. Khaled, M.S. Kamel, H.N.A. Hassan, H. Abdel-Gawad, H.Y. Aboul-Enein, Performance of a portable biosensor for the analysis of ethion residues, Talanta 119 (2014) 467–472.

THE JOURNAL OF PHYSICAL CHEMISTRY B

Article

pubs.acs.org/JPCB

Evaluation of Diffusion Coefficient of Thiocholine in Enzyme-Loaded Polypyrrole Composite Film through Different Methods and Electrode Polarization

Sudarshan Gogoi, Himadri Borah, Rekha R. Dutta, and Panchanan Puzari*

Department of Chemical Sciences, Tezpur University, Tezpur, Assam 784028, India

Supporting Information

ABSTRACT: In this work, the diffusion of thiocholine ion into an enzyme-loaded polypyrrole film was evaluated by different methods, and the results were compared to identify the most suitable method. The enzyme-loaded polypyrrole film was coated with a thin layer of gelatin and gluteraldehyde so as to prevent enzyme leaching. Diffusion coefficients under normal and prepolarized conditions were calculated by five different methods, namely, the Cottrell method, the method of Peerce and Bard, the theoretical impedance model, the electrochemically stimulated conformational relaxation (ESCR) method, and the direct impedance measurement method. The theoretical model of Vortynstev was used to calculate the parameters from the impedance spectra using simplex technique in MATLAB. The results indicate that under normal unpolarized condition the ESCR method gives a diffusion coefficient close to that given by Vortynstev method, but under polarized conditions the Cottrell method can provide a better value of diffusion coefficient than ESCR. The diffusion coefficient of thiocholine in PPy composite film from an electrolytic background of phosphate buffer of pH 7.4 was found to be 1.00×10^{-8} cm^2 s^{-1} based on Vortynstev method. The mechanism of thiocholine diffusion into the positively charged/polarized matrix is attributed to be through the formation of a dinegative ion between thiocholine and phosphate anion via electrostatic attraction.

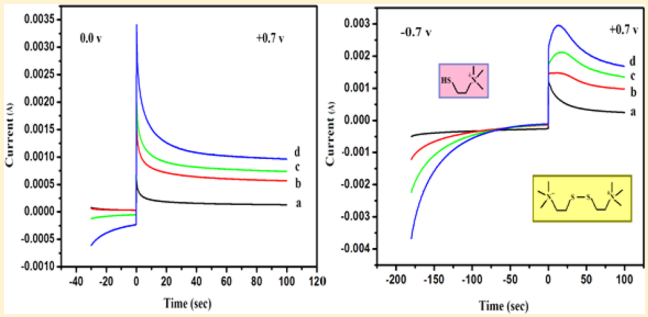

1. INTRODUCTION

Conducting polymers have been attracting increasing interest over last 30 years due to their interesting electrical and electrochemical properties and also due to their potential application in miniaturized electronic devices. Polypyrrole (PPy), a key member of the organic conducting polymers, has peculiar properties of reversal of conductivity and composition during its reversible electrochemical oxidation−reduction process[1] and also a high room-temperature conductivity (~40−100 S cm^{-1}). The possibility to develop many electrochemical devices such as artificial muscles, smart windows, polymeric batteries, artificial glands, electron ion transducers, and biosensors exploiting those properties has been demonstrated by different workers.[2] All devices related to those properties work either under the diffusion kinetic control of the counterion required for the charge balance or under slower relaxation kinetic control of the conformational structure. The best way to design the most suitable practical kinetic conditions for the different devices will be to acquire prior knowledge on diffusion and its control, which, in turn, depends on identification of reliable method(s) for determining diffusion coefficients of ions involved in the device inside the constituent polymer.

Different techniques such as the chronoamperometric method using the Cottrell equation[3−5] or electrochemical impedance[6−9] have been used to measure ion diffusion. Among these, the most commonly used one is the Cottrell model. Because the Cottrell equation was originally meant for diffusion of ions in solution electrolyzed with a bare electrode, so its applicability to ionic diffusion in films of coated electrode is a debatable topic. Some workers have suggested that the equation can be used for coated electrode provided a proper time scale is chosen; for example, in coated electrode, a short time scale gives the diffusion coefficients of the ions within the film, while a long time scale gives the same in the solution,[10] but examples are found in the literature where the Cottrell equation has been used to evaluate diffusion coefficients without making any distinction of the diffusion type. So one aim of the present work was to study whether the Cottrell equation can be applied to evaluate the diffusion coefficient of an ion in an electroactive polymeric composite film such as polypyrrole coated with gelatin and gluteraldehyde, taking thiocholine cation as the target ion. Thiocholine is the hydrolysis product of acetylthiocholine, a substrate for the cholinesterase enzymes (acetylcholinesterase, AChE; or butyrylcholinesterse, BChE), during in vitro study of the activities of those enzymes. Thus, thiocholine behaves as a biomarker for the biological effect of some pesticides and nerve agents that

Received: February 10, 2015
Revised: March 17, 2015
Published: March 17, 2015

DOI: 10.1021/acs.jpcb.5b01383
J. Phys. Chem. B 2015, 119, 4749−4757

inhibit the activity of the cholinesterase enzymes in muscles and nerve tissues.[11] On the basis of this fact, different varieties of AChE-based electrochemical biosensors have been designed by immobilizing the enzyme AChE in different matrix on solid electrode support, the signal intensity and reproducibility of which depend to a greater extent on the diffusion characteristic of thiocholine in the matrix. In a recent work,[12] we have shown that thiocholine gets oxidized on polypyrrole surface with a diffusion-controlled process. It was observed during the study that there exists a distinct difference between the shapes of the chronoamperogram (CA) of normal oxidation (normal oxidation means initial potential of 0 V applied for 30 s, followed by 0.7 V for 100 s) and prepolarized oxidation (prepolarized oxidation means initial voltage −0.7 V applied for 180 s, followed by 0.7 V for 100 s) of thiocholine on PPy matrix. The decay pattern of the CA in the case of normal oxidation looks like the Cottrell type, that is, the exponential decay, but in the case of the prepolarized one, the decay pattern is different due to huge faradaic current (Figure 2A,B), and thus it takes a very long duration for the CA to attain the state of steady-state oxidation. So it is an obvious question of whether the Cottrell equation can be applied to such systems or not, especially at the short time range. So we have calculated diffusion coefficients of both normal and prepolarized oxidation throughout the total time interval to study the applicability of Cottrell equation for such systems and compared the results with a few other methods. The diffusion coefficient under normal and prepolarized conditions was calculated by five different methods, namely, the Cottrell method, the method of Peerce and Bard, the curve fitting method using theoretical impedance model, the electrochemically stimulated conformational relaxation (ESCR) method, and the direct impedance measurement method, and compared. The theoretical model of Vortynstev was used to calculate the impedance spectra using a nonlinear simplex technique in MATLAB. The polypyrrole composite film was enzyme-loaded so that it reflects a practical situation of biosensor functioning, and the kinetics is mostly diffusion-controlled due to creation of diffusion channels.

2. EXPERIMENTAL SECTION

2.1. Reagents. Acetylcholinesterase (Type VI−S, EEL, 500 UN mg^{-1}), acetylthiocholinechloride, and phosphate buffer (PB) were procured from Sigma-Aldrich, USA. Pyrrole monomer was procured from E-Merck, Germany.

2.2. Instruments. PAR 273 A potentiostate/galvanostate was used for film deposition and chronoamperometric study. Platinum working electrode (diameter 3 mm, surface area 0.0707 cm^2) was obtained from CH instrument, USA. The impedance analyzer used was SP 150, Biologics, USA.

2.3. Electrode Fabrication. Enzyme-loaded, gelatin−gluteraldehyde−polypyrrole-coated platinum electrode (Pt/PPy-AChE-Glut-Geltn electrode) was prepared according to the published procedure.[12] In brief, AChE was electro-entrapped in polypyrrole at 0.7 V from a 0.5 M solution of the pyrrole in PB. Subsequently, gluteraldehyde and gelatin were added in steps and the electrode was kept for an aging period of 5 days in −20 °C before use.

2.4. Chronoamperometric Measurements. CA measurements were made under static solution condition in thiocholine prepared in phosphate buffer (pH 7.4) using three-electrode cell setup comprising Pt/PPy-AChE-Glut-Geltn electrode as the working electrode, Ag/AgCl-saturated NaCl reference electrode, and platinum coil as the auxiliary electrode. Two different sets of potentials were used, respectively, for normal and prepolarized state of thioholine ion. Parameters were 0.0 V for 30 s, followed by 0.7 V for 100 s in normal and −0.7 V for 180 s, followed by 0.7 V for 100 s in the pre polarized state.

Before each new experiment the working electrode was subjected to a few CV and CA runs in the negative potential region (from 0 to −0.8 V) until the prediffused materials were totally ejected (when the baseline was reproduced). Also, the electrodes were potentiostated for 10 min at +0.5 V time to time between experiments to recover the reversible damage to the Ag/AgCl electrode.

CA was used to calculate the thiocholine diffusion coefficient using the Cottrell equation (eq 1) in two different ways (named Cottrell A and Cottrell B). Under Cottrell A, plots of i versus $t^{-1/2}$ were obtained for three different concentrations. The slopes of the lines thus obtained were again plotted against concentrations of the diffusing species to evaluate D from its slope.[5]

$$I = \frac{nFAD^{1/2}C}{\pi^{1/2}t^{1/2}} \tag{1}$$

In Cottrell method B the integrated form of the previous equation (eq 2) was used to calculate the diffusion coefficient from the plot of Q versus $t^{1/2}$.

$$Q = \frac{2zFACD^{1/2}}{\pi^{1/2}}t^{1/2} \tag{2}$$

In these equations, z is the charge transfer during oxidation ($z = 1$), F is the Faraday constant (96 485.3365 C mol^{-1}), A is the geometric area of the electrode, C is the bulk concentration of the thiocholine ion, and D is the diffusion coefficient in cm^2 s^{-1}.

Under the ESCR model, eq 3 was used to calculate the diffusion coefficient.[13]

$$\ln\left[1 - \frac{Q}{Q_t}\right] = -\frac{2D}{\delta^2}t \tag{3}$$

Here Q is the charge consumed at every time t after the potential step, Q_t is the total charge obtained by integration of the CA within the time range of interest (calculated by numerical trapezoidal method), and δ is the thickness of the swollen film. The slope of the plot of $\ln(1 - Q/Q_t)$ versus t gave the diffusion coefficient, D.

CAs were also used to calculate the diffusion coefficient through the equation developed by Peerce and Bard for modified electrode (eq 4).[10]

$$\frac{i(\tau)}{i_d(\tau)} = \frac{K}{\gamma}\left[1 + 2\sum_{i=1}^{\infty}\left[\frac{1 - \frac{K}{\gamma}}{1 + \frac{K}{\gamma}}\right]^j \exp\left(-\frac{j^2}{\tau}\right)\right] \tag{4}$$

where $i(\tau)$ is the current passed at the polymer modified electrode and $i_d(\tau)$ is that at the bare electrode, that is, the Cottrell current given by eq 1. Here K is the extraction coefficient.

$\gamma = [D_s/D_m]^{1/2}$ and $\tau = D_m t/\delta^2$, where D_m, D_s, and δ are, respectively, the diffusion coefficient of ion in the film, the diffusion coefficient of ion in solution, and the thickness of the solvent swollen film.

DOI: 10.1021/acs.jpcb.5b01383
J. Phys. Chem. B 2015, 119, 4749−4757

The experimental $i(\tau)/i_d(\tau)$ ratios were plotted against $\log(t)$ in the time range at which the plot of $i_d(t) \times t^{1/2}$ versus $\log(t)$ was linear with a zero slope and compared with the theoretical $i(\tau)/i_d(\tau)$ ratio as per eq 4 for the same time zone. From the average deviation of the experimental curve from the theoretical one, the diffusion coefficient was calculated by using eq 5.

$$\log(\tau) - \log(t) = \log(D_m/\delta^2) \quad (5)$$

2.5. Curve Fitting Using Impedance Measurement and Vortynstev Model. The theoretical AC impedance model of Vorotynstev[14,15] was used to calculate the diffusion coefficient. Equations 4−9 of ref 15 were processed and fitted to the experimental impedance data for evaluation of the diffusion coefficient applying nonlinear least-squares with simplex technique in MATLAB. AC amplitude of 5 mA was applied for impedance analysis at a potential of 0.7 V in the frequency range 0.1 Hz to 0.8 MHz.

2.6. From Warburg Impedance. According to literature,[16] the low-frequency Warburg impedance is related to the diffusion coefficients of oxidants and reductants by eq 6.

$$z_f = \left(\frac{2}{w}\right)^{1/2} \frac{RT}{F^2A\sqrt{2}}\left(\frac{1}{D_0^{1/2}C_0^*} + \frac{1}{D_R^{1/2}C_R^*}\right) \quad (6)$$

where D_0 and D_R are the diffusion coefficients of the oxidized and reduced form of the species and C_0^* and C_R^* are their bulk concentrations.

In the present case, thiocholine and oxidized thiocholine are involved in the diffusion process. Assuming equal diffusion velocities for both and considering $C_0^* = C_R^*$ at least for the initial state of the reaction, eq 6 can be written as

$$z_f = \left(\frac{2}{w}\right)^{1/2} \frac{RT}{F^2A\sqrt{2}}\left(\frac{2}{D^{1/2}C^*}\right) \quad (7)$$

D was calculated using eq 7 through measurement of the low-frequency Warburg impedance from the impedance spectra.

Thiocholine was obtained through hydrolyzing acetylthiocholine for 1 h using a separate enzyme electrode, and the final concentration was determined by Ellman method.[17]

3. RESULTS AND DISCUSSION

3.1. Film Thickness Measurement. The thickness of the dry film was measured through SEM (Figure 1) at three different lateral sites, and the average was found to be 88 μm; that of the solvent swollen film measured through digital slide caliper (Mitutoyo-Japan) was found to be 110 μm. Figure 1 (left) shows the SEM image of an enzyme-loaded Ppy-gelatin film in the dry state (lateral view).

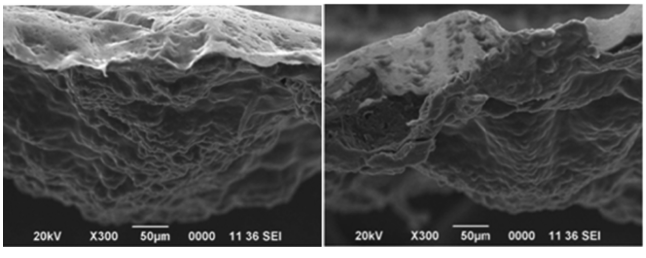

Figure 1. SEM image (lateral view) of PPy-AChE-Glut-Geltn film.

3.2. Chronoamperometric Study. Figure 2A,B shows the CAs, respectively, for normal and prepolarized oxidation of thiocholine at 0.7 V recorded with the enzyme-loaded PPy working electrode. The Figures reveal that in the absence of prepolarization the amperometric current quickly drops and becomes equilibrated soon, but in the prepolarized case the current decay is slow and it takes a longer time to get equilibrated. This indicates that faradaic current is greater when preconcentration is applied. This faradaic current due to thiocholine oxidation increases with concentration, as is obvious from the gaps in the current jump between the successive CAs for different concentrations after attaining the final potential (Figure 2B). The CA pattern indicates an uncommon diffusion characteristic and hence creates suspense on the feasibility of using the Cottrell equation to evaluate the diffusion coefficient under forced conditions, while in the normal case (Figure 2A) the feature of the CA apparently indicates the possibility of applying the same.

In both the CAs (Figure 2A,B) the conformational relaxation[18] seems to be missing probably either due to enzyme loading or due to surface coating with gelatin or gluteraldehyde or both. When conformational relaxation is present the CA peak current decreases immediately after the final potential is obtained, followed by a steady increase. In the present case we see a steady increase only, immediately after the final potential, followed by an exponential decay after certain time (inset i in Figure 2A,B). The steady upward rise after the initial jump is attributed to the charging current in conjugation with oxidative current of thiocholine oxidation. The fact that thiocholine oxidation is also involved in this region is obvious from the fact that the slope of the rising portion became steeper when thiocholine concentration was gradually increased (Figure 2B). The increase in the peak maxima with increasing amount of thiocholine in Figure 2B indicates that thiocholine oxidation affects the CA peak maxima in a quantitative manner. Results of cyclic voltammetric experiment also corroborate this point (Figure 3).

3.3. Diffusion Coefficient (*D*). *3.3.1. Cottrell Equation. 3.3.1.1. Cottrell A.* As mentioned in the literature,[19] the polymer-coated electrode application of Cottrell equation in the short time range gives the diffusion characteristic in the film and at longer time range the diffusion characteristic in solution, so we have chosen both short- and long-time range for the evaluation of the diffusion coefficient through the Cottrell equation. It is observed that in the CAs (normal and polarized) the current increases up to certain time and then decreases exponentially (Figure 2B and the inset i in Figure 2A). The Cottrell calculations were done separately for both regions before and after the peak current and up to the time when the curve became steady. Figure 4A,B shows typical plots of the i versus $t^{-1/2}$ and the slope versus c curve obtained within 3.9 to 4.9 s in the post-peak region.

Diffusion coefficients found are listed in Table 1. While calculating the diffusion coefficients the PB current was subtracted to correct for the charging current. The shown values are the average of three calculations performed at three different time slots in the pre- or post-peak region. The different time zones used for the calculations and the corresponding plots are shown in Table T_s in the Supporting Information.

3.3.1.2. Cottrell B. Under this procedure the diffusion coefficients have been calculated from the plots of consumed charge, Q versus $t^{1/2}$ (eq 2) for both normal and polarized

DOI: 10.1021/acs.jpcb.5b01383
J. Phys. Chem. B 2015, 119, 4749−4757

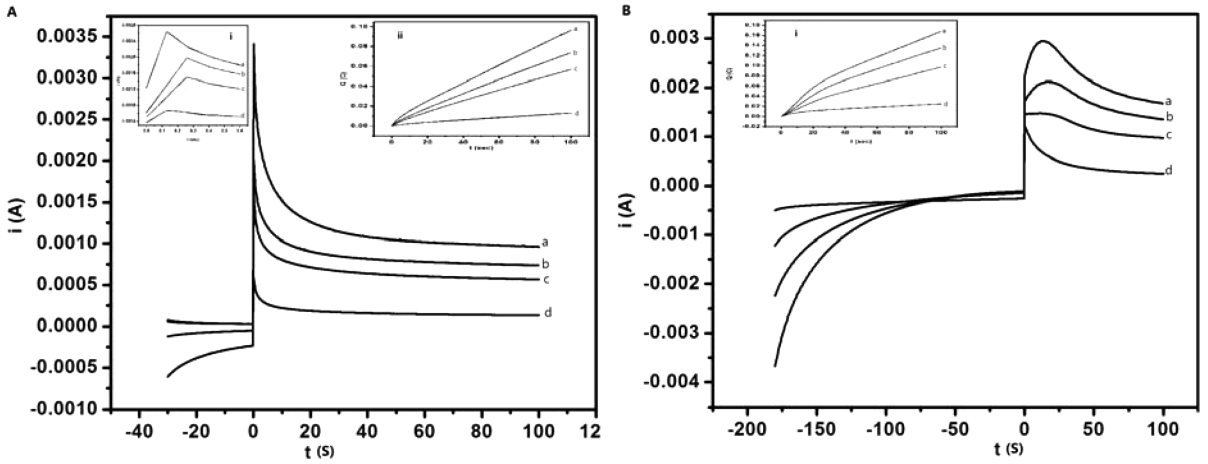

Figure 2. Chronoamperograms in thiocholine solution with Pt/PPy-AChE-Glut-Geltn electrode under normal (A) and polarized (B) conditions with thiocholine in PB of concentrations (a) 0.0353, (b) 0.0264, and (c) 0.0176 mM and (d) only PB. Inset i in panel A is the expanded CA in the time range 0 to 0.6 s to show the hidden charging current. Inset ii in panel A and inset I in panel B are the chronocoulograms corresponding to the CAs. The negative time range covered by the curves indicate the durations of application of the negative potential (−0.7 V).

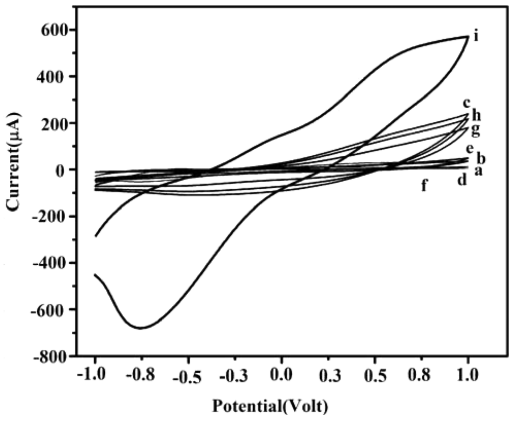

Figure 3. Cyclic voltammograms at scan rate 20 mV/s of (a) Pt electrode in PBS, (b) Pt-PPy in PBS, (c) Pt-PPy in 2 mM ACTh, (d) Pt-Glut-Geltn electrode in 2 mM ATChCl, (e) Pt-PPy-Glut-Geltn electrode in PBS, (f) Pt−Ppy-AChE-Glut-Geltn in PBS, (g) Pt-PPy-Geltn electrode in 2 mM ATChCl, (h) Pt-PPy-Glut-Geltn in 2 mM ATChCl, and (i) Pt-PPy-AChE-Glut-Geltn in 2 mM ATChCl.

conditions. Chronocoulograms thus obtained from the CA plots are shown in the Supporting Information.

The diffusion coefficients found are shown in Table 1.

3.3.2. ESCR Method. ESCR method restricts the selection of time scale based on consideration of the relaxation process. Under that restriction the time scales for both the normal and polarized cases were after the peak, that is after 0.13 s and 15 s respectively for normal and polarized cases. Diffusion coefficients were calculated by using eq 3 after elimination of charging currents. The diffusion coefficients found are shown in Table 1.

3.3.3. Method of Peerce and Bard. Under this method the time range for D calculation was chosen as the region where the plot of $i_d(t)\cdot t^{1/2}$ versus $\log(t)$ was linear with a zero slope (Figure 5A). In both the normal and the polarized cases this range fell at the peaks, that is, from 0.13 to 1 s in normal case and in 14.5 to 15 s in the polarized case. Experimental and theoretical i_t/i_d ratios within the selected time range were calculated for a range of K/γ ratios from 7.2 to 7.6 (Figure 5B). The best overlap was seen in the case of K/γ =7.6 (Figure 5C) and used to evaluate the ion (thiocholine) diffusion coefficient

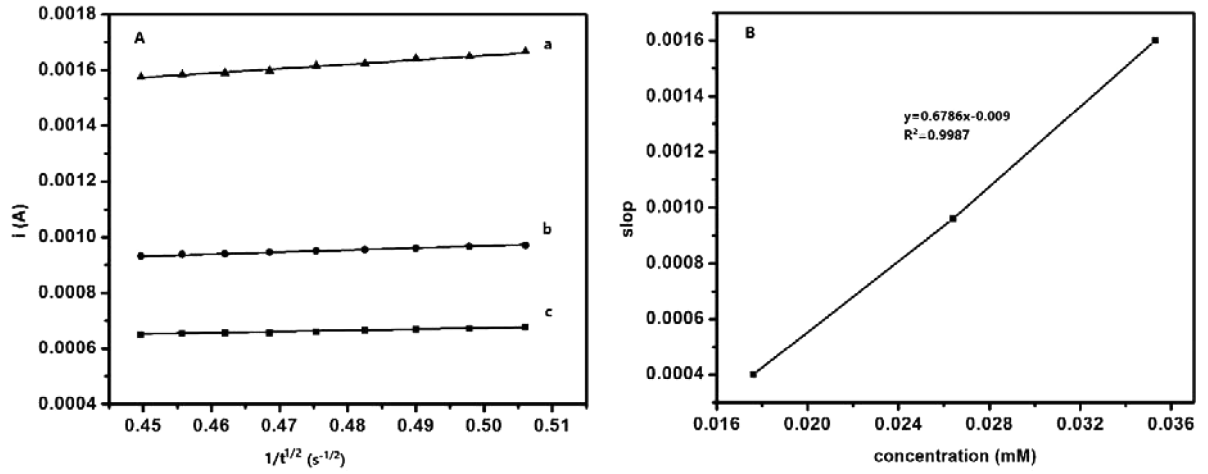

Figure 4. Plot of current, i, versus $t^{-1/2}$ for three different concentrations of thiocholine (A). Plot of slopes versus [TCh] (B) for calculation of D as per eq 1. The corresponding CAs are shown in Figure 2A: (a) 0.0353, (b) 0.0264, and (c) 0.0176 mM TCh solution.

DOI: 10.1021/acs.jpcb.5b01383
J. Phys. Chem. B 2015, 119, 4749−4757

Table 1. Comparison of Diffusion Coefficients Obtained from Cottrell and ESCR Calculations for Different Concentrations and at Different Regions of the Chronoamperograms

thiocholine concentraion	D (cm^2 s^{-1}) for normal condition			D (cm^2 s^{-1}) for forced condition		
	Cottrell A	Cottrell B	ESCR	Cottrell A	Cottrell B	ESCR
C_1 = 0.0176 mM						
before the peak	3.45 (±0.01) × 10^{-9}	1.96 (±0.03) × 10^{-9}		2.82 (±0.65) × 10^{-8}	1.08 (±0.03) × 10^{-6}	
on the peak		4.40 × 10^{-9}			2.20 × 10^{-6}	
after the peak	3.66 (±0.35) × 10^{-8}	1.77 (±0.03) × 10^{-8}	5.57 (±0.04) × 10^{-7}	6.40 (±0.1) × 10^{-7}	2.61 (±0.04) × 10^{-6}	4.00 (±0.6) × 10^{-7}
C_2 = 0.0264 mM						
before the peak	3.45 (±0.01) × 10^{-9}	1.55 (±0.03) × 10^{-9}		2.82 (±0.02) × 10^{-8}	2.28 (±0.03) × 10^{-6}	
on the peak		4.76 × 10^{-9}			2.92 × 10^{-6}	
after the peak	3.66 (±0.20) × 10^{-8}	1.64 (±0.05) × 10^{-8}	5.57 (±0.03) × 10^{-7}	4.60 (±0.12) × 10^{-7}	3.02 (±0.01) × 10^{-6}	1.33 (±0.01) × 10^{-7}
C_3 = 0.0353 mM						
before the peak	3.45 (±0.01) × 10^{-9}	4.40 (±0.10) × 10^{-9}		2.82 (±0.02) × 10^{-8}	1.54 (±0.04) × 10^{-6}	
on the peak		2.66 × 10^{-8}			2.48 × 10^{-6}	
after the peak	3.66 (±0.20) × 10^{-8}	2.48 (±0.04) × 10^{-8}	5.32 (±0.03) × 10^{-7}	4.60 (±0.12) × 10^{-7}	2.58 (±0.03) × 10^{-6}	1.94(±0.03) × 10^{-7}

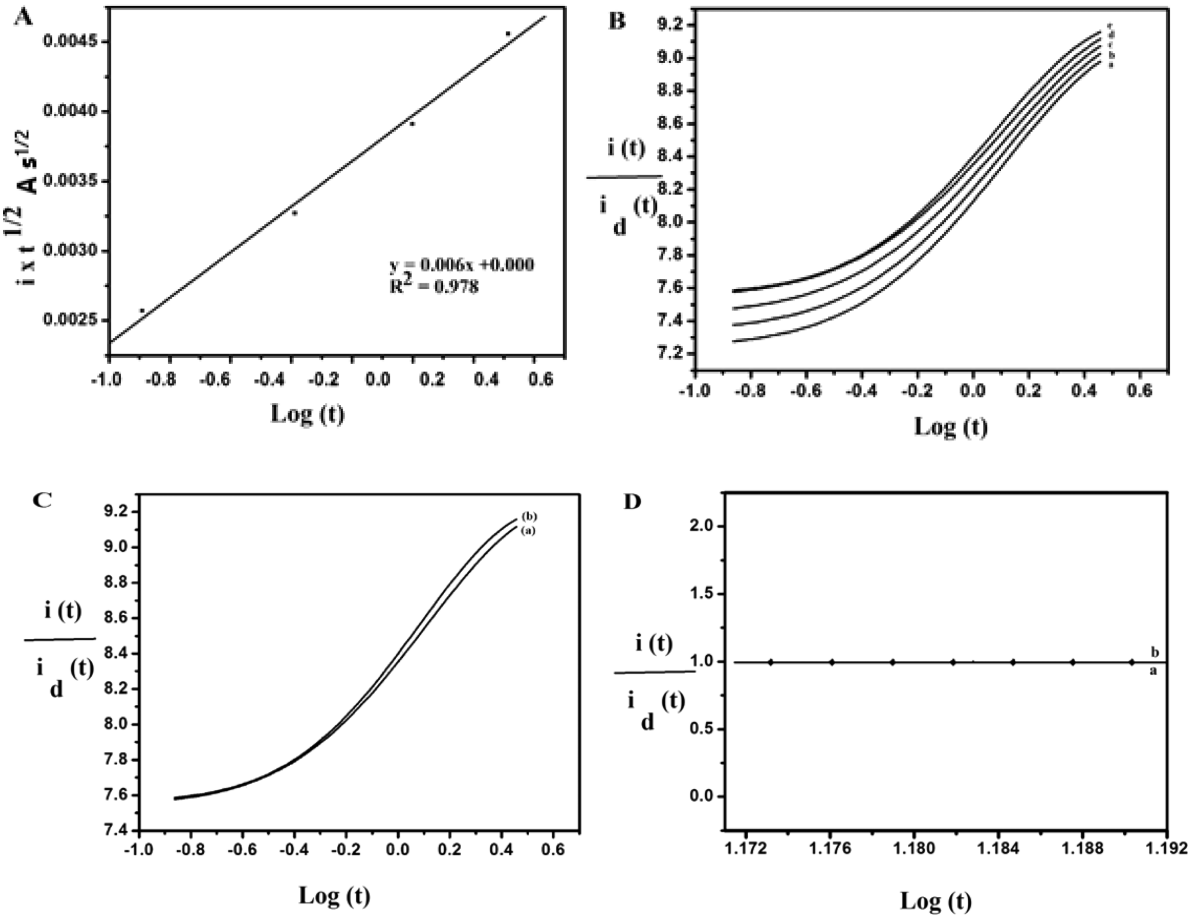

Figure 5. Comparison of experimental and theoretical chronoamperograms calculated as per eq 4. (A) Plot of $i_d(t) \times t^{1/2}$ versus $\log(t)$ for the normal condition. (B) Plot of all theoretical curves with K/γ ratios from 7.2 to 7.6. in the same time range under normal condition. (C) Overlap of experimental curve (a) with theoretical one (b) with K/γ = 7.6 under normal conditions and (D) overlap of theoretical curve with the experimental one in the time range 14.5 to 15 s under prepolarized condition. $i(t)$ is the current passed at the Pt/PPy-AChE-Glut-Geltn electrode and $i_d(t)$ is the same in bare electrode in 0.0353 mM thiocholine solution.

in the film, $D_{m,}$ by using eq 5. Similar curves for the polarized case are shown in Figure 5D. For the polarized case we did not get sigmoidal curves but one straight line that overlaps almost totally with the experimental one. The diffusion coefficients found were 1.31 × 10^{-8} and 1.81 × 10^{-8} cm^2 s^{-1}, respectively, for normal and polarized case. The diffusion in solution D_S could not be calculated due to the lack of extraction coefficient (K) value and also because it was not a part of the objectives of this study.

It is worth mentioning that along the same line of the foundation of this method we consider the blocking film at the electrode surface as a membrane through which the ions diffused toward the electrode surface before they eventually get oxidized. The possibility of pinhole diffusion[20] has been ignored

DOI: 10.1021/acs.jpcb.5b01383
J. Phys. Chem. B 2015, 119, 4749−4757

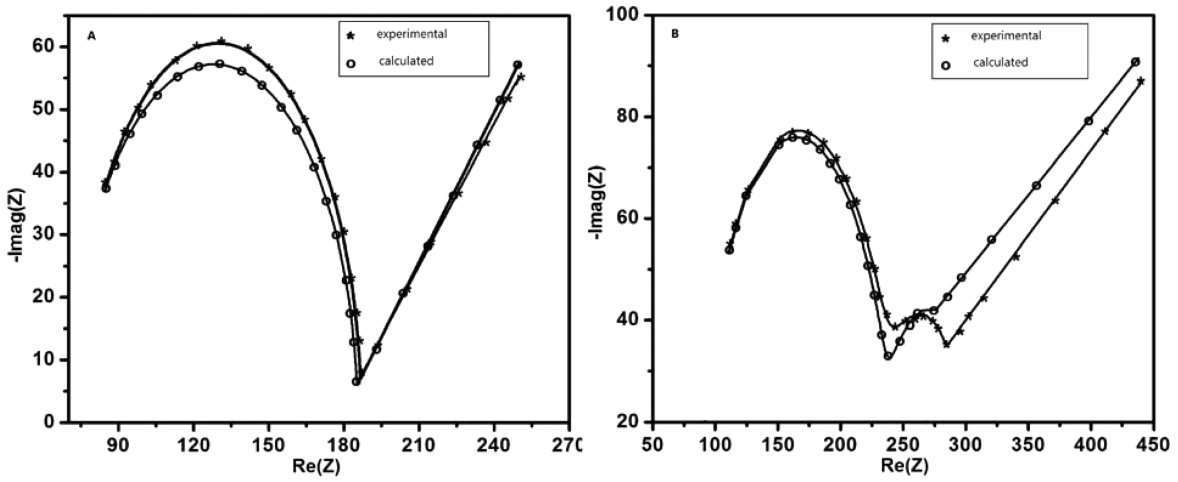

Figure 6. Experimental (*) and theoretical (○) impedance spectra of the film-modified electrode in 0.0353 mM thiocholine solution. (A) Impedance spectra in normal condition and (B) impedance spectra recorded after subjecting the film to polarization. Impedance was recorded in the same thiocholine solution where the prepolarization was applied. The parameters were (A) R_s = 70.00 Ω, C_e = 1.00 × 10^{-3} mF, C_i = 1.00 × 10^{-2} mF, R_e = 140.00 Ω, R_i = 200.00 Ω, R_p = 1.00 Ω, Z_{inf} =630.00 Ω, D_e =1.00 × 10^3 cm^2 s^{-1}, D_i = 1.00 × 10^{-6} cm^2 s^{-1}; (B) R_s = 86.00 Ω, C_e = 8.00 × 10^{-3} mF, C_i = 0.20 mF, R_e = 210.00 Ω, R_i = 165.00 Ω, R_p = 3.00 Ω, Z_{inf} =500.00 Ω, D_e =1.00 × 10^6 cm^2 s^{-1}, D_i = 1.00 × 10^{-8} cm^2 s^1.

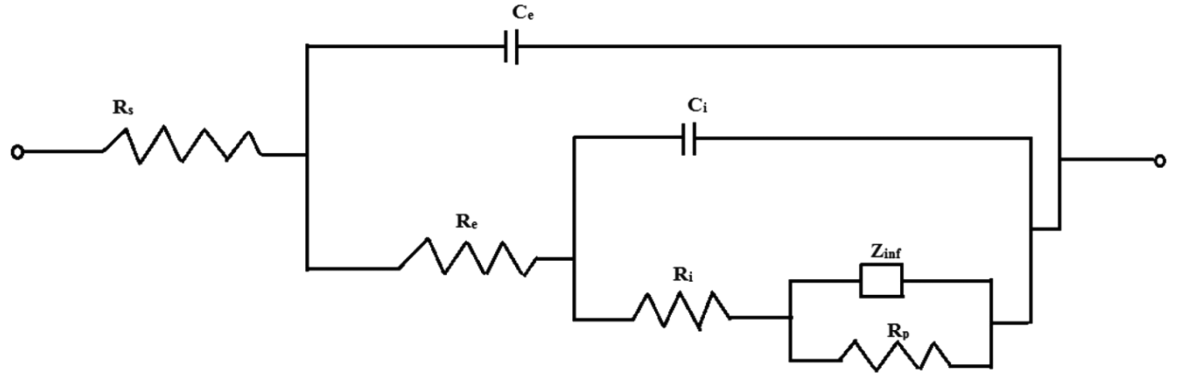

Figure 7. Equivalent circuit for the impedance model. R_s, Solution resistance; R_e, metal/film interfacial charge transfer resistance to the electrons; R_i, film/electrolyte interfacial resistance to the ions; R_p, resistance of the bulk film; C_e, double-layer capacitance of the metal/film interface; C_i, double layer capacitance of the film/electrolyte interface; Z_{inf}, resistance due to distributed elements.

considering the excess thickness and the viscous nature of the solvent swollen film.

3.3.4. By Vortynstev Impedance Equation. AC impedance spectra of the wet, swollen film recorded in thiocholine solution of molarity 0.0353 mM in normal and prepolarized conditions are shown in Figure 6A,B. The theoretical spectra were calculated by using equation eq 8

$$Z = R_s + \frac{Z_{ME}(w)\cdot Z_{inf}}{Z_{ME}(w) + Z_{inf}} \quad (8)$$

where Z_{ME} is the complex impedance calculated through eq 4 of ref 15. R_s is the series electrolytic resistance and Z_{inf} is the empirical resistance added parallel to the modified electrode impedance so as to account for nonideal blocking of the film−electrolyte interface (distributed element).

The evaluated parameters have been shown in the captions of Figure 6A,B. The relevant equivalent circuit is shown in Figure 7.

In the polarized case a higher value of solution resistance but a lower charge-transfer resistance at the film electrolyte interface (R_i) is obtained, which is in accordance with the expectation. In the polarized case decrease in R_i occurs due to weakening of interfacial double layer because of two opposite migration of ions: expulsion of prediffused but unoxidized TCh from the film toward the solution on one hand and migration of phosphate end of the compound ion toward the film after reorientation on the other hand. The increase in solution resistance is attributed to be due to the increase in the proportion of negative charge, that is, free phosphate anions in the post-polarized solution as compared with the pre-polarized one. The flat area in the Nyquist plot (Figure 6B) represents the hindered mass-transfer region, which is indicative of the change of film composition during prepolarization. The change in capacitive contribution due to diffusion of thiocholine ions into the film is adjusted through the Z_{inf} value, and hence no separate component has been included in the equivalent circuit. The thiocholine ion diffusion coefficients found were 1.00 × 10^{-6} and 1.00 × 10^{-8} cm^2 s^{-1}, respectively, for the normal and polarized case. The corresponding electron diffusion coefficients were found to be 1.00 × 10^3 and 1.00 × 10^6 cm^2 s^{-1}, respectively.

3.3.5. By Direct Impedance Measurement Method. The minimum Warburg impedance was calculated from the Nyquist plot using the equation (eq 6),[16] followed by its modified form eq 7.

DOI: 10.1021/acs.jpcb.5b01383
J. Phys. Chem. B 2015, 119, 4749−4757

From the experimental value of the impedance corresponding to the lowest Warburg region in the Nyquist plot, the diffusion coefficients were calculated and found to be 1.75×10^{-4} and 1.35×10^{-3} cm^2 s^{-1}, respectively, for normal and polarized cases.

Table 1 shows a comparison of the diffusion coefficient values calculated by using the two most commonly used methods for chronoamperometric determination of diffusion coefficient, namely the Cottrell and the ESCR. As mentioned in Section 3.3.1, the Cottrell method has been classified as Cottrell A and B based on the process of application. Under normal conditions Cottrell A and B each gave two sets of values for pre- and post-peak regions. Both values ranged from 10^{-9} to 10^{-8} with some variation in magnitude, but ESCA gave a steady value of $5.32\ (\pm 0.03) \times 10^{-7}$ cm^2 s^{-1}. Cottrell values are lower than ESCR. Under forced conditions, Cottrell A gave two sets of values ranging from 10^{-7} to 10^{-8}, but both Cottrell B and ESCR gave steady values of order 10^{-6} and 10^{-7}, respectively. Unlike the normal case, here the post-peak Cottrell values are higher than ESCR. From a comparison of the D values calculated by different methods (Table 2), it is clear that for normal diffusion ESCR-based value is closer (5.32×10^{-7} cm^2 s^{-1}) to the Vortynstev's impedance-based method (1.00×10^{-6} cm^2 s^{-1}). It implies that under normal type of diffusion the ESCR method is more reliable than other three methods.

Table 2. Comparison of Diffusion Coefficients Obtained by the Various Methods with 0.0353 mM Thiocholine

TCh polarization type	method	ionic diffusion coefficient (D_i) cm^2 s^{-1}	electron diffusion coefficient (D_e) cm^2 s^{-1}
normal	Cottrell A[a]	$3.45\ (\pm 0.01) \times 10^{-9}$ (pre peak region)	
		$3.66\ (\pm 0.2) \times 10^{-8}$ (post peak region)	
	Cottrell B[a]	$4.40\ (\pm 0.10) \times 10^{-9}$ (pre peak region)	
		$2.48\ (\pm 0.04) \times 10^{-8}$ (post peak region)	
	ESCR[a]	$5.32\ (\pm 0.03) \times 10^{-7}$	
	Peerce and Bard	1.31×10^{-8}	
	Vortynstev method	1.00×10^{-6}	1.0×10^{3}
	direct impedance measurement	1.75×10^{-4}	
polarized	Cottrell A[a]	$2.82\ (\pm 0.02) \times 10^{-8}$ (pre peak region)	
		$4.60\ (\pm 0.12) \times 10^{-7}$ (post peak region)	
	Cottrell B[a]	$1.54\ (\pm 0.04) \times 10^{-6}$ (pre peak region)	
		$2.58\ (\pm 0.03) \times 10^{-6}$ (post peak region)	
	ESCR[a]	$1.94\ (\pm 0.03) \times 10^{-7}$	
	Peerce and Bard	1.83×10^{-8}	
	Vortynstev method	1.00×10^{-8}	1.0×10^{6}
	direct impedance measurement	1.35×10^{-3}	

[a]Values shown are the average value calculated in three different time zones.

Under polarized conditions the diffusion coefficient obtained from Vortynstev's method is 1.00×10^{-8} cm^2 s^{-1}. The magnitude-wise Cottrell A value in the prepeak region is more close to this impedance-based value. So, it has been concluded that under normal conditions the ESCR method and under polarized conditions the Cottrell A methods are the alternate to the impedance-based method for determination of the diffusion coefficient of thiocholine in the PPy composite film.

Then, the obvious question is why two different methods and two different time zones become necessary for obtaining the correct diffusion value of the ion? The answer is the conclusion that the two conditions, normal and polarized, resulted into two distinctly different types of diffusions. In the former case, the diffusion is in the film electrolyte double layer with diffusion direction from the solution side toward the film, while in the latter case the diffusion is that of oxidized thiocholine molecules inside the film and toward the solution side from the film. The oxidation of prediffused thiocholine molecules occurs immediately after the final potential in the prepolarized case, and hence in this case the short time range is crucial for determination of the diffusion coefficient. This also supports the applicability of Cottrell equation for the purpose because here true charge decay occurs immediately after the final potential that falls in line with the Cottrell hypothesis. In the normal case it takes certain time for stabilization or proper orientation of the anionic (phosphate anion) sheet of the double layer, that is, until the disturbance due to the increasing charging current is stabilized at the peak. So here the true diffusional behavior can be seen only after the peak. This is why the ESCR model that allows diffusion calculation after this period (termed as relaxation period) is able to give good results in the normal case.

Under polarized conditions the diffusion coefficient obtained from impedance measurement is 1.00×10^{-8} cm^2 s^{-1}, which is much lower than the diffusion coefficient value obtained under normal conditions (1.00×10^{-6} cm^2 s^{-1}). This also supports the previously described conclusion of two different types of diffusion associated with the two processes (normal and polarized). In the polarized case, the diffusion is hindered diffusion inside the film, and hence a low diffusion is observed. In the normal case the diffusion is mostly at the interface and hence less hindered, resulting in a high value of diffusion coefficient.

Thus, based on Vortynstev's method the thiocholine diffusion coefficient in the prepared composite film of polypyrrole, enzyme, gelatin, and gluteraldehyde is concluded to be 1.00×10^{-8} cm^2 s^{-1}, and the same in the film/electrolyte boundary is 1.00×10^{-6} cm^2 s^{-1}. The latter value is almost the same with the reported value of 1.7×10^{-6} cm^2 s^{-1} in ref 4 and 0.6×10^{-6} cm^2 s^{-1} in ref 5, both determined through Cottrell method but in a matrix not having electroactive polymer. A lower value of 2.3×10^{-7} cm^2 s^{-1} was obtained by Turdean et al. in the polymer matrix consisting of polyvinyl alcohol and styrilpyridinium ion (PVA-SBQ) through RDE measurement.[21]

The method of Peerce and Bard gave a value of 1.83×10^{-8} cm^2 s^{-1} in the polarized case, which is even more closure to the impedance-based method when the calculation was done with a solution of molarity 0.0353 mM; however, when the concentration is different the deviation of experimental and theoretical curve becomes greater (Figure.S3 in Supporting Information), resulting in significant deviation of the diffusion coefficient from the impedance-based value. Moreover, in the normal case the value obtained was lower than the impedance-

DOI: 10.1021/acs.jpcb.5b01383
J. Phys. Chem. B 2015, 119, 4749−4757

based method. Therefore, this method, although it gives an excellent value of diffusion coefficient in electro-inactive polymer, it may not be the right choice for electroactive polymer like polypyrrole. The direct impedance measurement method gave an exceptionally high value, indicating its mismatch with the situation of application.

3.4. Mechanism of Thiocholine Diffusion. It has been attributed that the thiocholine cation forms a compound ion with the phosphate anion through weak electrostatic interaction, whereby the positive charge on the nitrogen atom is neutralized by one of the negative charges of the phosphate anion. The compound ion thus acquires a dinegative character. Under the influence of positive polarization the compound ion with its negative head moves toward the electrode, and the phosphate end of the ion enters in to the bulk of the film while keeping the thiocholine moiety mostly toward the outside of the film. Under negative polarization the situation becomes reversed; the thiocholine moiety gets more inside the film, leaving the phosphate group at the surface. At the extreme of strong polarization, the thiocholine unit becomes detached from the phosphate group. The situation is represented in Scheme 1.

Scheme 1. Formation of Dinegative Ion between Thiocholine and Phosphate Ion through Electrostatic Interaction

4. CONCLUSIONS

We have compared the performance of five different methods used for the evaluation of the diffusion coefficient from chronoamperometric data taking Vortynstev's impedance-based method as the benchmark and for the system of thiocholine diffusion in an enzyme-loaded polypyrrole composite film. For the normal type of diffusion in which the diffusion is basically at the film electrolyte interface, ESCR method can be reliably applied for calculation of diffusion coefficient, but for the calculation of diffusion coefficient inside the film that can be studied under prepolarized conditions, Cottrell method A is found to be more suitable. The diffusion coefficient of thiocholine in the enzyme-loaded PPy composite film and from an electrolytic background of phosphate buffer of pH 7.4 is 1.00×10^{-8} cm^2 s^{-1}, and the same for thiocholine diffusion at the film/electrolyte boundary is 1.00×10^{-6} cm^2 s^{-1}.

The work has implied that it is important to specify diffusion type (in film and in solution) while calculating diffusion through chronoamperometric method. This philosophy was rightly taken care of in the work of Peerce and Bard, although the method has the drawback of concentration dependency. In most of the recent work, this point is ignored. A modified diffusion equation with initial derivation along the same line as that of Peerce and Bard is expected to provide a very effective diffusion equation that can distinguish between film diffusion and solution diffusion.

The mechanism of positive ion (thiocholine) diffusion into a positively polarized matrix is attributed to the migration of a dinegative ion pair formed between thiocholine and PO_4^{3-} through electrostatic interaction.

■ ASSOCIATED CONTENT

Supporting Information

Detailed calculations of the diffusion coefficients under various methods and the associated figures. This material is available free of charge via the Internet at http://pubs.acs.org.

■ AUTHOR INFORMATION

Corresponding Author

*Phone: (+91) 3712275061. Fax: (+91) 3712 267005, 3712 267006. E-mail: pancha@tezu.ernet.in.

Notes

The authors declare no competing financial interest.

■ REFERENCES

(1) Otero, T. F.; Bengoechea, M. UV−Visible Spectroelectrochemistry of Conducting Polymers. Energy Linked to Conformational Change. *Langmuir* **1999**, *15*, 1323−1327.

(2) Ramanavicius, A.; Ramanaviciene, A.; Malinauskas, A. Electrochemical Sensors based on Conducting Polymer—Polypyrrole. *Electrochim. Acta* **2006**, *51*, 6025−6037.

(3) Cottrell, F. G. Application of the Cottrell Equation to Chronoamperometry. *Z. Phys. Chem.* **1902**, *42*, 385−431.

(4) Rotariu, L.; Zamfir, L.-G.; Bala, C. Low Potential Thiocholine Oxidation at Carbon Nanotube-Ionic Liquid Gel Sensor. *Sens. Actuators, B* **2010**, *150*, 73−79.

(5) Arduini, F.; Cassisi, A.; Amine, A.; Ricci, F.; Moscone, D.; Palleschi, G. Electrocatalytic Oxidation of Thiocholine at Chemically Modified Cobalt Hexacyanoferrate Screen-Printed Electrodes. *J. Electroanal. Chem.* **2009**, *626*, 66−74.

(6) *Impedance Spectroscopy: Emphasizing Solid Materials and Systems*; John Wiley & Sons: New York, 1987.

(7) Strauss, E.; Golodnitsky, D.; Ardel, G.; Peled, E. Charge and Mass Transport Properties of LiI-P(EO)n-Al2O3-based Composite Polymer Electrolytes. *Electrochim. Acta* **1998**, *43*, 1315−1320.

(8) Xie, Z.; Holdcroft, S. Polarization-Dependent Mass Transport Parameters for Orr in Perfluorosulfonic Acid Ionomer Membranes: An EIS Study Using Microelectrodes. *J. Electroanal. Chem.* **2004**, *568*, 247−260.

(9) Barreira, S. V. P.; García-Morales, V.; Pereira, M. C.; Manzanares, A. J.; Silva, A. J. Electrochemical Impedance Spectroscopy of Polyelectrolyte Multilayer Modified Electrodes. *J. Phys. Chem. B* **2004**, *108*, 17973−17982.

(10) Peerce, P. J.; Bard, A. J. Polymer Films on Electrodes Part II. Film Structure and Mechanism of Electron Transfer with Electrodeposited Poly (vinylferrocene). *J. Electroanal. Chem.* **1980**, *112*, 97−115.

(11) Schulze, H.; Vorlova, S.; Villatte, F.; Bachmann, T. T.; Schmid, R. D. Design of Acetylcholinesterases for Biosensor Applications. *Biosens. Bioelectron.* **2003**, *18*, 201−209.

(12) Dutta, R. R.; Puzari, P. Amperometric Biosensing of Organophosphate and Organocarbamate Pesticides Utilizing Polypyrrole Entrapped Acetylcholinesterase Electrode. *Biosen. Bioelectron.* **2014**, *52*, 166−172.

(13) Suárez, J. I.; Otero, F. T.; Márquez, M. Diffusion Coefficient in Swelling Polypyrrole: ESCR and Cottrell Models. *J. Phys. Chem. B* **2005**, *109*, 1723−1729.

(14) Vorotynste, M. A.; Daikhin, L. I.; Levi, M. D. Modelling the Impedance Properties of Electrodes Coated with Electroactive Polymer Films. *J. Electroanal. Chem.* **1994**, *364*, 37−49.

(15) Deslouis, C.; Moustafid, T. EL.; MumNIt, M. M.; Tribollet, B. Mixed Ionic-Electronic Conduction of a Conducting Polymer Film. Ac Impedance Study of Polypyrrole. *Electrochim. Acta* **1996**, *41*, 1343−1349.

(16) Bard, A. J.; Faulkner, L. R. *Electrochemical Methods: Fundamentals and Applications*, 2nd ed.; John Wiley: New York, 2001.

DOI: 10.1021/acs.jpcb.5b01383
J. Phys. Chem. B 2015, 119, 4749−4757

(17) Ellman, G. L.; Courtney, K. D.; Andres, V., Jr.; Featherstone, R. M. A New and Rapid Colorimetric Determination of Acetylcholinesterase Activity. *Biochem. Pharmacol.* **1961**, *7*, 88−95.
(18) Otero, T. F.; Grande, H.-J.; Rodríguez, J. Reinterpretation of Polypyrrole Electrochemistry after Consideration of Conformational Relaxation Processes. *J. Phys. Chem. B* **1997**, *101*, 3688−3697.
(19) Leddy, J.; Bard, A. J. Polymer Films on Electrodes Part XII. Chronoamperometric and Rotating Disk Electrode Determination of the Mechanism of Mass Transport through Poly (vinyl ferrocene) Films. *J. Electroanal. Chem.* **1983**, *153*, 223−242.
(20) Gueshi, T.; Tokuda, K.; Matsuda, H. Voltammetry at Partially Covered Electrodes Part I. Chronopotentiometry and Chronoamperometry at Model Electrodes. *J. Electroanal. Chem.* **1978**, *89*, 247−260.
(21) Turdean, G. L.; Popescu, I. C.; Oniciu, L.; Thevenot, D. R. Sensitive Detection of Organophosphorous Pesticides Using a Needle Type Amperometric Acetylcholinesterase-based Bioelectrode. Thiocholine Electrochemistry and Immobilised Enzyme Inhibition. *J. Enzyme Inhib. Med. Chem.* **2002**, *17*, 107−115.

DOI: 10.1021/acs.jpcb.5b01383
J. Phys. Chem. B 2015, 119, 4749−4757